TRANSCRIPTIONAL REGULATION OF THE HUMAN HYALURONAN SYNTHASE GENES: FOCUS ON HYALURONAN SYNTHASE 2

James Monslow BSc

Thesis Presented for the Degree of Philosophiae Doctor

March 2005

Institute of Nephrology
Wales College of Medicine
Cardiff University
Heath Park
Cardiff
CF14 4XN

ProQuest LLC
789 East Eisenhower Parkway
P.O. Box 1346
Ann Arbor, MI 48106-1346

DEDICATION

For the Rebel Alliance

ACKNOWLEDGEMENTS

Firstly, I gratefully acknowledge the Kidney Wales Foundation for funding the project.

Sincere thanks to everyone in the Institute for their advice, encouragement and support, especially at the start of the project. Thank you to John Martin, Gareth Thomas, Rachel McLoughlin and Rob Jenkins in particular, for being in the right place at the right time on countless occasions.

Thank you to Professor John Williams for his encouragement and support, and for his constructive criticism of the thesis. Thanks also to Aled Phillips, Bob Steadman and Nick Topley for their advice and innumerable good ideas in lab meetings.

Thank you to those scientific collaborators who gave their time and expertise so selflessly, in particular Dipak Ramji (School of Biosciences), Paul Buckland and Carol Guy (Dept. of Psychological Medicine).

An enormous thank you to Tim Bowen, for his constant enthusiasm, friendship and for being a fantastic supervisor over the past three and a half years.

Finally, I'd like to express my utmost gratitude to my close friends and family for their support, and especially to mum and dad, for believing in me.

SUMMARY

This thesis examines the transcriptional regulation of the human hyaluronan synthase (*HAS*) genes, with particular focus on hyaluronan synthase 2. The data details the reconstruction of the genomic structures of each HAS isoform for the first time, as well as analysis of the activity of each HAS proximal promoter. The HAS2 promoter region was then investigated in detail, beginning with the reconfiguration and confirmation of the *HAS2* transcription initiation site. The transcription factor stimulating protein 1 (Sp1) was then identified as an important regulator in the constitutive expression of the *HAS2* gene. Finally, the mechanism involved in the induced expression of the *HAS2* gene by the pro-inflammatory cytokine interleukin-1 beta was investigated. The study identified that the NF-κB pathway was not solely responsible for the increase in *HAS2* transcription, indicating that another, possibly novel mechanism was involved.

PUBLICATIONS AND PRESENTATIONS ARISING FROM THIS THESIS

Peer-reviewed publications

Monslow J, Williams JD, Jones SA et al. Transcriptional regulation of the human hyaluronan synthase 2 gene. *Manuscript in preparation*

Monslow J, Williams JD, Guy CA et al. (2004). Identification and analysis of the promoter region of the human hyaluronan synthase 2 gene. *J Biol Chem* **279**, 20576-20581

Monslow J, Williams JD, Norton N et al. (2003). The human hyaluronan synthase genes: genomic structures, proximal promoters and polymorphic microsatellite markers. *Int J Biochem Cell Biol* **35**, 1272-1283

Published abstracts

Monslow J, Williams JD, Norton N et al. (2003). The human hyaluronan synthase genes: genomic structures and polymorphic microsatellites. *Int J Exp Path* **84**, A34

Bowen T, **Monslow J**, Williams JD, et al. (2003). Characterisation of the proximal promoters of the human hyaluronan synthase genes. *Int J Exp Path* **84**, A64

Oral presentations

Monslow J, Williams JD and Bowen, T (2003). The human hyaluronan synthase genes: putative mediators of renal fibrosis. *Presented at the 2nd Annual General Meeting of the Cardiff Institute for Tissue Engineering and Repair (CITER), University of Wales Aberystwyth, Aberystwyth, UK.*

Monslow J, Williams JD, Spicer AP et al. (2003). The human hyaluronan synthase genes: putative mediators of renal fibrosis. *Presented at Hyaluronan 2003, Cleveland Clinic, Cleveland, OH, USA (to be published in conference proceedings, 2005).*

Monslow J, Williams JD, Guy CA et al. (2004). Identification and analysis of the promoter region of the human hyaluronan synthase 2 gene. *Presented at the 16th meeting of the European Renal Cell Study Group, Seabank Hotel, Porthcawl, UK.*

Monslow J, Williams JD, Craig JK et al. (2004). Identification and analysis of the promoter region of the human hyaluronan synthase 2 gene. *Presented at the 3rd Annual General Meeting of the Cardiff Institute for Tissue Engineering and Repair (CITER), University of Wales Swansea, Swansea, UK.*

Poster presentations

Monslow J, Williams JD, Spicer AP et al. (2003). The human hyaluronan synthase genes: putative mediators of renal fibrosis. *Presented at Hyaluronan 2003, Cleveland Clinic, Cleveland, OH, USA.*

Monslow J, Norton N et al. (2003). The human hyaluronan synthase genes: genomic structures and polymorphic microsatellites. *Int J Exp Path* **84**, A34

ABBREVIATIONS

ATP	Adenosine triphosphate
BRE	TFIIB recognition element
cDNA	coding deoxyribonucleic acid
CTGF	Connective tissue growth factor
CTP	Cytidine triphosphate
D-MEM	Dulbeccos' modified eagle medium
DNA	Deoxyribonucleic acid
dNTP	deoxy-nucleotide triphosphate
DPE	Downstream promoter element
DTT	Dithiothreitol
ECACC	European collection of cell cultures
ECM	Extracellular matrix
EDTA	Diaminoethanetetra-acetic acid
EGF	Epidermal growth factor
EMSA	Electro-mobility shift assay
ERK	Extracellular signal regulated kinase
ESRD	End stage renal disease
EST	Expressed sequence tag
ET-1	Endothelin 1
FCS	Foetal calf serum
FGF	Fibroblast growth factor
GAG	Glycosaminoglycan
gDNA	Genomic deoxyribonucleic acid
GFR	Glomerular filtration rate
HA	Hyaluronan
HAS	Human hyaluronan synthase
Has	Murine hyaluronan synthase
HEK	Human embryonic kidney cell
HK-2	Human kidney 2 cell
HPMC	Human peritoneal mesothelial cell
HTGS	High-throughput genomic sequence
HYAL	Hyaluronidase

IαI	Inter-alpha-trypsin inhibitor
ICAM-1	Intracellular adhesion molecule 1
IFN-γ	Interferon gamma
IGF-1	Insulin-like growth factor 1
IHABP	Intracellular HA binding protein
IL-1β	Interleukin-1 beta
Inr	Initiator
LYVE1	Lymphatic vessel endothelial HA receptor 1
MCP-1	Monocyte chemoattractant protein 1
MCS	Multiple cloning site
MMP	Matrix metalloproteinase
mRNA	messenger ribonucleic acid
NADase	Nicotinamide adenine dinuclease
NCBI	National Centre of Biotechnology Information
NF-1	Nuclear factor 1
NF-κB	Nuclear factor kappa B
NF-Y	Nuclear factor Y
OD	Optical density
ORF	Open reading frame
PBS	Phosphate-buffered saline
PCR	Polymerase chain reaction
PDGF	Platelet-derived growth factor
RACE	Rapid amplification of cDNA ends
RANTES	Regulated upon activation normal T-cell expressed and secreted
RHAMM	Receptor for hyaluronic acid mediated motility
RNA	Ribonucleic acid
RT	Room temperature
RT-PCR	Reverse transcriptase polymerase chain reaction
SAP	Shrimp alkaline phosphatase
SDS	Sodium dodecylsulphate
Sp1	Stimulating protein 1
Sp3	Stimulating protein 3
SPARC	Secreted protein acidic and rich in cysteine
TBM	Tubular basement membrane

TBP	TATA-box binding protein
TFBS	Transcription factor binding site
TGF-β	Transforming growth factor beta
TIMP	Tissue inhibitor of metalloproteinase
TIS	Transcription initiation site
T_M	Annealing temperature
TNF-α	Tumour necrosis factor alpha
TSG-6	Tumour necrosis factor stimulated gene 6
TTP	Thymidine triphosphate
UCSC	Universtity of California Santa Cruz
UDP	Uridine diphosphate
UTR	Untranslated region
UV	Ultra-violet
VCAM-1	Vascular adhesion molecule 1

CHAPTER ONE

INTRODUCTION

1.1 INTRODUCTION: RENAL FIBROSIS, THE EXTRACELLULAR MATRIX AND HYALURONAN

Renal fibrosis is a common feature of many progressive renal diseases that lead to end stage renal disease (ESRD) [Stahl and Felsen, 2001; Muller et al, 2000; Remuzzi and Bertani, 1998]. It can be induced by several injury mechanisms, but will finally produce identical fibrotic changes within the kidney. The rate at which fibrosis develops depends on the type of renal disease, and also on the patient. In some cases, the fibrotic process stops, and kidney function is retained. For a significant proportion of cases, this does not occur, and renal function declines until the only treatment options are dialysis or kidney transplantation. ESRD is one of the most expensive diseases to treat on a per-patient basis [Chatziantoniou et al, 2004]. Therefore the emerging challenge for clinicians is to arrest the decline of renal function and, if possible, to achieve regression of renal fibrosis and restoration of renal structure.

The current model of progressive renal fibrosis is derived from a series of *in vitro* and *in vivo* observations. No single molecule acting in isolation is able to trigger the full spectrum of events that typify fibrosis. Instead, the integration of several molecular players is required including inflammatory agents, cytokines, vasoactive agents and enzymes [Eddy, 2000; Chatziantoniou et al, 2004]. The early stages of fibrosis are typically characterised by inflammation and the disturbance of normal homeostatic mechanisms. This leads to qualitative and quantitative changes to the composition of tubular basement membranes (TBMs), interstitial matrix, tubular atrophy, cellular transformation and the accumulation of myofibroblasts [Stahl and Felsen, 2001; Abrass et al, 1999; Brito et al, 1998; Miner, 1999; Sibalic et al, 1998].

Under normal conditions, the formation of extracellular matrix (ECM) is a dynamic equilibrium between systems that promote its synthesis and those that favour its degradation. In pathophysiological conditions that lead to the development of fibrosis, this equilibrium is broken due to exaggerated rates of ECM synthesis, a diminished capacity of degradation or due to a combination of both. This process occurs irrespective of the underlying disease and originating compartment, indicating a final common pathway independent of the primary cause. Adopting this hypothesis, identifying and targeting the systems participating in this pathway may provide an

efficient treatment against renal fibrosis and kidney failure regardless of the initiating pathology.

One such molecule prominent during the early stages of the fibrotic process is hyaluronan (HA). HA is a high molecular weight glycosaminoglycan and a major constituent of the ECM in many tissues. In normal conditions in the kidney, it is found predominantly in the inner medulla and papilla [Hällgren et al, 1990]. However, in the pathophysiological processes observed in the early stages of fibrosis (e.g. inflammation), a significant deposition of HA is observed in the tubular interstitial space of the outer medulla and renal cortex. At the onset of fibrosis, HA is removed, leaving the fibrotic lesions consisting predominantly of fibrillar collagens. The accumulation and swift degradation of HA from the interstitial space appears crucial to fibrogenesis, however, its exact role is not fully understood.

1.2 HYALURONAN (HA)

1.2.1 Structure

HA is a linear glycosaminoglycan (GAG) that was first isolated from the vitreous of the eye [Meyer and Palmer, 1934]. Unlike other GAGs, HA contains no sulphate groups or epimerised uronic acid residues. Instead, its structure is made of D-glucuronic acid and D-N-acetylglucosamine residues that are linked together via alternating β-1,4 and β-1,3 glycosidic bonds [Weissman and Meyer, 1954]. This disaccharide structure (Figure 1.1) is then repeated to form a hyaluronan molecule or HA chain.

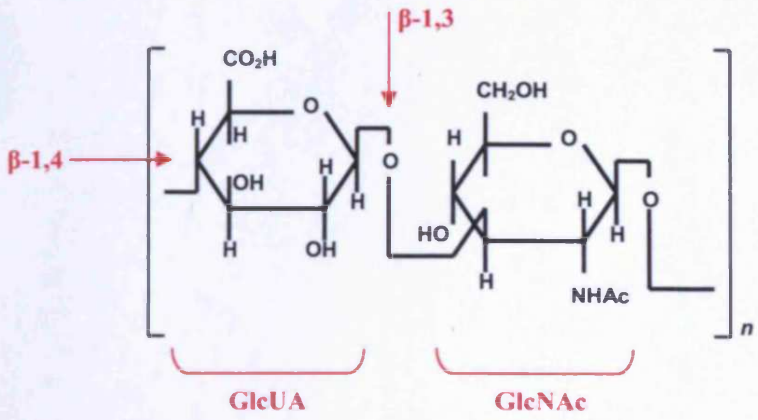

Figure 1.1. Chemical structure of HA. The repeating disaccharide unit is made of D-glucuronic acid (GlcUA) and D-N-acetylglucosamine (GlcNAc) linked via alternating β-1,4 and β-1,3 glycosidic bonds.

The number of repeat disaccharides in a completed HA chain can approach 30,000 units in some tissues. It can therefore have a molecular mass of up to 10 x 10^6 Da and an extended length of 25 μm (Figure 1.2), much larger than any other member of the GAG family [Toole, 2000]. In free solution under physiological conditions of pH and strength, HA forms a stiffened and expanded random coil due to hydrogen bonding of adjacent sugar units and mutual repulsion between carboxyl groups. In dilute solution it occupies a very large solvent domain but as the concentration increases, individual molecules entangle and form a continuous network. Its confirmation can also be modified by interaction with numerous specific binding proteins [Toole, 2001].

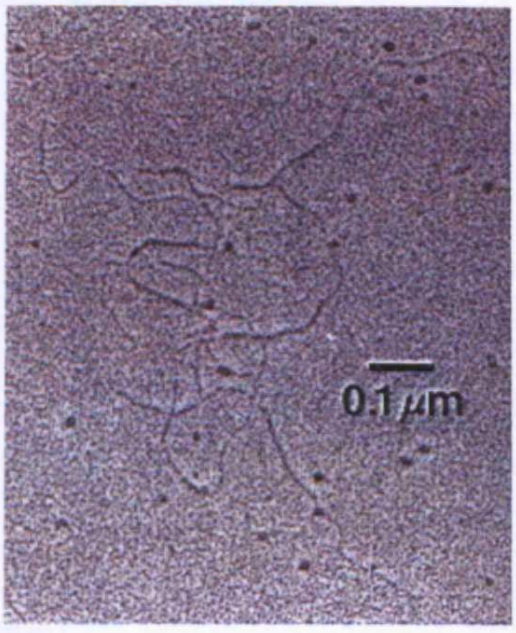

Figure 1.2. Electron micrograph of intertwined HA cables. They have been deposited on a flat surface and rotary shadowed with heavy metal for contrast [Hascall and Laurent, 1997].

1.2.2 Localisation of HA

HA is present in all vertebrates, and has also been found in the capsule of some strains of Streptococci that quite likely pirated the enzymatic machinery for its synthesis from vertebrate hosts. HA is a major constituent of the extracellular matrix (ECM) in which most tissues differentiate. It is also an essential component of many ECMs in mature tissues. HA has also been found on the cell surface, and inside the cell [Tammi et al, 2001]. Fifty percent of the total HA in the body (7-8 g) is contained in skin tissue (0.5 mg/ml in the dermis, 0.1 mg/ml in the epidermis), but is at higher concentrations in other tissues, e.g., synovial joint fluid (around 3-4 mg/ml). Even in low amounts, HA can still serve as an integral structural element (e.g. in hyaline cartilages). HA is also capable of binding other molecules, e.g., aggrecan, through specific HA-protein interactions which mask the HA backbone [Hascall, 2000].

1.2.3 Synthesis, degradation and turnover

Synthesis

Unlike other GAGs (e.g., heparin sulphate or chondroitin sulphate), HA is not assembled in the rough endoplasmic reticulum and Golgi apparatus, and is not covalently linked to a protein backbone during synthesis [Toole, 2000]. The HA synthases (HAS – discussed in detail later) are multipass trans-membrane enzymes situated at the plasma membrane. They extrude HA through the plasma membrane onto the cell surface or into the ECM while it is being synthesised, as an unmodified polysaccharide. In addition, HA is elongated at the reducing, rather than the non-reducing terminus [Weigel et al, 1997].

Degradation

HA can be degraded via the action of oxygen free radicals, peroxynitrites, ultra-violet (UV) irradiation or by the hyaluronidase (HYAL) family of enzymes [Schenck et al, 1995; Li et al, 1997]. In humans, six HYAL genes have been identified. They occur in clusters of three at two chromosomal locations. HYAL1, HYAL2 and HYAL3 make up the cluster on chromosome 3p21.3 and share about 40% similarity. HYAL4, HYALP1 and PH20 make up the second cluster on chromosome 7q31.3. With the possible exception of HYAL4 and HYALP1 (a pseudogene), all the HYALs degrade HA [Csoka et al, 2001; Lokeshwar et al, 2002].

The degradation of HA occurs in a stepwise fashion with quantum decreases in polymer size. From the cluster on chromosome 3, HYAL1 and HYAL2 constitute the major hyaluronidases of somatic tissues. HYAL2 cleaves high molecular weight HA to a limit product of approximately 20 kDa and is bound to the plasma membrane by a GPI-anchor [Stern, 2000; Lepperdinger et al, 2001]. HYAL1 is thought to be lysosomal, cleaving the 20 kDa chains into small HA disaccharides. [Stern, 2000]. Very little is known about HYAL3. Transcripts have been found in the brain and liver, but its protein product remains uncharacterised [Triggs-Raine et al, 1999]. PH20 is expressed in testis and has a role in fertilisation [Cherr et al, 2001]. At first thought to be sperm-specific, it is now known to be expressed in the prostate [Vines et al,

2001], female genital tract [Zhang and Martin-DeLeon 2003], breast [Beech et al, 2002] and foetal tissues [Csoka et al, 1999].

Turnover

HA has an extraordinarily high rate of turnover in vertebrates. However, this rate differs from tissue to tissue. Metabolic studies have shown that the half-life of a HA molecule in cartilage, for example, is normally 2-3 weeks whereas keratinocytes in the epidermis turn-over HA in less than 24 hours. The half-life of HA in the blood is extremely short, only a few minutes. In addition, certain cells may predominantly synthesise or catabolise HA, rather than keep a constant concentration in the tissue. For example, cells in the dermis actively synthesise more HA than they degrade. A larger proportion of HA escapes from this tissue only to be rapidly captured by receptors on reticulo-endothelial cells in lymph nodes and in the liver which internalise them for subsequent catabolism in lysosomes. It has been estimated that approximately one-third (~5 g) of total HA in the human body is metabolically removed and replaced during an average day [Fraser et al, 1997; Hascall, 2000].

1.2.4 Physiological and cell biological functions of HA

The molecular functions of HA fall into three partially overlapping categories. Firstly, HA occupies an enormous hydrodynamic domain that greatly influences the hydration and physical properties of tissues. Secondly, it can interact with a variety of extracellular molecules, such as link proteins and proteoglycans, to form a composite extracellular or pericellular matrix. Thirdly, it can bind to several specific cell surface receptors that activate intracellular signalling pathways and therefore influence cell behaviour [Camenisch and McDonald, 2000; Toole, 2000]. All three of these functions contribute to its roles in cell adhesion, proliferation, migration, differentiation, tissue remodelling, inflammation and diseases such as cancer and atherosclerosis [Toole, 2001; Itano et al, 2002; Lee and Spicer, 2000].

Physical properties of HA

HA solutions of concentrations similar to those found in soft connective tissue exhibit interesting physical and chemical properties. HA has therefore been assigned various roles in the homeostasis of the extracellular space [Comper and Laurent, 1978], e.g., the non-ideal osmotic behaviour of HA making it efficient as an osmotic buffer. The osmotic contribution of polysaccharide networks gives them a role in the homeostasis of tissues [Laurent and Fraser, 1992; Laurent et al, 1996]. At physiological concentrations, HA molecules entangle and form a random network of chains. These networks interact sterically with other macromolecular components [Comper and Laurent, 1978]. HA excludes other macromolecules that cannot find space in the network, and also retards the diffusion of other substances trying to penetrate it. By these properties, HA regulates the distribution of plasma proteins in tissues [Laurent and Fraser, 1992].

The rheological properties that HA solutions exhibit (e.g., in synovial fluid) have also led to speculations about its role in the lubrication of joints and tissues. HA solutions demonstrate similar visco-elastic properties shown by joint fluid. Reports also show that HA separates many tissue surfaces that slide along one another, e.g., fibrils in skeletal muscle [Gibbs et al, 1968; Laurent et al, 1996].

HA interactions with extracellular molecules

The interaction of HA with specific extracellular molecules is important in the assembly of a functional extracellular or pericellular matrix. These HA binding proteins are known collectively as hyaladherins. Among the best characterised hyaladherins are the HA and proteoglycan link protein family (HAPLNs), in particular, cartilage link protein, and the aggregating proteoglycan family, such as aggrecan, versican, brevican and neurocan. Cartilage link protein contains a HA binding domain consisting of a tandemly repeated peptide sequence [Goetinck et al, 1987] and also a separate distinct proteoglycan binding domain [Périn et al, 1987]. As well as forming its own interactions with HA, cartilage link protein can also stabilise HA-proteoglycan interactions by binding to both molecules simultaneously [Hardingham, 1979]. The aggregating proteoglycans have two structurally similar

HA-binding domains (termed link modules) with characteristic disulphide-bonded loops and sequence homologies of 30 – 40%. [Day, 1999]. The link module consists of two alpha helices and two triple-stranded anti-parallel β-sheets arranged around a large hydrophobic core, resembling the C-type lectin module [Kohda et al, 1996]. In aggrecan, for example, two link modules and adjacent sequences in the G1 globular domain are required for high avidity HA binding [Watanabe et al, 1997]. In contrast, the hyaldherin tumour necrosis factor-stimulated gene-6 (TSG-6) only contains a single link module. TSG-6 is secreted in response to inflammatory stimuli [Horton et al, 1998; Camenisch et al, 2000] and is still sufficient for high affinity interactions with HA [Papakonstantinou et al, 1998].

There are however, those hyaldherins that do not contain a link module. One example is the serine protease inhibitor, inter-α-trypsin inhibitor (IαI). This serum protein is composed of a light chain, also known as bikunin, and two heavy chains which are covalently cross-bridged by chondroitin sulphate. This was one of the first proteins found to associate with HA [Day and Prestwich, 2002]. This is an unusual proteoglycan essential during ovulation, acting to stabilise the HA-rich cumulus ECM with which it forms a covalent complex [Huang et al, 2000]. It has also been reported that IαI can bind non-covalently to HA, as is the case for all other HA-protein interactions [Rao et al, 1997]. CD38, a type II membrane glycoprotein, has also been reported as a non-link module hyaladherin. This protein has NADase activity, and this property has been studied much more extensively than its HA binding function for which no biological role has yet been determined [Bourguignon, 1992].

The interaction between HA and its hyaladherins is intertwined with their normal functions. Removing one part of the equation causes unravelling of tightly controlled biological systems. For instance, mice lacking the cartilage link module aggrecan, die shortly after birth due to severe defects in cartilage development [Watanabe and Yamada, 1999].

HA receptors

HA has become accredited as a signalling molecule, due to the identification of HA cell surface receptors that can initiate signal transduction cascades. Of these, CD44

and RHAMM (receptor for hyaluronic-acid-mediated motility) are established signal-transducing receptors that influence cell proliferation, survival and motility. Other cell surface hyaladherins, such as lymphatic vessel endothelial hyaluronan receptor 1 (LYVE1) and TOLL4 have also been identified [Turley et al, 2002; Toole, 2004].

CD44 is a widely distributed cell-surface glycoprotein that contains an extracellular domain, a trans-membrane domain and a cytoplasmic domain [Stamenkovic et al, 1989; Aruffo et al, 1990; Ponta et al, 2003]. The extracellular domain includes an amino terminal HA binding domain that is related to the link modules of the hyaladherins [Day and Prestwich, 2002]. The region of the *CD44* gene that encodes the extracellular domain contains a site into which many exon products are spliced in numerous combinations [Lesley et al, 1993]. Although HA is the main ligand for CD44, several other molecules interact with this protein, many of which bind to carbohydrate side groups that are attached to the 'spliced-in' regions including fibroblast growth factors, osteopontin and matrix metalloproteinases (MMPs) [Toole, 2004].

RHAMM is alternatively spliced and the different forms of the resulting protein are found both on cell surfaces and inside cells. Although RHAMM mRNA does not contain a recognisable leader sequence, the protein is transported to the cell surface where it binds HA. Like CD44, it also transduces signals that influence cell growth and motility [Turley et al, 2002]. There is no link module domain in RHAMM, but it does contain a HA binding motif present in several other hyaldherins [Yang et al, 1994]. Although RHAMM can bind to other extracellular macromolecules, the significance of this binding is not yet clear.

1.2.5 HA and pericellular matrix formation

Several cell types exhibit highly hydrated, HA-dependent pericellular matrices or 'coats'. They are usually 5-10 μm in thickness and can be destroyed by HYAL treatment [Lee et al, 1993; Knudson and Knudson, 1993; Nishida et al, 1999]. These pericellular matrices provide the environment in which numerous cellular activities take place and influence cell behaviour. During tissue formation or remodelling, such matrices provide a hydrated, fluid environment in which assembly of other matrix

components and presentation of growth and differentiation factors can readily occur without interference from the highly structured fibrous matrix usually found in fully differentiated tissues. Embryonic mesenchymal cells, including the precursors of muscle and cartilage, embryonic glial cells, neural crest cells and even some embryonic epithelial cells exhibit prominent pericellular matrices. In some cases, such as cartilage, the pericellular coat is a unique structural component that protects cells and contributes to the characteristic properties of the differentiated tissue. [full review in Toole, 2000].

1.2.6 HA and cellular signalling

The biochemical mechanisms by which HA-CD44 interactions are transduced into intracellular signals that bring about cellular effects are the subject of ongoing investigations. The binding of CD44 isoforms to HA affect cell adhesion to ECM components and is implicated in the processes of aggregation, proliferation, migration and angiogenesis [Lesley et al, 1993; Bourguignon et al, 1992; Bourguignon et al, 1998; Lokeshwar et al, 1996]. It is clear, that in some cell types, the multivalent interaction of polymeric HA with CD44 causes clustering of CD44 in the plasma membrane and that this event is associated with phosphorylation of CD44, interactions with the cytoskeleton and changes in cell behaviour [Lokeshwar et al, 1994; Sleeman et al, 1996]. It has been shown that activation of various components of intracellular signalling pathways including Rac1 [Oliferenko et al, 2000; Bourguignon et al, 2000], phosphoinositide 3'-kinase [Kamikura et al, 2000], erbB-2 [Bourguignon et al, 1997], c-Src kinase [Bourguignon et al, 2001] and NF-κB [Mckee et al, 1997; Fitzgerald et al, 2000] and that rearrangement of cytoskeletal elements, e.g. ankyrin [Zhu and Bourguignon, 2000] and ezrin [Yonemura et al, 1998] result from interaction of HA with CD44 in different cell types. These pathways are reviewed in greater detail by Knudson and Knudson [2000].

The binding of exogenous HA to cell surface RHAMM plays a key role in activating signal cascades, probably as a co-receptor for integral membrane proteins. Although the role(s) of intracellular RHAMM protein forms are not yet known, their ability to associate with kinases [Hall et al, 1996; Zhang et al, 1998], calmodulin [Assmann et al, 1999; Lynn et al, 2001] and the cytoskeleton [Assmann et al, 1999; Entwistle et al,

1996] predicts that they play key roles in cytoskeletal assembly. Cell surface RHAMM has been shown to activate signalling pathways including Src [Hall et al, 1996], extracellular signal regulated kinase (Erk) [Lokeshwar and Selzer, 2000], and Ras [Wang et al, 1998; Mohapatra, 1996], and are reviewed in greater detail by Turley et al [2002].

CD44 and RHAMM can perform separate functions in regulating cell signalling. For instance, CD44, but not cell surface RHAMM, can mediate adhesion of endothelial cells and thymocytes to HA and regulate proliferation. In contrast, cell surface RHAMM, but not CD44, is required for migration [Masellis-Smith et al, 1996; Savani et al, 2001]. In addition, cell surface RHAMM but not CD44 appears to be essential for activation of protein tyrosine kinase cascades by endothelial cells in response to HA [Lokeshwar and Selzer, 2000]. On the other hand, HA-CD44 but not RHAMM interactions have been implicated in the cellular uptake of HA, which in turn effects growth regulation and tissue integrity [Kaya et al, 1997; Teder et al, 2002]. Deletion of either CD44 or RHAMM does not result in embryonic lethality and therefore either these two proteins share some functions and/or other cellular hyaladherins are able to compensate for the loss of CD44 or RHAMM [Turley et al, 2002]

1.2.7 Intracellular HA

There is growing evidence for the presence of intracellular HA. It was first found to be intracellular when it was isolated from rat brain nuclei in 1976 [Margolis et al, 1976] but this report did not receive widespread attention. More recently, intracellular HA has been detected in the cytoplasm of vascular smooth muscle cells during late prophase/early prometaphase of mitosis and in key subcellular compartments such as the nucleus and lamellae during cell locomotion and following serum stimulation [Collis et al, 1998; Evanko and Wight, 1999]. In addition, the identification of intracellular HA binding proteins (IHABPs), including RHAMM, P32, CDC37 and IHABP4 lends further support to the intracellular presence of HA [Day and Prestwich, 2002; Assmann et al, 1998; Hofmann et al, 1998; Huang et al, 2000].

Intracellular HA can be derived from either the extracellular environment by internalisation [Collis et al, 1998; Lee and Spicer, 2000] or synthesised from an as yet

unidentified intracellular source [Evanko and Wight, 1999]. There is evidence that intracellular HA is seen during mitotic events after viral infection [de la Motte et al, 2003] and following the onset of endoplasmic reticulum (ER) stress [Majors et al, 2003]. These reports identify HA cable-like structures originating from nuclear and ER membranes, extruding through the plasma membrane and extending out into the ECM. Furthermore, it is suggested that these structures may be important in cellular defence mechansims during inflammation [Hascall et al, 2004].

1.3 HA AND FIBROSIS

1.3.1 Localisation and function of HA in the kidney

HA is the dominant GAG in the renal papillary interstitium. It is normally distributed at 50-100 times higher concentrations in the inner medullary and papillary segments than in the cortical and outer medullary portions of the kidney, which contain almost no HA [Hällgren et al, 1990]. Besides having a role in the urinary concentrating process [Ginetzinsky, 1958; MacPhee, 1998; Hansell et al, 2000; Knepper et al, 2003], HA accounts for the main stability of the tubular and vascular structures of the inner medulla and the papilla [Pitcock et al, 1988, Fraser et al, 1997].

1.3.2 Pathophysiology of interstitial fibrosis

In recent years, the effect of renal fibrosis on the reduction of glomerular filtration rate (GFR) has correlated better with tubular interstitial fibrosis than with glomerulosclerosis, and has therefore been studied intensely [Strutz and Muller, 1995; Bohle et al, 1996]. The interstitial fibrogenic cascade can be divided into four arbitrary phases; cellular activation and injury, fibrotic signalling, fibrogenesis, and decline in renal function.

1.3.3 HA and interstitial fibrosis

In disease states, a significant accumulation of HA is observed in the interstitial space of the outer medulla and renal cortex. This accumulation occurs during fibrogenesis, and is a feature of many inflammatory renal diseases, including ischemic injury [Johnsson et al, 1996; Göransson et al, 2004], interstitial nephritis [Sibalic et al, 1997], crescentic glomerularnephritis [Nishikawa et al, 1993; Jun et al, 1997], lupus nephritis [Feusi et al, 1999] and diabetic nephropathy [Mahadevan et al, 1995; 1996; Jones et al, 2001; Takeda et al, 2001]. In addition, marked increases of HA in the cortex have been reported in allograft rejection [Wells et al, 1990; 1993]. Once accumulated, it may then play a role in further fibrotic signalling mechanisms and/or cellular activation.

1.3.4 Phase 1 - Cellular activation and injury

Tubular cell activation

Tubular cells have the facility to produce molecules that propagate renal injury, facilitate interstitial inflammation and/or directly contribute to fibrosis, e.g., they may produce endothelin-1 (ET-1) in response to proteinuria [Zoja et al, 1995]. Vasoconstriction induced by peptides such as ET-1 and angiotensin II may propagate tubular damage due to ischemia [Eddy, 2000]. Tubular activation may also be modulated in response to other events that occur during the course of chronic renal insufficiency including increased filtration of other urinary proteins (chemoattractants, complement proteins and cytokines), increased ammoniogenesis, ischemia, lipiduria, tubular hypermetabolism and crystal deposition [Jernigan and Eddy, 2000].

Interstitial inflammation

As a source of several profibrotic molecules, monocytes and macrophages directly contribute to the fibrogenic process [Nathan, 1987]. While their presence may originate in small part from *in situ* proliferation of resident interstitial macrophages [Lan et al, 1995], most of these cells have migrated from the circulation into the

interstitial space. The stimulus for this efflux is thought to be chemoattractant molecules that are either secreted across the basolateral membrane of tubules or that pass between tubular cells moving from the tubular lamina directly into the interstitium [Eddy, 2000]. Chemokines are thought to play an important role, e.g., monocyte chemoattractant protein 1 (MCP-1) [Wang et al, 1997; Grandaliano et al, 1996; Tang et al, 1997; Okada et al, 2000], along with complement proteins [Biancone et al, 1994; Nomura et al, 1997; Nangaku et al, 1999], leukocyte adhesion molecules [Ricardo et al, 1996; Morrissey and Klahr, 1998], antigen expression [Weiss et al, 1994] and profibrotic growth factors such as insulin-like growth factor 1 (IGF-1) and transforming growth factor beta (TGF-β) [Wang et al, 1999]. Increased HA in the cortex is also coupled with certain inflammatory responses [Gerdin and Hällgren, 1997]. For example, in tubular epithelial cells, it can directly stimulate the expression of the cell adhesion molecules intracellular adhesion molecule-1 (ICAM-1) and vascular adhesion molecule-1 (VCAM-1) [Oertli et al, 1998], as well as MCP-1 [Beck-Schimmer et al, 1998].

Appearance of interstitial myofibroblasts and the activation of resident interstitial fibroblasts

Studies have shown that the presence of interstitial myofibroblasts correlates with the risk of progressive renal disease [Alpers et al, 1994; Goumenos et al, 1994; Roberts et al, 1997]. Myofibroblasts, unlike traditional interstitial fibroblasts are characterised by their expression of the myocyte protein alpha smooth muscle actin. In addition to their unique phenotype, myofibroblasts, are considerably more profibrotic. Furthermore, they are able to produce high amounts of HA as a result of decreased HA degradation [Jenkins et al, 2004]. The origin of these cells seems to be the proliferation and/or differentiation of resident fibroblasts, migration of perivascular cells and the transdifferentiation and migration of tubular cells [Eddy, 2000]. TGF-β has been shown to transform fibroblasts into myofibroblasts and to induce alpha smooth actin expression and phenotypic changes in cultured tubular epithelial cells [Fan et al, 1999]. The transformation of the phenotype, function and number of tubular interstitial cells sets the stage for subsequent events. At this early phase, renal damage may be repaired and kidney function restored to normal levels. However, if renal

injury persists passed this point, changes in tubular cells and ongoing interstitial inflammation will result in destructive renal scarring [Eddy, 2000].

1.3.5 Phase 2 - Fibrogenic signalling

Coincident with, or as a consequence of the cellular events, a series of molecules are elaborated and their cognate receptors expressed by tubular interstitial cells to result in matrix accumulation along tubular basement membranes and within the interstitial space. These include TGF-β [Jernigan and Eddy, 2000], connective tissue growth factor (CTGF) [Ito et al, 1998; Riser et al, 2000], angiotensin II [Cruz et al, 2000; Gilbert et al, 1998; Nagamatsu et al, 1999; Otsuka et al, 1998; Szabo et al, 2000], ET-1 [Eddy, 2000], PDGF [Kliem et al 1996; Fellström et al, 1989; Gesualdo et al, 1994], fibroblast growth factor (FGF) [Ray et al, 1994], tumour necrosis factor alpha (TNF-α) [Guo et al, 1999] and interleukin-1 (IL-1) [Lan et al, 1993]. Many of these are known to directly stimulate HA production in the kidney as well as in other cellular systems, including PDGF [Heldin et al, 1992], TGF-β1 [Haubeck et al, 1995], IL-1 [Ito et al, 1993] and TNF-α [Sampson et al, 1992].

One of the fundamental pathways to fibrogenesis is dominated by TGF-β. This is known to be an important regulator of interstitial matrix production and its over-production has been associated with renal fibrosis. Three mammalian isoforms have been identified although it is only TGF-β1 has been extensively investigated with regards to renal fibrosis. Both resident kidney cells and infiltrating leukocytes may be stimulated to produce latent TGF-β. It may also be filtered from the plasma during proteinuria [Eddy, 2000]. Numerous factors are known to stimulate its production including angiotensin II, ET-1, ischemia, high glucose and insulin. It may also induce its own expression [Jernigan and Eddy, 2000].

Activation of TGF-β triggers several events that promote fibrosis. This includes the transcription of matrix-encoding genes, inhibitors of matrix degrading enzymes, inhibition of matrix binding integrin receptors, transformation of fibroblasts into myofibroblasts, transdifferentiation of tubular epithelial cells into myofibroblasts and chemotaxis of fibroblasts and monocytes [Jernigan and Eddy, 2000]. Upregulated expression of TGF-β is a feature of all human and experimental models of renal

fibrosis. For example, transgenic mice overexpressing TGF-β develop glomerular and interstitial fibrosis [Kopp et al, 1996; Clouthier et al, 1997]. In addition, treatment of rats with replication-defective adenoviral vectors that express the soluble TGF-β type II receptor attenuates interstitial collagen accumulation in models of proteinuria and ureteral obstruction [Jernigan and Eddy, 2000].

Evidence also suggests that HA-mediated signalling may contribute during the pro-inflammatory response acting via CD44 signalling. [Wüthrich, 1999]. CD-44 is scarcely expressed in the kidney except by passenger leukocytes [Roy-Chaudhury et al, 1996; Benz et al, 1996]. However, in inflammatory renal diseases, CD44 expression is markedly enhanced, particularly in crescents and injured tubules [Roy-Chaudhury et al, 1996; Sibalic et al, 1997; Florquin et al, 2002]. As previously mentioned, HA can induce the expression of MCP-1 [Beck-Schimmer et al, 1998], and it has been found that this occurs via HA-CD44 signalling [Wüthrich, 1999]. The expression of other pro-inflammatory cytokines, e.g. TNF-α and RANTES (regulated upon activation normal T-cell expressed and secreted) can also be induced by this mechanism [Wüthrich, 1999]. Interestingly, an absence of CD44 causes increased tubular damage, but reduces fibrosis [Rouschop et al, 2004], suggesting also a protective role for HA in the fibrogenic pathway.

1.3.6 Phase 3 - Fibrogenesis

The synthesis, secretion and activation of one or more of the fibrogenic molecules discussed above results in the activation of genes that leads to the accumulation of extracellular molecules within the interstitial space. This excessive accumulation can cause progressive renal scarring and is the consequence of increased synthesis and decreased degradation acting simultaneously.

Increased extracellular matrix production

Evidence for increased matrix protein synthesis has been shown by increased mRNA levels of matrix genes within the kidney. This suggests that transcription may be a rate-limiting step for the production of some matrix molecules, and also the *de novo* appearance of proteins not normally present in the interstitium. The interstitial scar

consists of several matrix molecules, including normal interstitial matrix proteins (collagens I, III, V, VII, XV and fibronectin) and proteins usually restricted to tubular basement membranes (collagen IV and laminin) [reviewed by Jerginan and Eddy, 2000]. Recent reports have shown that interstitial myofibroblasts are the primary source of these proteins with a smaller contribution originating from tubular and other interstitial cells [Tang et al, 1997]. In addition to providing structural support, these matrix proteins can also interact with cellular receptors, including integrins. As a consequence, the nature of the interstitial matrix can influence the behaviour of neighbouring cells. Fibronectin also has chemotatic properties that may influence inflammation [Eddy, 2000].

Other constituents of the fibrotic interstitium include increased proteoglycans, polysaccharides and glycoproteins. Like the matrix proteins, these molecules do much more than provide structural support. Examples of these molecules include HA, SPARC (secreted protein acidic and rich in cysteine), thrombospondin, decorin and biglycan. SPARC has been reported to accumulate in the interstitium during fibrosis [Pichler et al, 1996], and has been shown to stimulate TGF-β expression and synthesis of collagen I and fibronectin [Francki et al, 1999]. Thrombospondin has also been shown to activate TGF-β, and in addition is also known to appear early in the development of interstitial fibrosis [Crawford et al, 1998; Hugo et al, 1998]. Proteoglycans are also important in fibrosis, and are known to act as a potential reservoir for growth factors such as FGF and TGF-β. Decorin and biglycan are small proteoglycans that have the ability to inhibit TGF-β and have been shown to accumulate in the kidney during progressive scarring [Diamond et al, 1997; Schaefer et al, 1998; Stokes et al, 2000].

Emerging evidence now suggests that the accumulation of HA in the corticointerstitium also has anti-inflammatory effects. In certain disease conditions, including diabetic nephropathy, the deposited HA forms cable-like structures [Wang and Hascall, 2004]. Monocytes, in particular, bind to these cable structures via CD-44, which stops them interacting with the resident cells and attenuates the inflammatory response [Hascall et al, 2004; Selbi et al, 2004]. The increased HA deposition has also been shown to attenuate TGF-β signalling by modulating the TGF-β1 receptor via CD44 interactions [Ito et al, 2004(1); 2004 (2)].

Decreased extracellular matrix degradation and impairment of matrix remodelling

Matrix turnover in normal conditions is a fine balance between the rate of synthesis of new molecules and the rate at which they are degraded. In disease conditions, this balance is lost. Under normal conditions, several matrix-degrading proteases are synthesised that help maintain the matrix architecture. During fibrosis, their activity is halted by the production of protease inhibitors. Therefore, at the same time that synthesis is increased, degradation enzymes are inactivated. In early fibrotic lesions this can be completely reversed, as reported in rats with acute nephritic syndrome [Jones et al, 1992] and in humans with diabetic nephropathy [Fioretto et al, 1998].

One example of this inhibitory effect is on the matrix metalloproteinases (MMPs). MMPs are a large family of endopeptidases involved in matrix degradation and turnover. Four major MMP inhibitors have been identified. These are the tissue inhibitors of metalloproteinases (TIMP) -1, -2, -3 and -4. TIMP-2 and TIMP-3 are expressed constitutively in normal kidneys. TIMP-1 has shown to be induced in many progressive renal diseases [reviewed by Jernigan and Eddy, 2000]. TIMP-1 can be synthesised by nearly all mesenchymal cells including fibroblasts, macrophages and tubular epithelial cells. Its expression can also be induced by TGF-β, TNF-α, IL-1 and thrombin [Eddy, 2000]. As well as being able to inhibit MMP activity directly, TIMP-1 has other effects, including inhibition of apoptosis and angiogenesis and the induction of changes in cell morphology [Gomez et al, 1997].

1.3.7 Phase 4 – Progressive decline in renal function

As matrix molecules continue to accumulate within and expand the interstitial space, they begin to have destructive effects on kidney structure and function. The renal tubules, accounting for 80% of total kidney volume, are victims of the fibrogenic process, which in many instances they helped initiate. The tubules atrophy, sometimes leaving behind normal appearing glomeruli lacking the distal nephron segment. This renders the nephron non-functional [Marcussen, 1992]. The post glomerular peritubular capillaries are also obliterated through this fibrotic destruction. Like the loss of tubules, a decrease in the surface area of the peritubular capillaries is a histological feature of progressive renal disease that closely correlates with loss of

renal function [Serón et al, 1990]. Endothelial cell apoptotic death has also been reported in progressive models of renal disease [Eddy, 2000].

1.4 HYALURONAN SYNTHASE (HAS)

1.4.1 Identification and chromosomal location of the HAS enzymes

The HA polymer was first described in 1934, but the enzymes from various vertebrates and microbes that catalyse HA synthesis, the HA synthases (HASs), were only identified in the 1990s. Since the discovery in 1993 of the first gene encoding a HA synthase from group A *streptococcus* [DeAngelis et al, 1993], many more similar *HAS* genes (or cDNAs) have been identified and cloned from other species. 1996 saw four different laboratories almost simultaneously identifying eukaryotic HAS cDNAs revealing that HAS was a multigene family encoding distinct isoforms. Two genes (*HAS1* and *HAS2*) were quickly discovered in the mouse and the human [Itano and Kimata, 1996 (1); 1996 (2); Shyjan et al, 1996; Spicer et al, 1996; Watanabe and Yamaguchi, 1996], with a third gene discovered slightly later [Spicer et al, 1997]. HAS cDNAs have also been identified in other species, including *Xenopus laevis* (African clawed frog), chicken, zebrafish, [Spicer and McDonald, 1998], rabbit [Ohno et al, 2001], *Pasteurella multocida* [DeAngelis, 1996] and even a virus that infects a type of algae, which in turn lives in a protozoan host [DeAngelis et al, 1997].

To date, four cDNAs have been identified and cloned in humans, and are numbered in the order they were discovered; *HAS1* [Shyjan et al, 1996], *HAS2* [Watanabe and Yamaguchi, 1996] and two variant transcripts from the *HAS3* locus, *HAS3* variant 1 [Spicer et al, 1997 (1); Sayo et al, 2002] and *HAS3* variant 2 [Sayo et al, 2002]. The map positions for the human *HAS* genes have also been elucidated, with *HAS1* at 19q13.3-13.4, *HAS2* at 8q24.12 and *HAS3* at 16q22.1 [Spicer et al, 1997 (2)].

1.4.2 Evolutionary background of HAS

Sequence analysis of the human (*HAS*) and mouse (*Has*) genes shows they share a very high degree of similarity. *HAS1* shares a 95% sequence identity to *Has1*, and *HAS2* a 98% sequence identity to *Has2* [Weigel et al, 1997]. In addition, localisation of the three *HAS* genes (for mouse and human) on different chromosomes, and the appearance of HA throughout the vertebrate class suggest that this gene family evolved through a series of sequential gene duplications followed by divergence [Weigel et al, 1997; DeAngelis, 1999; Spicer and McDonald, 2000]. Reports stipulate that an initial ancestral *HAS* gene in animals was duplicated to form a *HAS1* lineage and a *HAS2* lineage. A subsequent pair of duplication events early in the vertebrate phylogenetic tree resulted in a) the formation of *HAS1* and a HAS-related homologue, and b) the formation of *HAS2* and *HAS3*. In *Xenopus*, the HAS-related gene (called *xHas-rs*) may be a pseudogene, as the recombinant protein was found to be inactive *in vitro*. In mammals, no such related counterpart has been detected, and it was suggested that this was probably lost from the chromosome [Spicer and McDonald, 1998].

The identity (approximately 30%) between the bacterial and eukaryotic HASs also suggests the likelihood of a common ancestral gene. It is possible that a bacterial ancestor to the present day Group A *streptococcus* species incorporated, from a eukaryotic host, a eukaryotic copy of a primitive HAS gene [Weigel et al, 1997]. However, based upon the location of the *streptococcus* HAS open reading frame (ORF) within the HAS operon, and the location of related polysaccharide capsule synthase ORFs in similar operons of other bacterial species, it is much more likely that the *streptococcus* HAS protein evolved from another polysaccharide capsule synthase as a result of functional convergent evolution [Spicer and McDonald, 2000; DeAngelis, 1999].

1.4.3 Structure

Peptide sequence

The amino acid sequences of the streptococcal and vertebrate HASs are rather distinct from the *Pasteurella* HAS. The streptococcal and vertebrate enzymes are more similar at the amino acid level to the chitin synthases, Nod transferases and certain bacterial capsule synthases [DeAngelis et al, 1999], and are designated Class I HASs. *Pasteurella* HAS is more similar to other distinct bacterial polysaccharide synthases and certain lipopolysaccharide glycosyltransferases [DeAngelis et al, 1998], and is designated as a Class II HAS. To date, *Pasteurella* HAS is the only known member of Class II [DeAngelis, 1999].

Class I HASs are comparable in size (approximately 400-600 amino acids), and appear to possess seven short sequence motifs located similarly throughout the central region of the polypeptide. A few of these putative motifs are similar to other glycosyltransferases that produce β-linked polysaccharides such as chitin, cellulose, and various bacterial capsular polysaccharides built from UDP sugars. However, the exact role of these motifs in the structure and/or function of the polypeptide are not yet known. Five to seven membrane associated regions are predicted in the various HASs, in agreement with the membrane localisation of the enzyme activity. There appears to be a central cytoplasmic domain of about 260-320 residues flanked by two membrane associated regions at the carboxyl terminus. Most of the polypeptide chain is not exposed to the cell exterior surface [DeAngelis, 1999; Weigel, 2004].

The *Pasteurella* Has, is the only known class II HAS enzyme. It is roughly twice the size of the class I enzymes, being 972 residues in size. There is a disagreement on whether it may be a transmembrane or soluble enzyme [DeAngelis, 1999]. However, the vast majority of the polypeptide chain is thought not to be associated with the membrane on the basis of its primary structure. *Pasteurella* Has enzyme activity is found associated with the membrane fraction after lysis of native [DeAngelis, 1996] or recombinant [DeAngelis et al, 1998] bacterial cells, and may therefore be associated with the membrane via an unknown binding protein [DeAngelis, 1999].

Topology

To date, the streptococcal HAS is the only HAS enzyme to be purified and partially characterised [DeAngelis and Weigel, 1994]. Mammalian HAS enzymes are thought to resemble the streptococcal HAS structure due to the similarity in their amino acid sequences [Weigel, 2004]. Figure 1.3 shows a schematic of streptococcal HAS at the plasma membrane. The majority of the protein, including both the amino and carboxyl termini, is inside the cell. Only four of the synthases' membrane domains appear to pass through the membrane, giving only two small loops of the protein exposed to the extracellular side. Another two or more regions of the protein, including the large central domain, may associate with the membrane as amphipathic helices or re-entrant loops that do not span the membrane [Weigel, 2004].

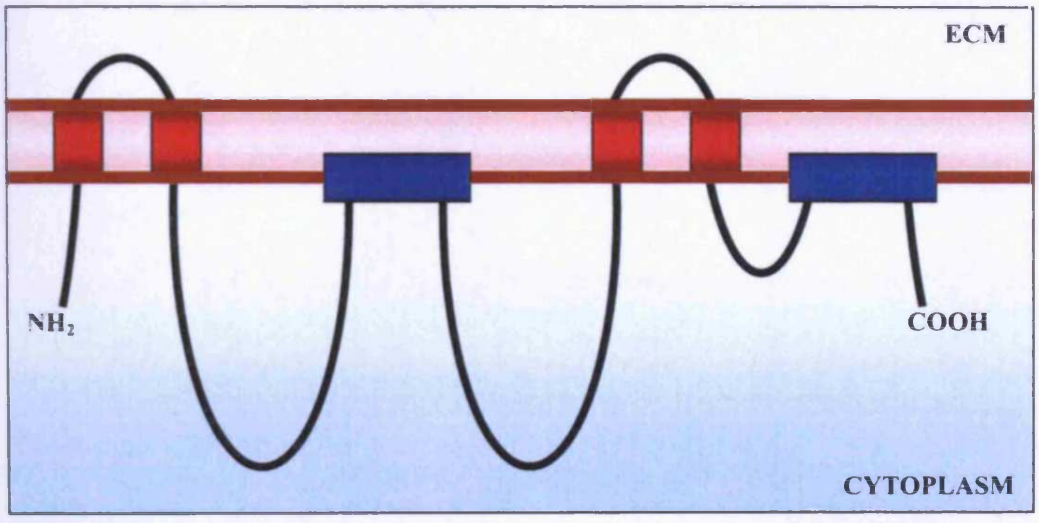

Figure 1.3. Organisation of the streptococcal HAS in the membrane. The polypeptide chain is shown by the black line with the transmembrane domains in red and the membrane associated domains in blue. The (NH_2) and carboxyl (COOH) ends of the protein are labelled.

1.4.4 Mechanism of HA synthesis

Virtually all known enzymes catalyse a reaction that uses one or two (or more rarely, three) substrates to produce one or two products. The HAS enzymes are an exception

to this rule. HA synthase has two different enzymatic activities within the same enzyme. The HA product after each sugar addition becomes a substrate for the next sugar addition. The overall reaction for the synthesis of one HA disaccharide unit is shown in Figure 1.4.

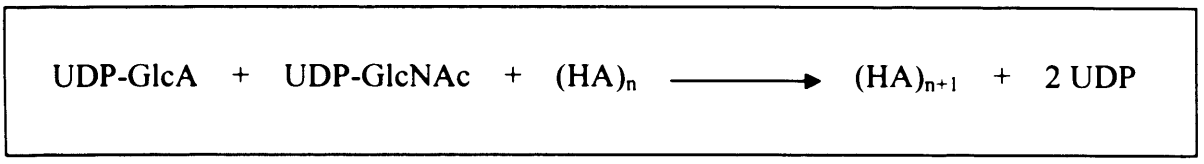

Figure 1.4. Overall reaction of HA synthesis by HAS. One HA disaccharide unit is added to the HA chain using the substrates uridine diphosphate glucuronic acid (UDP-GlcA) and uridine diphosphate N-acetylglucosamine (UDP-GlcNAc). The number of disaccharide units in the HA molecule is represented by n.

Although the synthase is only adding one HA disaccharide unit, it must exhibit six different functions to achieve this process. It requires two specific binding sites for the UDP-GlcA and UDP-GlcNAc sugar precursors and two different glycosyltransferase activities for the addition of the substrates to the HA chain by β-1,3 and β-1,4 linkages. It also requires a binding site that anchors the growing HA polymer to the enzyme and a ratchet-like transfer reaction that moves the growing polymer one sugar at a time [Weigel, 2004]. This later activity is likely coincident with the stepwise advance of the polymer through the membrane.

1.4.5 Functional relationship of the *HAS* genes *in vitro*

Expression of any one of the different human HAS isoforms can lead to HA synthesis, demonstrating that each isoform functions independently as a synthase. However, the rate of synthesis, and HA chain length differs for each isoform. HAS1 and HAS2 generate HA chains in excess of 1 x 10^6 Da, whereas HAS3 synthesises much smaller HA chains, in the region of 1 x 10^5 Da *in vitro*. The HA elongation rates of HAS1 and HAS2 are also significantly faster than that demonstrated by HAS3, however, HAS3 appears to be the most active [Itano et al, 1999]. HA chains of different lengths have been reported to have different effects on cell behaviour. Short HA chains have been

reported to stimulate cell proliferation and to initiate signalling cascades [Noble et al, 1996]. They may also be involved in angiogenesis and inflammatory responses [West et al, 1985]. It was originally thought that short HA chains were generated by the degradation of extracellular HA, for instance, through the action of the HYAL enzymes or oxidative species. The discovery that distinct HAS proteins synthesise short HA chains *in vitro* therefore adds another level of HA regulation [Spicer and Nguyen, 1999; Spicer and McDonald, 2000].

1.4.6 Functional relationships of the *HAS* genes *in vivo*

How the functional *in vitro* characteristics of the *HAS* genes translate to their functions *in vivo*, and relate to the various biological functions that have been reported for HA is the subject of ongoing investigation. Expression patterns of the *HAS* genes are different in embryonic development and in adult tissues [Spicer and McDonald, 1998]. Thus, promoter sequences and enhancer sequences have diverged substantially since this small gene family arose through gene duplication [Spicer and McDonald, 1998; Spicer and Nguyen, 1999]. However, it remains unclear as to whether or not the enzyme functions of the three HAS proteins have also diverged. Gene knockout studies in the mouse indicate that Has2 is essential for embryonic development. Mice deficient in this protein were not obtained because the mutation was lethal, with the embryos showing severe defects in the yolk sacs and cardiac development. In addition, they were almost entirely deficient in HA [Camenisch and McDonald, 2000]. Mice lacking Has1 and Has3 were however viable, underlining the importance of Has2 in embryonic development. The phenotypic effects of the Has1 and Has3 deficient mice are the subject of current investigation. It is possible that phenotypes may arise with age, for instance, relating to joint dysfunction, other skeletal disorders or immune-related dysfunction. In addition, there may be some degree of functional compensation built into this system [Spicer and McDonald, 1998].

1.4.7 Regulation of HAS and HA synthesis

HA is widely expressed throughout the human body, with varying amounts observed in different tissues (see section 1.2.2) and coincides with the differential tissue expression of the HAS enzymes [Spicer and McDonald, 1998]. Each HAS isoform

must therefore be under different mechanisms of transcriptional control depending on the tissue. More importantly, the control mechanisms of each HAS enzyme in one tissue, may not be the same in other tissues that demonstrate similar expression patterns.

Increased HA levels are observed in a number of disease states, including inflammation [Mohamadzadeh et al, 1998], wound healing, [Weigel et al, 1997; Knudson et al, 1989; Turley, 1989], renal injury [Strutz, 2001], atherosclerosis [Toole et al, 2002] rheumatoid arthritis [Laurent and Fraser, 1992] and cancer progression [Ropponen et al, 1998; Catterall et al, 1997; Setala et al, 1999]. Therefore, changes in HA metabolism must occur in order that this increased synthesis is brought about. In many situations, this is most likely to be two events occurring in parallel; an increase in the enzymatic activity and/or expression of the HASs that make HA, and a decrease in the enzymatic activity and/or expression of the HYALs that degrade it.

Prior to the identification of the mammalian *HAS* genes in 1996, laboratories were only able to record changes in HA levels. Increases in HA had been observed in many different cell lines after treatment with a variety of stimuli, many of which are now known to be involved in a number of the disease conditions stated above. These included PDGF [Heldin et al, 1992], TGF-β1 [Haubeck et al, 1995], IL-1 [Ito et al, 1993] TNF-α [Sampson et al, 1992], IFN-γ [Sampson et al, 1992] and even serum [Klewes and Prehm, 1994]. HA production had also been shown to be inhibited using such molecules as periodate-oxidised (po) UDP-GlcNAc and po-UDP-GlcA [Prehm, 1985], as well as colchicine and cytochalasin [Brecht et al, 1986]. Some of these reports demonstrated that the increases in HA production occurred in conjunction with a higher level of synthase activity, and deduced that this was due to newly synthesised enzymes in the plasma membrane [Ito et al, 1993; Klewes and Prehm, 1994]. However, they were not able to prove whether it was a direct consequence of an increase in HAS expression.

Since 1996, many reports have taken these findings a step further and demonstrated that many of the above factors that alter HA production also affect *HAS* gene expression. For instance, PDGF [Jacobson et al, 2000; Usui e al, 2000], TGF-β [Stuhlmeier et al, 2003; Usui et al, 2000], IL-1 [Ijuin et al, 2001; Kennedy et al, 2000;

Yamada et al, 2004], TNF-α [Ijuin et al, 2001; Kennedy et al, 2000; Ohkawa et al, 1999] and serum [Jacobson et al, 2000] have all been reported to increase expression levels of one or more of the *HAS* genes. In addition, many other stimuli have been discovered that also increase HA synthesis as a result of increasing *HAS* gene expression, including chorionic gonadotrophin [Stock et al, 2002], vasodilatory prostoglandins [Sussmann et al, 2004], keratinocyte growth factor [Karvinen et al, 2003], epidermal growth factor (EGF) [Pasonen-Seppänen et al, 2003; Pienimäki et al, 2001], osteogenic protein-1 [Nishida et al, 2000], retinoic acid [Sayo et al, 2002] and the ginsenoside, compound K [Kim et al, 2004]. HAS expression can also be directly inhibited by certain glucocorticoids [Stuhlmeier and Pollaschek, 2003], and high concentrations of the compound 4-methylumbelliferone [Kakizaki et al, 2004].

There are other reports (since the discovery of the HAS enzymes in 1996) that still show changes in HA levels that are independent of alterations in *HAS* expression. Endothelial cells from microvascular origin demonstrate increased HA synthesis after stimulation with TNF-α and IL-1 independent of increases in HAS expression [Mohamadzadeh et al, 1998]. In addition, HA synthesis can be inhibited by vesnarinone [Ueki et al, 2000] and moderate concentrations of 4-methylumbelliferone [Kakizaki et al, 2004] without altering HAS transcription patterns.

The regulation of HA synthesis can occur on many levels; 1) transcription of the *HAS* genes, 2) translation of HAS mRNA, 3) synthesis of the HAS enzymes, 4) insertion of the HAS enzymes into the plasma membrane, 5) activity of the active enzymes, 6) the availability of HA substrates, 7) at the breakdown/turnover of the HA chains and 8) the half-life of the active HAS protein. Difficulties arise in measuring the activity and turnover of the active HAS enzymes as an efficient method for their purification remains problematic. In addition, antibodies for the identification of the enzymes as a whole, or for those that distinguish between the different isoforms are currently unavailable. The mechanisms involved in the regulation of HA synthesis at the transcriptional level are also poorly understood. However, the techniques and resources are available to allow control of HA synthesis at this level to be investigated.

1.5 GENE EXPRESSION AND TRANSCRIPTIONAL REGULATION OF THE *HAS* GENES

1.5.1 Background

The eukaryotic cell is confronted with the challenge of properly regulating each of its tens of thousands of genes. When it is considered that each gene has its own unique expression program, it becomes evident that the control of gene activity requires an enormous amount of resources in terms of information (*i.e.* instructions for the regulation of each gene) and effectors (*i.e.* factors that mediate the gene expression programs). The most characteristic and fundamental requirement of gene control in multicellular organisms is the execution of precise decisions so that the right gene is activated in the correct cell at the required time, and in many genes, the regulation 'switch' is at the level of transcriptional initiation [Kadonaga, 2002; Lewin, 2000].

To date, very little work has been carried out on characterising the mechanisms involved in the expression of the *HAS* genes. The genomic structures for the mouse *Has* genes have been elucidated [Spicer and McDonald, 1998], and preliminary analysis of the murine *Has1* gene and promoter had been published [Yamada et al, 1998]. No work, however, had been carried out on the human forms of the *HAS* genes, and with growing evidence indicating their importance in disease, it poses an area of great interest.

1.5.2 Role of chromatin structure in gene expression

Within the eukaryotic nucleus, DNA is complexed with histones to form a polymer termed chromatin. The fundamental structural unit of chromatin is the nucleosome which consists of approximately 146 base pairs of DNA wrapped around an octamer of histones containing two copies each of four core histone proteins (H2A, H2B, H3 and H4) [Luger, 2003]. In addition to the four core histones, a fifth class of histone, the linker histone H1 associates with DNA between nucleosomes and may facilitate the formation of higher order chromatin organisation such as chromatin fibres [Hansen, 2002]. Packaging genomic DNA into chromatin therefore presents a

significant physical barrier for regulatory proteins such as transcription factors to access their DNA target sites [Felsenfeld and Groudine, 2003].

Unlike many transcription factors, some nuclear receptors are capable of binding to their hormone response DNA elements (HRE) embedded in chromatin [Urnov and Wolffe, 2001]. Upon ligand activation, nuclear receptors bind to HRE and recruit many transcriptional cofactors including chromatin remodelling factors to the target gene promoters. Two distinct classes of chromatin remodelling protein complexes have been identified. The first class are ATP-dependent complexes which are capable of directly changing the chromatin structure [Eisen et al, 1995]. They contain a core ATPase catalytic subunit that belongs to the SNF2/SWI2 family of DNA helicases. The second class of chromatin remodelling complex consists of the histone modifying enzymes including histone acetyltransferases, deacetylases, methyltransferases, kinases and ubiquitin ligases [Fischle et al, 2003]. The recruitment of these various cofactors instigates changes in the chromatin structure allowing other essential transcription factors to bind and activate or repress transcription [Acevedo and Krauss, 2004; Kinyamu and Archer, 2004].

1.5.3 Role of the promoter in constitutive gene expression

Core promoter region

The core promoter region encompasses the transcription initiation site (TIS) and typically extends approximately 50 bp upstream, to 40 bp downstream from it. The key function of the core promoter is to direct the initiation of transcription by the basal RNA polymerase II machinery. It is often incorrectly assumed that all core promoters are essentially the same. There is, in fact, considerable variability in the DNA elements that constitute core promoters. These elements include the TATA box, the TFIIB recognition element (BRE), the initiator (Inr) and the downstream promoter element (DPE). It is important to note that there are no universal core promoter elements. Each of these motifs is found only in a subset of core promoters [Kadonaga, 2002].

The TATA box was the first eukaryotic core promoter motif to be identified [Goldberg, 1979; Breathnach and Chambon, 1981] and is found in a high proportion of promoters. It is typically located approximately 25 to 30 nucleotides upstream of the TIS and its consensus sequence is TATAAA. At present, it is unknown if the promoters for each of the human *HAS* genes contain TATA box motifs. The murine Has1 promoter does not contain a TATA box [Yamada et al, 1998] and it is therefore highly likely, due to the high degree of sequence conservation between the two species, that the human HAS1 promoter does not contain this motif. Whether this proves to be the case for the HAS2 and HAS3 promoters remains to be determined.

In the absence of a TATA box, transcription initiation depends more heavily on other sites in order to recruit the RNA polymerase II machinery [Crawford et al, 1999]. The Inr element encompasses the TIS and has been identified in mammals, *Drosphilia* and yeast [Corden et al, 1980; Breathnach and Chambon, 1981; Hultmark et al, 1986; Struhl, 1987]. The DPE was first identified in a study of binding of purified *Drosphilia* TFIID to TATA-less core promoters [Burke and Kadonaga, 1996]. It is found most commonly in TATA-less promoters, although there are examples of promoters that contain both motifs [Kutach and Kadonaga, 2000]. It has also been reported to act co-operatively with the Inr element in binding the TFIID subunit of RNA polymerase II [Burke and Kadonaga, 1996]. The murine HAS1 promoter has not yet been analysed for the presence of these motifs. Whether the human HAS promoters also contain these elements is unknown.

Proximal promoter region

The proximal promoter region is defined as the DNA region directly upstream of the TIS. In many known genes, it extends approximately 300 bp upstream, however there is no truly defined size. Typically, they contain recognition sequences for other proteins (transcription factors) that are required for constitutive transcription of the gene of interest. Their purpose is to modulate transcription of the core promoter elements and act as transcriptional enhancers [Lewin, 2000]. Common examples of recognition sequences found in proximal promoters include GC boxes for the transcriptional factor family stimulating protein-1 (Sp1) and CCAAT boxes for nuclear factor-1 (NF-1) and nuclear factor-Y (NF-Y). The murine Has1 promoter

region contained a putative CCAAT box motif [Yamada et al, 1999], however its role in the transcription of the *Has1* gene is yet to be investigated. The presence of these sites in the human *HAS* gene promoters is unconfirmed.

1.5.4 Gene expression in response to external stimuli

Gene expression in eukaryotic cells can be altered in a semi-permanent way as cells differentiate, or in a temporary, easily reversible way in response to extracellular signals (inducible gene expression). Environmental cues such as the extracellular concentrations of certain ions, small nutrient molecules, temperature and shock can result in dramatic alteration of gene expression patterns. Changes in gene expression can also arise as a result of changes in cell signalling. This can take different forms, but the end point is always the same; a previously inactive transcription factor is specifically activated by the signalling pathway and then subsequently binds to specific regulatory sequences located in the promoters of target genes, thereby activating transcription [Strachan and Read, 2000].

A number of reports have illustrated the activation of certain signalling pathways by external stimuli that bring about changes in HAS expression. TGF-β has been shown to increase the transcription of *HAS1* in human fibroblast-like synoviocytes via the p38 mitogen activated protein (MAP) kinase pathway [Stuhlmeier and Pollaschek, 2004 (1); 2004 (2)] and *HAS2* in corneal endothelial cells via Smad signalling [Usui et al, 2000]. In addition, IL-1 has been reported to increase HAS2 expression in proximal tubular epithelial cells via NF-κB signalling [Jones et al, 2001]. These reports clearly show evidence of signalling pathways leading to increases in *HAS* transcription, but the mechanisms by which these pathways interact with the HAS promoters, and the transcription elements that are required remain a mystery.

1.6 AIM OF THESIS

1.6.1 Aim

The introduction had identified a role for HA in the pathological changes and inflammatory responses that occur in the early stages of renal fibrosis. As with many biological products the control of HA synthesis occurs at several levels. The aim of the thesis was to examine the mechanisms involved in controlling the transcription of the *HAS* genes. The first step was to reconstruct the genomic structures of the human *HAS* genes. A more detailed analysis of the HAS2 promoter was then carried out due to its reported involvement in a number of different disease conditions, and in particular, its upregulation in tissue injury in the kidney.

1.6.2 Scope of the thesis

Chapter 3 documents the reconstruction of all the human *HAS* genes using a variety of computational and laboratory-based methods. In addition, the proximal promoter region for each isoform was tested for transcriptional capability, and microsatellite markers for each gene were identified.

Chapter 4 details the repositioning of the TIS for the human *HAS2* gene. It also includes a more in-depth analysis of transcriptional activity of the HAS2 proximal promoter, and expression of the HAS2 message in a number of different cell lines.

Chapter 5 investigates the mechanisms involved for constitutive expression of the HAS2 gene. It details a closer investigation of the transcriptional activity of the HAS2 core promoter region, and identifies transcription factors required for HAS2 expression.

Chapter 6 documents the effects of IL-1β stimulation on the expression of the *HAS2* gene. This includes investigation into its effect on the HAS2 promoter, and the role of NF-κB in the IL-1β-induced expression of HAS2.

CHAPTER TWO

METHODS

2.1 COMPUTATIONAL-BASED METHODS

2.1.1 Genomic structure reconstruction

cDNAs for each human *HAS* gene had previously been elucidated. The sequences for *HAS1* (accession number NM_001523) [Shyjan et al, 1996], *HAS2* (NM_005328) [Watanabe et al, 1996], *HAS3* variant 1 (NM_005329) [Sayo et al, 2002; Spicer et al 1997] and *HAS3* variant 2 (NM_138612) [Sayo et al, 2002] were retrieved from the National Center for Biotechnology Information (NCBI) database at http://www.ncbi.nlm.nih.gov. Using the programs BLAST [Altschul et al, 1997] and BLAST2 [Tatusova et al, 1999] clones were identified in the high-throughput genomic sequences (HTGS) database, mapping to the relevant gDNA regions that covered the entire cDNA sequence for each gene. In addition, each clone contained >10kbp upstream of the transcription start sites for each isoform.

2.1.2 Determination of precise intron/exon boundaries

Precise locations of intron/exon boundaries were confirmed by comparison of the human sequences with their murine orthologues that had already been elucidated [Spicer and McDonald, 1998], and with the known 5' and 3' exon/intron splice site consensus sequences (Figure 2.1).

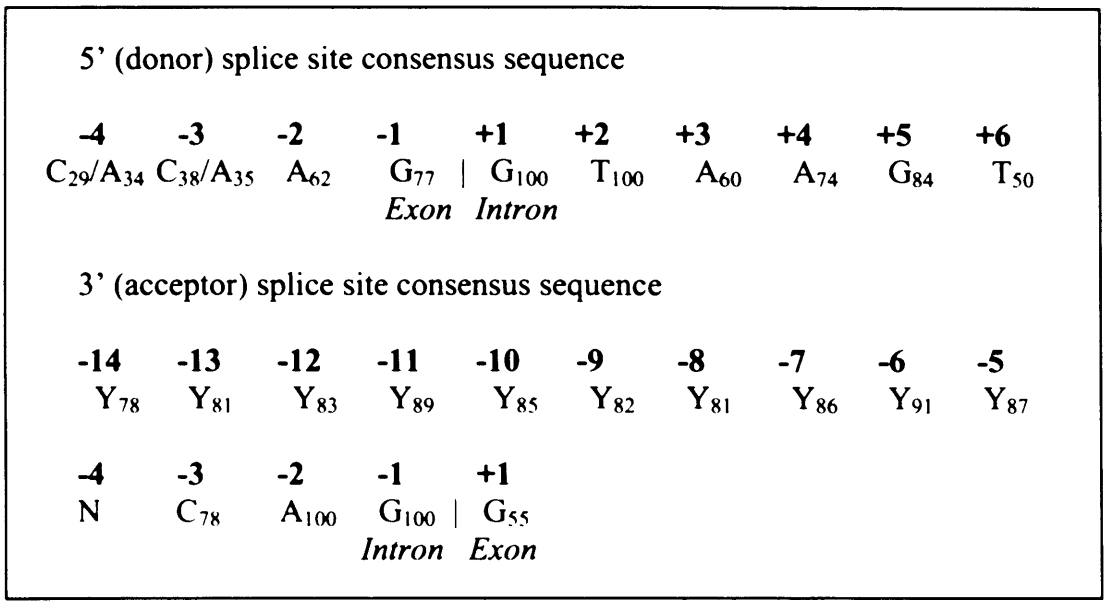

Figure 2.1. 5' and 3' splice site consensus sequences for intron/exon junctions. Bases are numbered relative to their position from the intron/exon boundary. Y indicates a pyrimidine base (C or T) and N represents any base (A, C, G or T). Subscript numerals refer to percentage frequency of occurrence [Krawczak et al, 1992].

2.1.3 Primer Design

All primers were designed using the Primer3 program at http://frodo.wi.mit.edu/cgi-bin/primer3/primer3_www.cgi and default parameters [Rozen and Skaletsky, 2000]. Most of the primers designed using this program had a GC content of 50-60 % and a T_M (annealing temperature) of approximately 60°C.

2.1.4 Alignment of HAS2 genomic sequences from different species

Alignments for the genomic sequences upstream of the *HAS2* genes from human, mouse, rat and horse were carried out using the ClustalW algorithm at the European Bioinformatics Institute (http://www.ebi.ac.uk/clustalw/index.html).

2.1.5 Identification of putative transcription factor binding sites in the HAS promoters

The proximal promoter region for each HAS isoform was screened for TFBSs using the MatInspector professional TFBS identification software [Quandt et al, 1995] at the internet-based Genomatix Suite (http://www.genomatix.de/cgi-bin/eldorado/main.pl), using standard parameters. The Chip2Promoter analysis program, also from Genomatix, was used for simultaneous comparative analysis to identify TFBSs common to 2 or more of the HAS proximal promoters.

2.1.6 Expressed Sequence Tag (EST) database analysis

BLAST and BLAT [Kent, 2002] analyses were used to compare the HAS2 sequences from human, mouse, rat, bovine and horse against expressed data in the EST database at NCBI (http://www.ncbi.nlm.nih.gov/blast/Blast.cgi) and the genome browser at the University of California Santa Cruz (UCSC) website (http://genome.ucsc.edu/).

2.1.7 RNA secondary structure prediction

The 5' untranslated region (UTR) for the human *HAS2* gene was examined for evidence of RNA secondary structure using software at the MFOLD web server (http://www.bioinfo.rpi.edu/applications/mfold) using default parameters.

2.2 CELL CULTURE

2.2.1 Cell lines and growth conditions

A variety of cell lines were used in this study. All cell lines were cultured in 75 cm^2 tissue culture flasks (unless stated) at 37°C in a humidified incubator (Cell House 170, Heto Holten, Derby, UK) with an atmosphere containing 5% CO_2. Medium was replaced with fresh growth medium every 3 to 4 days until the cells reached 100% confluence.

2.2.2 Human kidney (HK) 2 cells

HK-2 is a clonal cell line derived from the transformation of human proximal tubular cells with Human Papilloma Virus 16 E6/E7 genes but retains the functional characteristics of fully differentiated proximal tubular cells [Ryan et al, 1994]. HK-2 cells were purchased from American Type Culture Collection (Manassas, VA, USA) and grown in 1:1 mix of D-MEM:F-12 medium (Gibco/BRL Life Technologies Ltd., Paisley, UK) supplemented with 20 mM HEPES (Gibco), 2 mM L-glutamine (Gibco), 5 μg/ml insulin (Sigma, Poole, Dorset, UK), 5 μg/ml transferrin (Sigma), 5 ng/ml sodium selenite (Sigma) 400 ng/ml hydrocortisone (Sigma) and 10% foetal calf serum (FCS; Autogen Bioclear Ltd., Mile Elm, Calne, UK).

2.2.3 TE671 cells

TE671 cells were a gift from Dr. P. Buckland (Dept. of Psychological Medicine, Cardiff University, Cardiff, UK). This cell line is listed in the European Collection of Cell Cultures (ECACC) catalogue as a human medulloblastoma cell line, but is also known to be identical to the human rhabdomyosarcoma RD cell line. TE671 cells were cultured in the same growth medium as for the HK-2 cell line.

2.2.4 Human embryonic kidney (HEK) 293t cells

HEK293t cells are a transformed sub-line of HEK293, using the SV40 T antigen. This cell line was also a gift from Dr. P. Buckland. HEK293t cells were cultured in the same growth medium as for HK-2 cells.

2.2.5 Human lung fibroblasts

Primary human lung fibroblasts (AG02262) were purchased from Corriel Cell Repositories (Coriell Institute for Medical Research, NJ, USA). Fibroblasts were grown in D-MEM supplemented with 2mM L-glutamine, 20 mM HEPES, 100 μg/ml penicillin (Sigma) 100 μg/ml streptomycin (Sigma) and 10% FCS.

2.2.6 Human peritoneal mesothelial cells (HPMCs)

HPMCs were isolated from the greater omental tissue obtained from consenting patients undergoing abdominal surgery [Stylianou et al, 1990]. The patients were free from any sign of infection and/or malignancy and once removed the portion of omentum was kept in sterile PBS (Gibco) at 4°C for a maximum of 24 h before processing. Firstly, the tissue was washed in PBS at room temperature (RT) to remove any excess red blood cells. The tissue was then carefully cut into pieces of approximately 5 cm^2. The mesothelial cells were recovered from the tissue by a series of enzyme digests as follows.

The tissue was submerged in 15 ml of trypsin/EDTA (Gibco) diluted 1:1 with PBS. The tissue was incubated for 20 min at 37°C with continuous rotation. 15 ml of growth medium (M-199 (Gibco) supplemented with 2 mM L-glutamine, 5 μg/ml insulin, 5 μg/ml transferrin, 400 ng/ml hydrocortisone, 100 μg/ml penicillin, 100 μg/ml streptomycin and 10% FCS) was then added and the cells recovered by centrifugation at 800 x g for 5 min. This digestion process was then repeated. Following the second digestion, pelleted cells were resuspended in 5 ml growth medium supplemented with 10% FCS, and seeded into a 25 cm^2 tissue culture flask. The primary culture was incubated at 37°C with 5% CO_2 for 48 h, to allow viable cells to adhere to the flask and subsequently elongate. The medium was removed to a new 25 cm^2 culture flask to allow any remaining viable cells the chance to attach, while fresh medium was added to the original flask. Primary cultures were subsequently grown to confluence and passaged into 75 cm^2 flasks. The cells were then again grown to confluence, passaged, and grown to confluence once more prior to experimental use.

2.2.7 Sub-culture

Confluent cell monolayers for passage were sub-cultured using the following method. Growth medium was removed and followed by a single wash with 10 ml PBS. Cells were then treated with 10 ml trypsin/EDTA diluted 1:1 with PBS. After 5-10 min incubation at RT, cells were detached from the flask with gentle agitation. 5 ml FCS was added to neutralize the protease activity and the cell suspension was transferred

to a 50 ml centrifuge tube. The cells were pelleted by centrifugation at 2,500 rpm at 4°C for 7 min. After removing the supernatant, the cells were suspended in 45 ml fresh supplemented medium containing 10% FCS and seeded into three 75 cm^2 tissue culture flasks.

2.2.8 Serum starvation/growth arrest

Some of the experiments in this study required the cells to be in a state of growth arrest prior to use. The growth medium was removed and the confluent cell monolayers were washed twice with PBS. Fresh growth medium was then added containing no serum. The cells were then incubated for a further 48 hr at 37°C in the presence of 5% CO_2.

2.3 POLYMERASE CHAIN REACTION (PCR)

2.3.1 Primer reconstitution

PCR primers were designed using the Primer3 program as previously described and purchased from Invitrogen (Invitrogen, Paisley, UK). Upon arrival, lypholised primers were reconstituted in 200 µl H_2O, vortexed briefly then left to stand for 30 min at 4°C. Primer solutions were then vortexed briefly for a second time and collected by pulsing using a bench-top centrifuge. 5 µl of the primer solution was then diluted 1:80 with 395 µl H_2O, vortexed briefly, and 100 µl was used for spectrophotometric analysis to determine the concentration of the primer solution.

The concentration of the primer solution was calculated as follows:

Concentration (µM) = Absorbance (Abs) @ 260 nm x (nmol/OD) x dilution factor

Abs @ 260 nm – determined by spectrophotometer

nmol/OD – supplied with primer on data sheet

dilution factor - 80

Primers were then diluted to a stock concentration of 10 μM.

2.3.2 Generation of PCR fragments

One randomly selected gDNA sample (a gift from Dr. T. Bowen) was used for the amplification of each HAS exon (with flanking sequences) as well as the proximal promoter fragments. They were all amplified in a GeneAmp PCR system 9700 Thermocycler (PE Applied Biosystems, Beaconsfield, UK) using the following touchdown PCR program (unless stated). A denaturation step of 94°C for 5 min was followed by an initial cycle comprising of 30 s at 94°C, 30 s at a T_M of 60°C and 30 s at 72°C. T_M was reduced by 0.5°C per cycle for the next 10 cycles, remaining at 55°C for the concluding 25 cycles (Figure 2.2). Reactions were performed in a volume of 12 μl comprising 1 x PCR buffer containing 1.5 mM $MgCl_2$ (Qiagen, Crawley, UK), 40 ng of gDNA, 20 pmol of each primer, 100 μM dNTPs (Invitrogen) and 0.5 U of *Taq* polymerase (Qiagen).

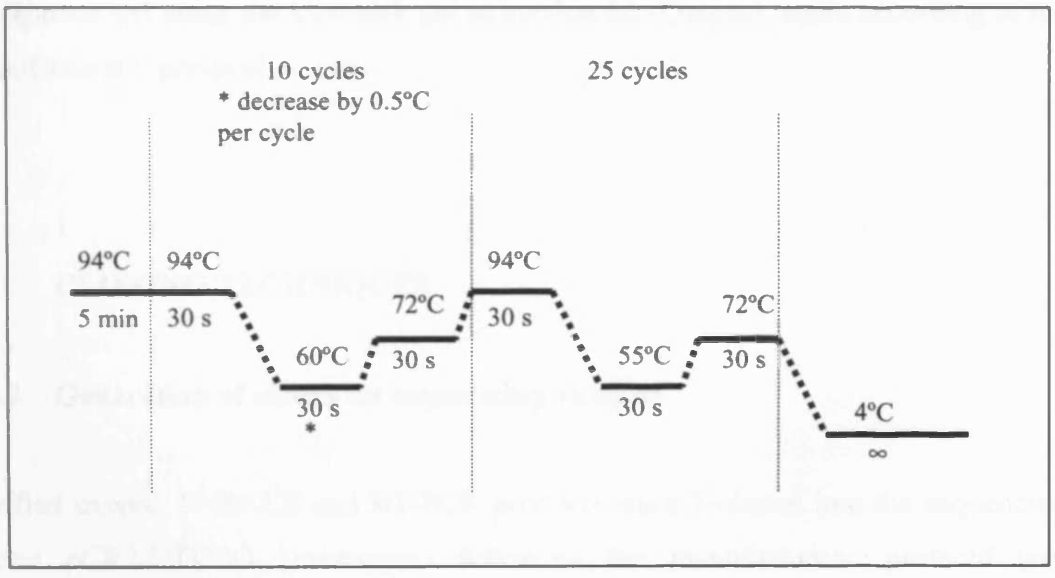

Figure 2.2. Schematic of touchdown PCR program used for the amplification of the HAS exons.

2.3.3 Sizing of PCR fragments

All PCR fragments were sized using submerged flat-bed electrophoresis. 5 µl of DNA loading buffer (H_2O containing 15% Ficoll Type 400 (Sigma), 0.25% Orange G (Sigma)) was added to each sample and mixed. Samples were then run through a 1.5% agarose gel (agarose purchased from Invitrogen) submerged in 1 x TAE buffer (Promega, Madison, WI, USA) at 90 v for approximately 90 min. PCR bands were then visualized under UV light by ethidium bromide (Sigma) staining using the Chemidoc apparatus (Bio-Rad, Hemel Hempstead, UK).

2.3.4 Purification of PCR fragments

PCR products were purified using the Qiaquick PCR purification kit (Qiagen) following the manufacturers' protocol with the following modification. Pure samples were eluted in 30 µl H_2O rather than 50 µl of TE buffer. When PCR reactions yielded more than one product, the band relating to the product of interest was excised from the agarose gel using the Qiaquick gel extraction kit (Qiagen), again according to the manufacturers' protocol.

2.4 CLONING TECHNIQUES

2.4.1 Generation of clones for sequencing analysis

Purified exonic, 5'-RACE and RT-PCR products were T-cloned into the sequencing vector pCR2.1/TOPO (Invitrogen) following the manufacturers' protocol (see appendix II for vector map). These were then transformed and amplified using the transformation procedure described in section 2.4.3.

2.4.2 Generation of luciferase constructs

Purified promoter fragments were cloned into a modified version of the pGL3-Basic luciferase reporter vector (Promega). The modified vector contained a *Kpn* I/*Hin* dIII

insertion from the pBluescript vector (Invitrogen) multiple cloning site (MCS) into the MCS of pGL3-Basic. The modified vector now contained a recognition site for the restriction endonuclease *Eco* RV, that cuts DNA producing blunt-ended products rather than sticky ends. The vector could therefore be used for T-cloning. The modified vector was gratefully provided by Dr. P Buckland. Appendix II shows a vector map of the modified vector (pGL3-Mod) including the original and altered sequences of the MCS.

Generation of proximal promoter constructs for each HAS enzyme

The HAS promoter constructs used in chapter 3 were designed using the following method. Proximal promoter fragments were T-cloned into pGL3-Mod. The pGL3-Mod T-vector was prepared as follows. 2 µg of the vector was digested with 5 U of *Eco* RV (NEB, Hitchin, Hertfordshire, UK) at 37°C for 2 h, in a reaction volume of 20 µl. After cleaning the digested product using the Qiaquick PCR Purification kit (section 2.3.4), thymine residues were added to each end using 5 U of Taq DNA polymerase (Qiagen) and 100 µM dTTP (Invitrogen) at 70°C for 2 h in a reaction volume of 100 µl.

5 µl of each PCR fragment was added to 1 µl of the prepared T-vector and ligated using 5 U of T4 DNA ligase (NEB) in a reaction volume of 10 µl overnight at 16°C.

Generation of nested HAS2 promoter constructs

The HAS2 promoter constructs used in chapters 4 and 5 were designed as follows. 5 µg of pGL3-Mod was digested with 5U of *Kpn* I (NEB) and 5 U of *Hin* dIII (NEB) and incubated at 37°C for 1 - 2 h. These enzymes both contained recognition sites within the MCS of pGL3-Mod, and were absent from the HAS2 proximal promoter region. The digested vector was then analysed by electrophoresis on 1.5% agarose before being extracted from the gel using the Qiaquick gel extraction kit (Qiagen) following the manufacturers' instructions. 2 µg of the digested product was treated with 2 U shrimp alkaline phosphatase (SAP - Promega) in a total volume of 30 µl and incubated at 37°C for 20 min. The sample was then heated to 65°C for 20 min to inactivate the SAP.

The nested HAS2 promoter fragments were amplified using sense strand primers tailed with a *Kpn* I site and a common antisense strand primer tailed with a *Hin* dIII site (see chapter 4.2 for primer sequences). PCR products were digested and gel extracted as described above before being cloned into the linearised, dephosphorylated pGL3-Mod vector in a reaction volume of 10 µl comprising 6 µl PCR product, 2 µl vector, 1 x ligase buffer and 5 U T4 DNA ligase. Samples were incubated at 16°C overnight.

2.4.3 Transformation

Ligated samples were transformed and amplified using JM109 *E. coli* competent cells (Promega). 40 µl cells (10^8 cfu/µg) were added to each sample and incubated on ice for 30 min. They were then subjected to heat-shock at 42°C for 90 s before being placed back on ice for a further 5 min. 150 µl SOC medium (Invitrogen) was then added, followed by incubation at 37°C for 90 min in an orbital shaker (200 rpm). Cells were then plated onto YT agar (Appendix I) containing 100 µg/ml carbenicillin (Sigma), and incubated at 37°C overnight.

2.4.4 Mini-prep

5 colonies per agar plate were grown in 5 ml YT broth (Appendix I) containing 100 µg/ml carbenicillin at 37°C for 8 h. Each culture was then screened for presence of the vector using the following mini-prep method. Cells from 1.5 ml of culture were pelleted by centrifugation at 13,000 rpm for 1 min. The excess medium was decanted leaving a residual volume of 50 - 100 µl. Pellets were resuspended by vortexing before the addition of 300 µl of TENS buffer (appendix I). The solutions were mixed by inversion, and incubated at RT for 5 min. 150 µl 2M sodium acetate (Sigma) was then added followed by centrifugation at 13,000 rpm for 4 min. Supernatants were transferred to a second vessel and 900 µl 100% ethanol (Sigma) was added. Samples were then centrifuged for a further 4 min at 13,000 rpm, followed by a second wash with 900 µl 70% ethanol. After a final centrifugation (same conditions as above), pellets were inverted and air-dried at RT, then resuspended in 20 µl of H_2O.

2.4.5 Screening of colonies for presence of inserts

5 µl mini-prep was then digested with the desired restriction enzymes (see Table 2.1 for enzymes used) to determine presence of cloned fragments. This was carried out in a reaction volume of 10 µl at 37°C for 1-2 h. Products were then sized on a 1.5% agarose gel. 1 µl ribonuclease A (10mg/ml – Invitrogen) was added to the DNA loading buffer to degrade the RNA in the preps. Colonies yielding vectors containing the desired inserts fragments were then re-picked and grown up in 5 ml YT broth as previously described. Cultures were then mini-prepped using the QiaSpin Mini-prep kit (Qiagen) following the manufacturers' protocol, with the following modification. Samples were eluted in 50 µl H_2O instead of the supplied TE buffer.

Proximal promoters	*HAS1* *HAS2* *HAS3* v1 *HAS3* v2	*Kpn* I *Eco* RI *Bam* HI *Sma* I
HAS2 promoter constructs	*Kpn* 1 and *Hin* dIII	
Exonic, 5'-RACE and RT-PCR fragments	*Eco* RI	

Table 2.1. Restriction endonucleases used to confirm successful generation of clones.

2.4.6 Sequencing analysis

All promoter, exonic, 5'-RACE and RT-PCR constructs were submitted for sequence analysis (The Sequencing Service, University of Dundee, Dundee, UK). This was to ensure the identity of the inserts and the fidelity of their amplification. Samples cloned into the pCR2.1/TOPO vector were sequenced using M13 forward and reverse primers (Table 2.2). Promoter constructs cloned into the pGL3-Mod vector were sequenced using the RV3 and GL2 primers (Table 2.2).

Primer	Sequence 5'-3'
M13-Forward	GTAAAACGACGGCCAG
M13-Reverse	CAGGAAACAGCTATGAC
RV3	CTAGCAAAATAGGCTGTCCC
GL2	CTTTATGTTTTTGGCGTCTTCC

Table 2.2. Oligonucleotide sequences of the primers used for sequence analysis. M13 forward (M13-F) and reverse (M13-R) primers were used to sequence fragments cloned into the pCR2.1/TOPO vector. RV3 and GL2 primers were used to sequence promoter fragments cloned into the pGL3-Mod vector.

2.5 LUCIFERASE ANALYSIS

2.5.1 HK-2 cells

Plate setup

HK-2 cells from a confluent 75 cm^2 flask were collected as previously described (section 2.2.7). After resuspension of the cells in 50 ml growth medium (supplemented with 10% FCS), they were plated out into 6-well plates, 2ml of the cell suspension per well. Cells were then grown to approximately 70% confluence prior to transfection.

Transfection

Transient transfection of HK-2 cells was performed using the mixed lipofection agent FuGene 6 (Roche, Lewes, East Sussex, UK). Initial characterisation experiments carried out by Fraser et al (2002) determined that a ratio of 3 µl FuGene to 1 µg DNA was optimal for transfection into HK-2 cells seeded in 6-well plates. With the cells at 70% confluence, the growth medium was removed and the cells were washed twice with PBS. They were then transfected with 1 µg of the required promoter construct, and 1 µg of the *Renilla* luciferase vector, according to the manufacturers' instructions.

The *Renilla* vector was used to determine transfection efficiency and to normalise the luciferase readings generated by the promoter constructs. The transfection was carried out in a low nutrient medium of a 1:1 mix of D-MEM:F-12 medium supplemented with 2 mM L-glutamine. 24 h after transfection the medium was replaced with fresh low nutrient medium for a further 24 h, containing additives as necessary for the experiment.

Reporter gene analysis

The growth medium was removed and the cells were washed once in PBS, before the addition of 500 µl of lysis buffer (Promega). The cells were then incubated at RT for 15 min with gentle agitation, to detach the cell monolayer. The remaining adhered cells were detached using a cell scraper, and the cell suspensions were transferred to 1.5 ml centrifuge tubes, followed by vortexing for 10 s. Luciferase activity was then measured using the Dual-Glo luciferase assay kit (Promega). 50 µl of each sample was transferred to a white 96-well luminometric plate. 100 µl of luciferase assay reagent II (supplied with kit) was added to each sample, and the luminescence of each sample recorded for 10 seconds using a luminometer (FLUOSTAR Optima, BMG Labtechnologies GmbH, Offenburg, Germany). Finally, 100 µl of Stop and Glo reagent (supplied with kit) was then added, and the luminescence of the *Renilla* luciferase in each sample was measured.

2.5.2 HEK293t and TE671 cells

Plate setup

An established luciferase reporter assay, as described by Coleman et al (2002), was also used to analyse promoter activity. Confluent monolayers of TE671 and HEK293t cells were collected as described in section 2.2.7. Pelleted TE671 cells were resuspended in 10 ml of growth medium supplemented with 10% FCS. 1.5 ml of this cell suspension was then added to a further 10 ml of supplemented growth medium. Cells were then seeded into a black, clear bottomed, 96-well luminometric plate, 100 µl per well. For HEK293t cells, the 96 well plates were first coated with poly-L-lysine (Promega) by adding 50 µl to each well. The solution was removed and the wells

were washed with 50 µl PBS. After air-drying the plates for 30 min, HEK293t cells were seeded as described for the TE671 cell line. Cells were then incubated until reaching approximately 70% confluence.

Transfection -TE671 cells

Each construct was assayed in multiples of 8. Once removing the growth medium, 100 µl Optimem medium (Gibco) was added per well comprising 500 ng Lipofectamine (Invitrogen), 2.25 µg Lipofectamine Plus reagent (Invitrogen), 100 ng promoter construct and 23 ng SPAP-CMV (secreted alkaline phosphatase) vector (a gift from Dr. P. Buckland). The SPAP-CMV vector was used to determine transfection efficiency and to normalise the luciferase data of the promoter constructs. Plates were then incubated for 24 h at 37 °C in the presence of 5% CO_2.

Transfection – HEK293t cells

Each promoter construct was again assayed in multiples of 8 for statistical significance. After removal of the growth medium, 100 µl of Optimem medium was added per well comprising 2 µg Lipofectamine, 100 ng promoter construct and 23 ng SPAP-CMV vector. Plates were then incubated for 24 h at 37 °C in the presence of 5% CO_2.

Post transfection – both cell lines

After 24 h incubation, the transfection solution was removed and the wells were washed once with 50 µl PBS. 100 µl of low nutrient growth medium (as used for HK-2 cells) was then added per well, and the plates were incubated for a further 24 h prior to luciferase assay.

Reporter gene analysis

13 µl of supernatant from each well was removed and used for the SPAP-CMV assay (Tropix, Bedford, MA, USA). Each 13 µl sample was transferred to a new 96-well black luminometric plate (with a black base). 50 µl of dilution buffer (supplied with

kit) was added to each well. The plates were then covered and incubated at 65°C for 30 min, after which they were placed on ice. 50 µl of phospha-assay buffer (supplied with kit) was added, and the samples were incubated at RT for a further 5 min. 50 µl of phospha-reaction buffer (also supplied) was then added to each well, and the samples were incubated for a further 15 min at RT in the dark. The luminescence of each sample was then measured; HEK293t samples were measured for 1 s and the TE671 samples for 10 s.

The luciferase activity of the promoter constructs was measured using the Bright-Glo luciferase assay kit (Promega). An additional 37 µl of supernatant from each well was removed and discarded. The transparent base of each plate was then covered with a non-transparent black adhesive film, and 50 µl of Bright-Glo assay reagent (supplied with kit) was added to each sample. Plates were incubated at RT in the dark for 10 min, after which the luminescence of each sample was recorded. As described above, the luminescence in each HEK293 sample was measured for 1 s and the TE671 samples for 10 s.

2.6 ANALYSIS OF *HAS* GENE MICROSATELLITE POLYMORPHISM

2.6.1 Identification and amplification of repeat sequences

Each human HAS gene was analysed for the presence of dinucleotide tandem repeat motifs (microsatellites) by visual inspection of the DNA sequences. Primers were designed to amplify one repeat motif unique to each *HAS* gene, the sense strand primer in each case 6-FAM-5'-end-labelled (Sigma). A pooled sample of 184 individual gDNA samples was used to analyse microsatellite polymorphism using the PCR conditions described in section 2.3.2 for each *HAS* gene. The same primers were then used in a second set of 48 separate PCR reactions for each isoform, using 48 individual gDNA samples to confirm the heterozygosity of the pooled sample. Products were then run and analysed on an ABI 3100 Genetic Analyser (PE Applied Biosystems).

2.7 RNA ANALYSIS

2.7.1 RNA extraction and quantification

Extraction

Total RNA was isolated from cell cultures using TRI reagent (Sigma). Confluent cell monolayers in 75 cm^2 culture flasks were lysed with 3 ml TRI reagent, before division of the lysate into 1 ml aliquots. 200 µl chloroform (Sigma) was added to each aliquot before mixing by inversion for 15 sec. Samples were incubated for 5 min at RT, then centrifuged with the brake off at 13,000 rpm for 15 min at 4°C. The aqueous layer (500 µl) was collected and an equal volume of isopropanol (Sigma) was added. Samples were then incubated at –20°C overnight then centrifuged at 13,000 rpm for 15 min at 4°C. The precipitated RNA was then washed with 1.5 ml 100% ethanol (Sigma), centrifuged (conditions as above), and the supernatant removed. This wash step was then repeated using 1.5 ml 70% ethanol. Samples were then air-dried for 1 h at RT before being resuspended in 20 µl double distilled H_2O by vortexing.

Quantification

The integrity of RNA was determined by flat-bed electrophoresis. 1 µl of RNA was run through a 3% agarose gel as previously described (section 2.3.3). The presence of two bands representing 18S and 28S subunits of ribosomal RNA indicated non-degraded RNA that could be used in further experiments.

Determination of RNA Concentration

The concentration of RNA was determined by spectrophotometric analysis using a Beckman DU 64 single beam spectrophotometer (Beckman Instruments, High Wycombe, UK). 1 µl RNA was diluted in 55 µl H_2O. Absorbance readings at 260 nm and 280 nm were taken. A 260/280 ratio of 1.7 or higher indicated a sufficiently pure sample. The concentration was then calculated using the following equation:

RNA conc (μg/ml) = Abs_{260} x Molar extinction coefficient x Dilution factor

Molar extinction coefficient for RNA = 40

Dilution factor = 55

2.7.2 Purification of messenger RNA (mRNA) from total RNA

mRNA was purified from 75 μg of total RNA using Oligo $(dT)_{25}$ Dynabeads (Dynal, Bromborough, Wirral, UK) following manufacturers' instructions. This typically yielded between 3 and 4 μg of mRNA diluted in 15 μl H_2O.

2.7.3 Primer extension

Primer extension was carried out on mRNA from HK-2 cells using the AMV Reverse Transcriptase Primer Extension Kit (Promega). HAS2-specific RNA primers (Table 4.1) were radiolabelled with 10 mCi/ml γ-^{32}P ATP (Amersham Biosciences, Chalfont St. Giles, Buckinghamshire, UK) following the manufacturers' protocol. 1 μg of purified mRNA was then used in each primer extension reaction as per manufacturers' instructions. Products were analysed on a 18 cm x 18 cm denaturing polyacrylamide gel containing 8% acrylamide (19:1 acrylamide:bis – Sigma), 7M urea (Sigma) and 1 x TBE buffer (Appendix I). Gels were run in 1 x TBE buffer at 250 V for approximately 8 h, after which they were wrapped in plastic film, and exposed to x-ray film (Hyperfilm MP, Amersham) overnight at -70°C. Films were then developed the next day.

2.7.4 5'-Rapid amplification of cDNA ends (5'-RACE)

First strand synthesis

Purified mRNA was used for 5'-RACE analysis using the SMART RACE kit (BD Biosciences Clontech, Cowley, Oxford, UK). 1 μg of mRNA was combined with 1 μl of 5'CDS primer and 1 μl of the SMART II^{TM} oligo (both supplied with kit) and incubated for 2 min at 70°C. Tubes were cooled on ice for a further 2 min, followed by the addition of the reaction mix. This comprised of 2 μl of 5 x first strand buffer, 1

µl 20 mM dithiothreitol (DTT), 1 µl 10mM dNTPs and 1 µl PowerScript™ reverse transcriptase (all supplied with RACE kit). Samples were then incubated for 42°C for 90 min followed by the addition of 20 µl Tricine-EDTA buffer (supplied). Samples were stored at –20°C until needed.

PCR

The generated cDNA was then amplified by PCR using the Advantage 2 PCR Kit (BD Biosciences Clontech). 2.5 µl of cDNA was amplified in a total volume of 50 µl according to the manufacturers' instructions with the RACE primer (see Table 4.1) using the following touchdown PCR program. A denaturation step at 94°C for 7 min was followed by 15 cycles comprising of 94°C for 1 min, 64°C for 1 min (this was decreased by 2°C every five cycles) and 72°C for 3 min. This was followed with 10 cycles comprising of 94°C for 1 min, 58°C for 1min and 72°C for 3 min. The reaction was concluded with a final extension step of 72°C for 10 min. The product generated was then used as a template in a nested PCR reaction using the RACE-N primer (table 4.1), using the same touch-down program as described above. Products were analysed on a 2% agarose gel by flat-bed electrophoresis.

2.7.5 Reverse transcription polymerase chain reaction (RT-PCR)

cDNA synthesis

Reverse transcription was carried out with 1 µg total RNA in a total volume of 20 µl comprising 100 µM random hexamers (Amersham), 5 mM dNTPs, 1 x PCR containing 1.5 mM $MgCl_2$ (PE Applied Biosystems) and 1 mM DTT (Invitrogen). The solution was heated to 95°C for 5 min followed by 4°C for 2 min. 40 U recombinant RNAsin ribonuclease inhibitor (Promega) and 200 U Supersricpt II Rnase H^- reverse transcriptase (Invitrogen) were then added. The solution was heated to 20°C for 10 min, 42°C for 60 min, 95°C for 5 min, and 4°C for 2 min. cDNA was stored at -20°C until needed.

PCR

2 µl of cDNA generated in the above method was used per 50 µl PCR reaction comprising of 1 x PCR buffer containing 1.5 mM $MgCl_2$ (PE Applied Biosystems), 5mM dNTPs, 2.5 U Amplitaq Gold *Taq* polymerase (PE Applied Biosystems) and 1mM of each primer. Cycling conditions were as follows. A denaturation step at 94°C for 2 min was followed by *n* cycles (26 for β-actin, 38 for HAS2) comprising 94°C for 30 s, 65°C for 30 s and 68°C for 90 s. Cycling was then followed by a final extension step at 68°C for 15 min (Figure 2.3). Reaction products were analysed on 1.5% agarose by flat-bed electrophoresis as previously described (section 2.3.3).

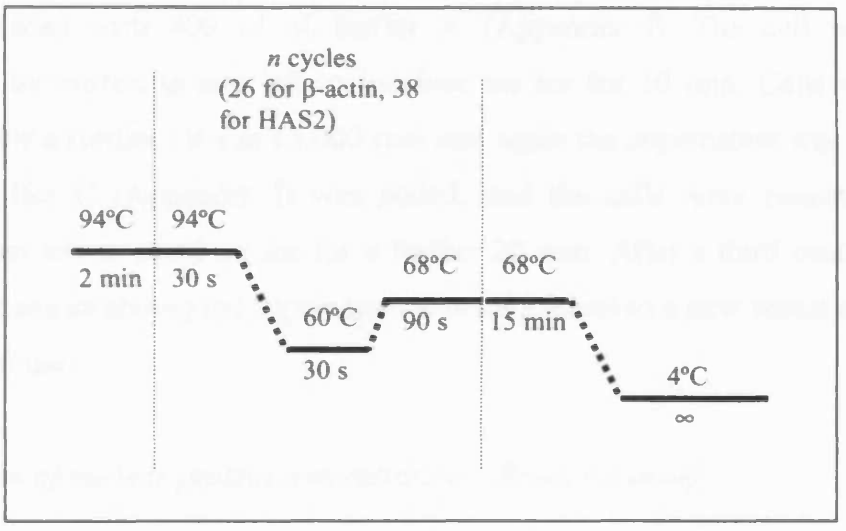

Figure 2.3. Schematic of the PCR cycling program used in RT-PCR experiments. The number of cycles (n) for β-actin and HAS2 are given.

2.8 ELECTRO-MOBILITY SHIFT ASSAY (EMSA)

2.8.1 Nuclear protein extraction and quantification

Preparation of cells

Nuclear protein was extracted from confluent 75 cm^2 flasks of TE671 and HK-2 cells. The cells were treated in the same way as prepared for the luciferase assays for

HEK293t and TE671 cells. At 70% confluence the growth medium was removed and replaced with 10 ml Optimem. This was left on the cells for 24 h, before being removed and replaced with 10 ml of low nutrient growth medium. A further 24 h later this was removed and the nuclear protein was extracted using the method described below.

Protein extraction

1.5 ml of ice cold PBS was added to each culture flask. Cells were then detached from the base of the flask by scraping. The cell-PBS suspension was then transferred to a 1.5 ml centrifuge tube and centrifuged for 10 s at 13,000 rpm. The PBS was aspirated off and replaced with 400 µl of Buffer A (Appendix I). The cell pellet was resuspended by vortexing and left to incubate on ice for 10 min. Cells were then centrifuged for a further 10 s at 13,000 rpm and again the supernatant was removed. 50 µl of Buffer C (Appendix I) was added, and the cells were resuspended by vortexing then left to stand on ice for a further 20 min. After a third centrifugation (same conditions as above) the supernatant was transferred to a new vessel and stored at –70°C until use.

Determination of nuclear protein concentration – Bradford assay

The Bradford dye binding assay was used to quantify nuclear protein extract concentrations. A standard curve of bovine serum albumin (Sigma) was prepared fresh for each assay, range 31.25 – 2000 ug/ml. Protein extracts were diluted 1:4 with buffer C so that their concentration fell within the range of the standards. 5 µl of each diluted sample was added in triplicate to a clear 96 well assay plate. 100 µl of Bradford reagent (Bio-Rad) was then added to each well and the absorbances at 595 nm taken immediately in a plate reader (FLUOSTAR Optima).

2.8.2 Probe preparation

Complementary single-stranded oligonucleotides were purchased from Invitrogen. Each contained a CGA sequence tagged on at the 5' end, which when annealed to its

complementary sequence created a three base overhang. The overhangs were then filled in using the Klenow reaction and a radiolabelled nucleotide (Figure 2.4).

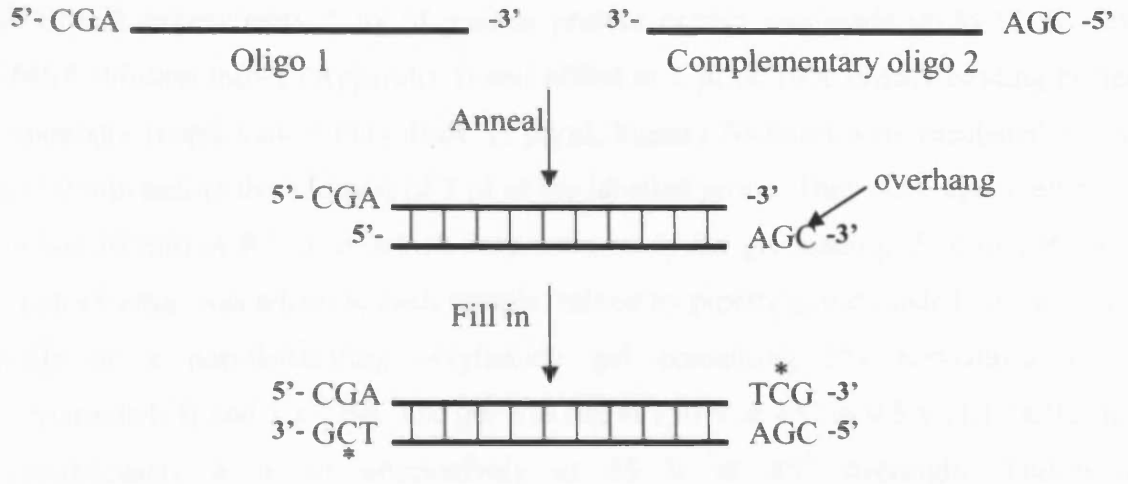

* labelled nucleotide

Figure 2.4. Generation of labelled DNA probes for EMSA experiments. Complementary oligonucleotide sequences were annealed and then end-labelled using the Klenow reaction.

1 µg of each oligonucleotide pair were annealed in 100 µl containing 1 x buffer 3 (NEB), at 100°C for 10 minutes. After boiling, samples were left to cool down for 1 h at RT. Probes were then labelled using the MegaPrime DNA labelling kit (Amersham) as follows. 25 ng of probe was labelled in a reaction volume of 50 µl containing 10 µl of labelling buffer, 2 µl of Klenow DNA polymerase, and 3 µl of 10 mCi/ml ^{32}P dCTP (Amersham). This was incubated for 15 min at 37°C followed by the addition of 5 µl 0.2M diaminoethanetetra-acetic acid (EDTA; Sigma)) to stop the reaction. Probes were then purified using ProbeQuant G-50 Micro Columns (Amersham) following the manufacturers' protocol.

2.8.3 EMSA binding reaction

The Hoefer SE 400 vertical slab gel electrophoresis system (Amersham) was used for all EMSA experiments. 5 μg of nuclear protein extract was made up to 13 μl with EMSA dilution buffer (Appendix I) and added to 2 μl of 10 x EMSA binding buffer (Appendix I) and 3 μl of Poly dI/dC (1 μg/μl, Sigma). Samples were incubated on ice for 10 min before the addition of 2 μl of the labelled probe. They were again left for a further 20 min at RT, after which they were ready for gel loading. 5 μl of 20% w/v Ficoll (Sigma) was added to each sample, mixed by pipetting and loaded into separate wells of a non-denaturing acrylamide gel containing 5% acrylamide (29:1 acrylamide:bis) and 1 x TBE. The gel was run at 150 V at 4°C in 0.5 x TBE buffer for approximately 4 h, or alternatively at 55 V at 4°C overnight. Following electrophoresis, the gel was carefully transferred onto 3mm filter paper (Whatman International, Maidstone, Kent, UK) and dried on a gel drier (model 543, Bio-Rad) at 80°C for 45 min. The dried gel was then exposed to x-ray film (Hyperfilm MP) at -70°C overnight and subsequently developed.

2.8.4 Competition EMSA

Demonstration that an excess of unlabelled probe of the same sequence as the radiolabelled probe prevents retardation by nuclear protein further suggests that the observed interactions are specific. Similarly, use of a different sequence in excess should not interfere with probe retardation. Competition EMSAs were therefore carried out using a 100-fold excess of the desired unlabelled probes. 5 μl of the desired unlabelled probe (20 ng/μl) was added to 5 μg of nuclear protein and the volume was made up to 13 μl with EMSA dilution buffer. The competition EMSA was then carried out as described above for the EMSA binding reaction (section 2.8.3).

2.8.5 Supershifts

Supershifts were carried out using antibodies specific to the proteins identified that were binding to the radiolabelled probes. 10 μg of the desired antibody (purchased

from Santa Cruz Biotechnology Inc., Santa Cruz, CA, USA) was incubated with 5 μg of nuclear protein for 20 min at RT prior to the addition of the radiolabelled probe, as described in section 2.8.3. Samples were then run down a 4% non-denaturing acrylamide gel at 150 V for 6 h at 4°C. Gels were then dried and exposed as previously described (section 2.8.3).

2.9 SYNTHESIS OF MUTATED PROMOTER CONSTRUCT

2.9.1 Template preparation

Two complementary oligonucleotides containing the mutated Sp1 binding sites of the HAS2 promoter (Table 2.3) were designed and purchased from Sigma. The 44 nucleotides at the 3' end of the sense strand oligonucleotide were complementary to the 44 nucleotides at the 3' end of the antisense strand nucleotide (for sequences see table 2.3). 1 μg of each oligonucleotide was diluted in 5 μl of H_2O, mixed together and annealed in a 100 μl reaction containing 10 μl 10 x buffer 3 (NEB) and 80 μl of H_2O. After boiling the mixture in a water bath for 10 minutes, the water bath was turned off, and the mixture was left to cool to until the water bath temperature reached RT. The 5' overhangs (65 bp at each end) of the annealed product were then filled in using the Klenow polymerase reaction (Megaprime kit, Amersham). 2.5 μl of the annealed product was added to 10 μl reaction buffer, 2 μl Klenow polymerase (both supplied with kit), 5 μl 0.5 mM dCTP (Invitrogen) and 80 μl H_2O. The mixture was incubated for 1 h at 37°C to generate the full-length double-stranded template. Finally, the product was purified using ProbeQuant G-50 Micro Columns as described in section 2.8.2.

2.9.2 Amplification of mutated and wildtype promoter sequences

The purified template was then used in a PCR reaction to amplify the full-length mutated promoter fragment. In addition, a non-mutated, wildtype promoter fragment of the same length was generated using gDNA as a template. The PCR reactions were carried out in a reaction volume of 15 μl comprising 6 μl of template, 1 x PCR buffer

containing 1.5 mM $MgCl_2$ (PE Applied Biosystems), 5mM dNTPs, 2.5 U Amplitaq Gold *Taq* polymerase (PE Applied Biosystems) and 1mM of each primer (purchased from Sigma – Table 2.3). Samples were then run using the following touchdown reaction. A denaturation step of 94°C for 5 min was followed by an initial cycle comprising of 30 s at 94°C, 30 s at a T_M of 65°C and 30 s at 72°C. T_M was reduced by 0.5°C per cycle for the next 10 cycles, remaining at 60°C for the concluding 25 cycles. Products were then sized using flat-bed electrophoresis as described in section 2.3.3.

Name	Oligonucleotide sequence
HAS2 mut-prom-F	AGCTCAGAGAAGGCTTTGAATGGCCAATTTCTCTCTCTCC TTCTCCACTAACCCGACTCCCGCTCTACCAACCTACCGCG CTCCCAGTTCCATACCCTCAGGGTTCCCC
HAS2 mut-prom-R	GGGTGTTTTAATAGGGCGGCGGAGGGAGTGGGGGGGTGAG GGAAGTGGAGAGGGAGGTGTGGACTGGGGAACCCTGAGGG TATGGAACTGGGAGCGCGGTAGGTTGGTA
HAS2-long-F3-F	CCGGTACCGAACCGGCCTGTAGCTCAGAGAAGGCTTTGAA
HAS2-long-F3-R	CCAAGCTTAAGTGAGCTGGTGGGTGTTTTAATAGGGCGGC

Table 2.3. Sequences of the oligonucleotides used to generate the mutated and wildtype HAS2 core promoter fragments. HAS2-mut-prom-F and -R were used to make the template used to generate the mutated fragment. HAS2-long-F3-F and –R were used to amplifiy the mutated and wildtype fragments by PCR. Mutated nucleotides are indicated in red.

CHAPTER THREE

RECONSTRUCTION OF THE HUMAN HYALURONAN SYNTHASE GENES

3.1 INTRODUCTION

Under normal conditions, HA can be found in the inner medulla and papilla of the kidney, with very little present in the outer medulla or the cortex [Hällgren et al, 1990]. It is well known however, that HA accumulates in the cortex in inflammatory diseases, including crescentic glomerulonephritis [Nishikawa et al, 1993; Jun et al, 1997], tubulointerstitial injury [Sibalic et al, 1997] and allograft rejection [Wells et al, 1990; 1993]. The mechanisms responsible for this accumulation however, are poorly understood.

Previous reports from this and other laboratories have demonstrated that in certain disease conditions and in particular during the processes of wound healing, increased HA synthesis is accompanied by an increase in the expression of the *HAS* genes. For example, in an *in vitro* model of diabetic nephropathy, treatment of human proximal tubular cells (HPTCs) with high levels of glucose increases the expression of HAS2 through an NF-κB dependent process [Jones et al, 2001]. In addition, scratch-wound studies using skin keratinocyte monolayers show an increase in HA following an upregulation of *HAS2* transcription [Pienimäki et al, 2001; Pasonen-Seppänen et al, 2003].

Increased HA levels are also observed during episodes of peritonitis. The peritoneal membrane forms the barrier across which solute transfer occurs in patients treated for chronic renal disease with peritoneal dialysis. The mesothelium plays a pivotal role in the response of the peritoneum to inflammation and tissue injury, maintaining peritoneal homeostasis via processes such as leukocyte trafficking and host defence [Topley et al, 1996; Topley and Williams, 1994; Yung et al, 1995; Yung and Davies, 1996]. During episodes of peritonitis which occur as a result of poor aseptic technique, levels of HA in the peritoneal fluid increase [Yung and Davies, 1996]. Reports from this laboratory have demonstrated that mechanical injury to HPMC monolayers *in vitro* leads to an upregulation of HA synthesis which follows a specific upregulation of *HAS2* transcription [Yung et al, 2000]. This provides further evidence suggesting that in certain cellular systems HA production may be specifically controlled at the transcriptional level of the genes encoding the HAS enzymes.

At the beginning of this study, little was known about the genomic organisation and transcriptional control of the human *HAS* genes. However, the genomic organisation of the corresponding mouse *Has* orthologues had been described, together with *in vitro* and *in vivo* functional studies [Spicer and McDonald, 1998]. In order to better understand the function and transcriptional regulation of the human *HAS* genes in both renal and peritoneal injury, the genomic structures for all four HAS isoforms were first reconstructed using a number of *in silico* techniques. These findings were then confirmed experimentally and were compared with their murine *Has* orthologues. The proximal promoter sequences for each *HAS* gene were identified and tested for their ability to drive transcription. The proximal promoters were also analysed for the presence of putative transcription factor binding sites (TFBSs). Finally, intragenic or proximal dinucleotide microsatellite sequences were identified for each HAS isoform and analysed for polymorphism.

3.2 METHODS

3.2.1 *in silico* reconstruction of human *HAS* genes

The genomic structures of the human *HAS* genes were reconstructed by combining a variety of *in silico* methodologies discussed in sections 2.1.1 and 2.1.2.

3.2.2 Primer design

Primer sequences used for the amplification of HAS exons plus their flanking sequences, promoter fragments, and microsatellites are listed in table 3.1.

Genomic *in silico* data was used to design PCR primers for the individual HAS1, HAS2, and HAS3 exons plus flanking sequences. HAS2 exon 4, and HAS3v1 exon 4 were amplified in two segments, *a* and *b*. This was for ease of amplification as both exons were greater than 2000 bp in length.

Primers were also designed to amplify approximately 500 bp upstream of each HAS exon 1. In all but one case, the antisense strand primer was designed to include the transcription start site and any downstream promoter elements but not ATG triplets which might falsely prime translation [Coleman et al. 2002]. To compensate for the ATG eight nucleotides from the transcription start site of HAS3v2 exon 1, a non-homologous trinucleotide was added to the antisense strand primer (shown in red in Table 3.1) to produce a stop codon after amplification and thus terminate any spurious translation products initiated from this site.

Gene	Amplified regio	Sense strand primer	Antisense strand primer	Predicted size
HAS1	Exon 1	CTGCGCTGGTCTTCAAATG	TCACTGTCAGGCACATGGAT	249
	Exon 2	GGGAAGGAAGGAAAGGATTTT	GGAAAGTGGGATTTGGGTGT	838
	Exon 3	CCTTCCTCTCAAGCATCAGC	TTTCCACCCCATCCACAG	335
	Exon 4	AGCATTGGAGTTGGTGTTGG	TTCATTGGCCTCCACACATA	244
	Exon 5	CATTTCTGCCTCCAGAATCC	TCCCCAATTCTCAATCATCC	1120
	Promoter	GAGGAGGCAAGAGAAGTGGA	GCGCAGTGGGTCTGGCCGGGCTCTCTCTT	570
	Microsatellite	CCCAGCTTAGCCTGACTGAC	TCACGTCAGGCACATGGAT	293
HAS2	Exon 1	AAAACACCCACCAGCTCACT	GGCCTGTTGGAGGACCTT	665
	Exon 2	CAAGTGTGGGACAATCATGG	GTTTGCCCTGGCAGGAAT	709
	Exon 3	TGAAATTTTGACTACAGGGAATG	ACAACAACACCTGGCACAGA	296
	Exon 4a	CAGGATGGAACAGGTTTTGC	GGCATTATCTGATGCCACAA	1084
	Exon 4b	TCATGCTTTTGACGCTGTATG	TGGCCTTGATTTTCAACGAT	966
	Promoter	TTACTTAGCTGAAGGGCACCAT	GCTGTTTCAAGTCTCTGGTTC	555
	Microsatellite	CCTTTCTGGGGACACAGGTA	AGTAAAACGCGCTGGGCTAT	242
HAS3 v1	Exon 1	GACTGGGATCCCTTGGGTTTTC	CCTGCATCCGCAGCCTAGGAG	323
	Exon 2	ACTGGAAATGCTGCCTCCT	CACAACCCAAGGGACCTAGA	794
	Exon 3	TGAGGTCAGAATGGGCTGA	CATTTCCCAGGCATATCCAA	218
	Exon 4a	GCCTCGTGGTCTCTGATGTC	ATTCCCCTTCCCTCCCTTAC	1051
	Exon 4b	GTGGCCCTCCTCATGCTAT	GTCCCTCTTTGGAAACTGGA	2548
	Promoter	TCAAAGTTTCGGAGGCTTGATGGAGAA	GCCAAGGCCAGCCAGCAAC	703
	Microsatellite	GGTCACTTACAAGCAGCCAGT	GAAGAGAAGCCAGAAATCCAG	188
HAS3 v2	Exon 1	CCCTCCCACTCTGGTCAACT	GAGGCTGGAAGAGGAGAGGATGC	457
	Exon 4	TCAAGCAGAAACTGCATTCG	GAATGTTGCCCCCTTAAACA	585
	Promoter	TTCTCTTCAGCGCCTCTTTC	CCTCAGGCCCGCGGCGGCTCCAT	629

Table 3.1. Oligonucleotide sequences in 5'-3' orientation for the amplification of human HAS exons, proximal promoters and microsatellites. Predicted sizes for PCR products are given. The changed nucleotides in the HAS3v2 antisense strand primer sequence (to produce a stop codon) are indicated in red.

3.2.3 Amplification and analysis of HAS exons

HAS exons were amplified and sized by agarose gel electrophoresis as discussed in section 2.3. They were then cloned into vector pCR2.1/TOPO (sections 2.4.1, 2.4.3 and 2.4.4), and their identity confirmed by sequencing with M13 forward and reverse primers (Invitrogen) as explained in section 2.4.5.

3.2.4 Amplification and analysis of HAS proximal promoter transcriptional activity *in vitro*

HAS promoters were amplified and sized by gel electrophoresis as discussed in section 2.3. These were then T-cloned into vector pGL3-Mod (section 2.4.2), and clones were screened for presence of the required promoter fragments using enzyme digestion (sections 2.4.3 and 2.4.4) followed by sequencing (section 2.4.5). Luciferase assays were carried out in HK-2 cells as explained in section 2.5.1, and in TE671 and HEK293t cells as described in section 2.5.2.

3.2.5 *in silico* analysis of proximal promoters for TFBSs

Each HAS proximal promoter was analysed individually for putative TFBSs, and the promoters were then compared for TFBSs common to more than one isoform, as described in section 2.1.5.

3.2.6 Identification of polymorphic microsatellite sequences proximal to each *HAS* gene

Dinucleotide tandem repeat CA/GT motifs within, or proximal to, the three *HAS* loci were located by visual inspection of sequence data. PCR amplification was carried out as for the HAS exons (section 2.3) using primers shown in Table 3.1. Each sense strand primer was labelled with 6-FAM at the 5' end. A pooled sample of 184 individual gDNA samples was used to analyse microsatellite polymorphism [Kirov et al. 2000]. Genotypes from a sample of 48 individual gDNAs were then used to estimate allele frequencies, and an established pedigree used to confirm stable

Mendelian microsatellite inheritance [Williams et al. 1999] as described in section 2.6.

3.3 RESULTS

3.3.1 *in silico* reconstruction of the human *HAS* genes

The accurate computational prediction of the genomic structures of eukaryotic genes and identification of their promoters by algorithmic means remains problematic. Using a combination of *in silico* and *in vitro* methodologies, the human *HAS* genes were reconstructed. The HAS reference cDNAs were compared with the high-throughput genomic sequences available via the NCBI database (http://www.ncbi.nlm.nih.gov). From these findings the putative genomic structures were reconstructed, together with their upstream proximal promoter regions. Table 3.2 details the predicted size of each human HAS genomic component. Figure 3.1 shows schematic representation of each human HAS genomic structure.

Gene	5'-UTR	Exon 1	Intron 1	Exon 2	Intron 2	Exon 3	Intron 3	Exon 4	Intron 4	Exon 5	3'-UTR	gDNA	cDNA
HAS1	35	44	4026	693	2012	226	579	133	2153	991	315	10857	2087
HAS2	538	538	11512	627	11507	102	2066	1739	N/A	N/A	809	28091	3006
HAS3 v1	156	156	1700	636	3409	102	800	3326	N/A	N/A	2402	10129	4220
HAS3 v2	60	60	3079	636	3409	102	4812	360	N/A	N/A	252	12458	1158

Table 3.2. Predicted sizes (bp) of exons, introns, UTRs, cDNA and gDNA distances for the human *HAS* genes.

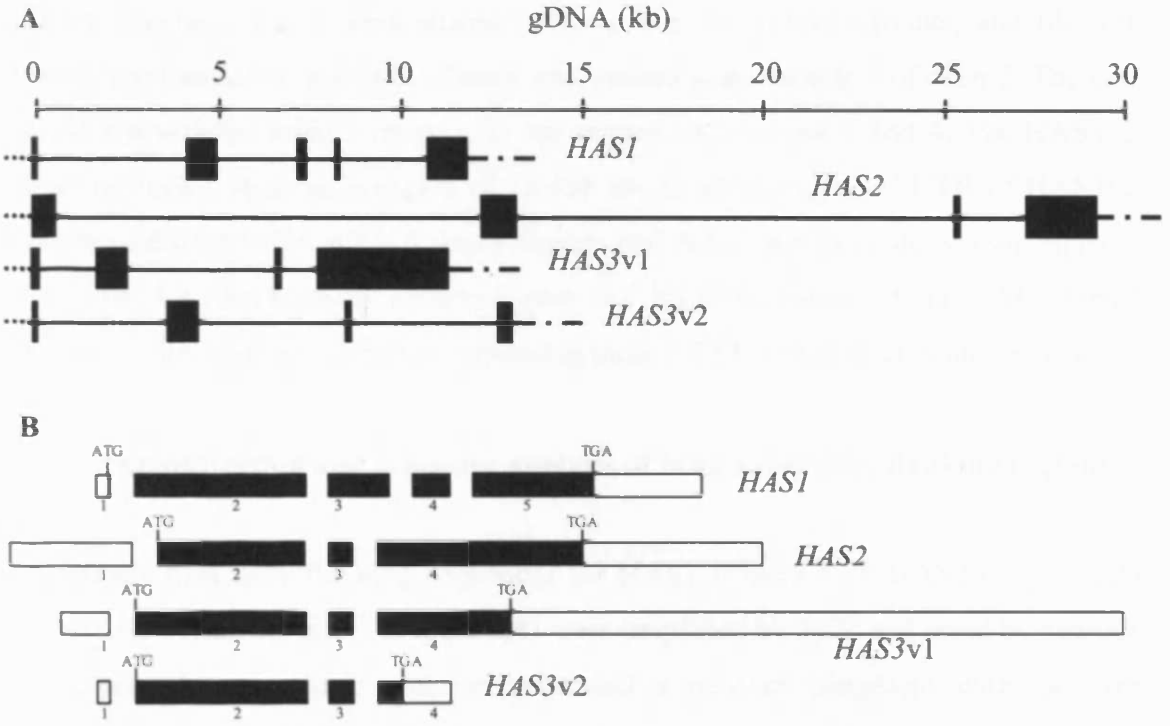

Figure 3.1. A. Genomic structures for the human *HAS* genes drawn to scale in 5'-3' orientation. Exons are represented as filled boxes and are separated by introns (solid lines). Promoter regions are represented by dotted lines and the downstream 3' sequences by dotted and dashed lines. B. Alignment of the human *HAS* genes in 5'-3' orientation. Exons are represented by numbered boxes, with the coding regions filled and the 5'- and 3'-UTRs unfilled. Translation start sites (ATG) and termination codons (TGA) are labelled.

The full reference *HAS1* cDNA sequence, NM_001523 was recovered from clone BAC BC330783 sequence AC018755 as five exons, the translation start site located 9 bp from the three prime (3') end of exon 1. Together with intervening intronic sequences, the gene extended over 10.857 kb of gDNA. The *HAS2* reference cDNA sequence, NM_005328, was recovered from clone RP11-3G20 sequence AC104233 as four exons. The gene extended over 28.091 kb of gDNA, with the translation start site located at nucleotide 1 of exon 2, with exon 1 comprising the 5'-UTR. Reference sequences for *HAS3*v1 (NM_005329) and HAS3v2 (NM_138612) were both recovered from clone RP11-123C5 sequence AC009027. The genomic structure of HAS3v1, the longer transcript, had strong overall similarity with that of HAS2. The four HAS3v1 exons together with their intronic sequences spanned 10.129 kb of

gDNA. Exons 2 and 3 were shared between the two HAS3 variants, and like for HAS2, the translation start site of each was located at nucleotide 1 of exon 2. The two HAS3 transcripts varied, however, in the sequences of exons 1 and 4. The HAS3v2 genomic region spanned a region of 12.458 kb. In addition, the 3'-UTR of HAS3v2 was devoid of ATTTA mRNA decay signals and AATAAA polyadenylation signals. The first AATAAA motif occurred over 4.5 kb downstream of the NM_138612 sequence, the intervening region containing three ATTTA pentanucleotide sequences.

3.3.2 Amplification and sequence analysis of HAS exons plus flanking regions

The exons plus their flanking sequences for HAS1 (Figure 3.2), HAS2 (Figure 3.3) and HAS3 variants 1 and 2 (Figure 3.4) were amplified by PCR and sized by agarose gel electrophoresis. Each reaction generated a product congruent with the size predicted *in silico*. PCR products were cloned into the sequencing vector pCR-TOPO/2.1 and sent for analysis. Results obtained revealed 99% identity with the respective gDNA and reference cDNA sequences.

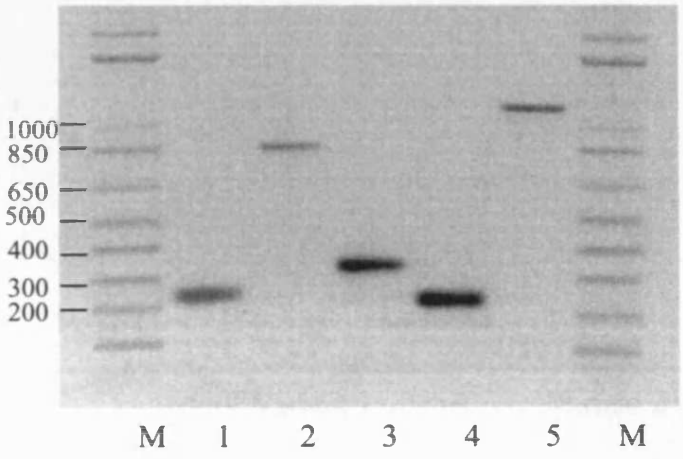

Figure 3.2. HAS1 exons amplified by PCR. Each exonic fragment is labelled (1-5; exon 1-5). Double-stranded DNA markers are given (M) with their sizes in bp.

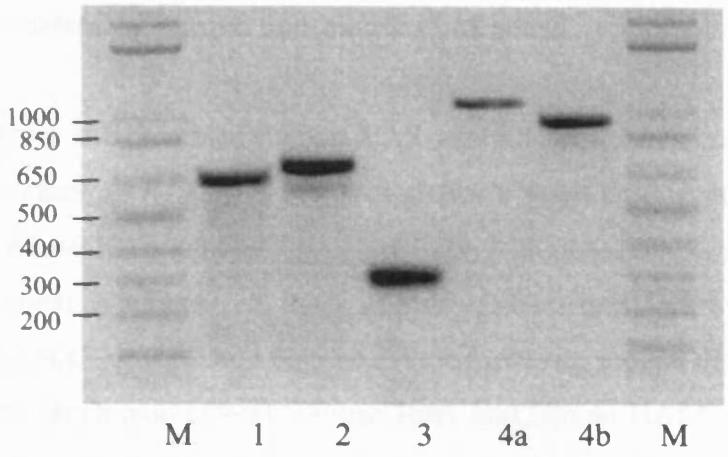

Figure 3.3. HAS2 exons amplified by PCR. Each Exonic fragment is labelled (1-4b; exon 1-4b). Double-stranded DNA markers are given (M) with their sizes in bp.

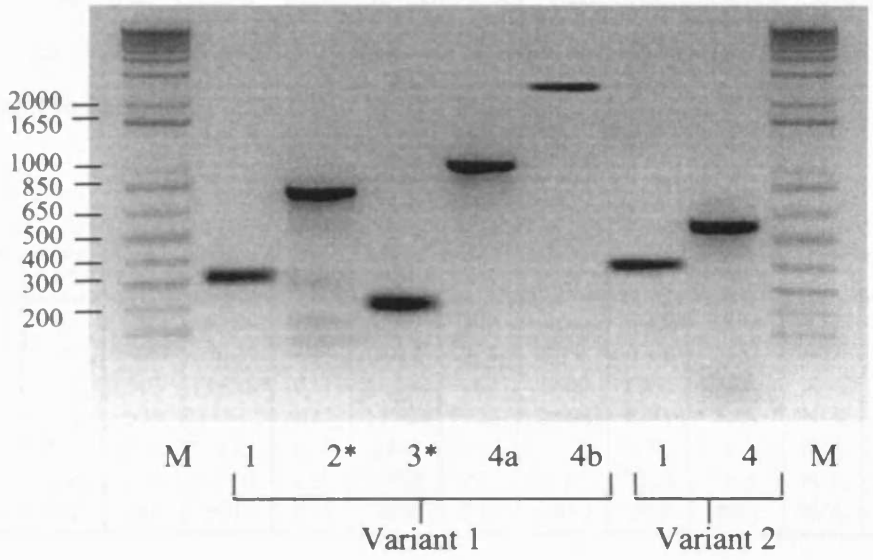

Figure 3.4. HAS3 exons amplified by PCR. HAS3v1 exons and HAS3v2 exons are labelled. Exons 2 and 3 (labelled with *) were identical to both HAS3 transcripts and so only needed to be amplified once. Double-stranded DNA markers are given (M) with their sizes in bp.

3.3.3 Comparison of human and mouse *HAS* genes

Table 3.3 shows the predicted human HAS genomic structures compared with their murine Has orthologues. Figure 3.5 also shows a schematic representation of each human and mouse HAS genomic structure. The human sequences had a high degree of organizational similarity to their murine counterparts, with the exception of HAS3v2. The *HAS* genes could also be divided into the groups described previously by Spicer and McDonald (1998). Mouse Has1 and human HAS1 were characterized by five exons, with the translation start site very close to the 3' end of exon 1. In contrast, the mouse and human HAS2 and HAS3 isoforms conformed to the second group, characterised by four exons with the translation start site at the beginning of exon 2. The huge increase in available bioinformatic data that took place over the course of this study allowed comparison of the HAS genomic structures described here with the results of algorithm based genomic structure predictions which are available at the UCSC Genome Browser (http://genome.cse.ucsc.edu/). These predictions concurred with our data for *HAS1* at 19q13.41, *HAS2* at 8q24.12 and *HAS3* at 16q22.1.

Gene	5'-UTR	Exon 1	Intron 1	Exon 2	Intron 2	Exon 3	Intron 3	Exon 4	Intron 4	Exon 5	3'-UTR	gDNA	cDNA
m*Has1*	42	51	4489	708	1567	226	464	133	3251	971	295	11860	2089
h*HAS1*	35	44	4026	693	2012	226	579	133	2153	991	315	10857	2087
m*Has2*	505	505	11528*	627	11590	102	1300	2960	N/A	N/A	2030	28612	4194
h*HAS2*	538	538	11512	627	11507	102	2066	1739	N/A	N/A	809	28091	3006
m*Has3*	173	173	3493	639	2345	102	911	5000	N/A	N/A	4076	12663	5914
h*HAS3* v1	156	156	1700	636	3409	102	800	3326	N/A	N/A	2402	10129	4220
h*HAS3* v2	60	60	3079	636	3409	102	4812	360	N/A	N/A	252	12458	1158

Table 3.3. Comparison of the predicted sizes (bp) of exons, introns, UTRs, cDNA and gDNA distances for the murine (m) and human (h) *HAS* genes. *mHas2 intron 1 contained a number of n residues, as the sequence was not complete.

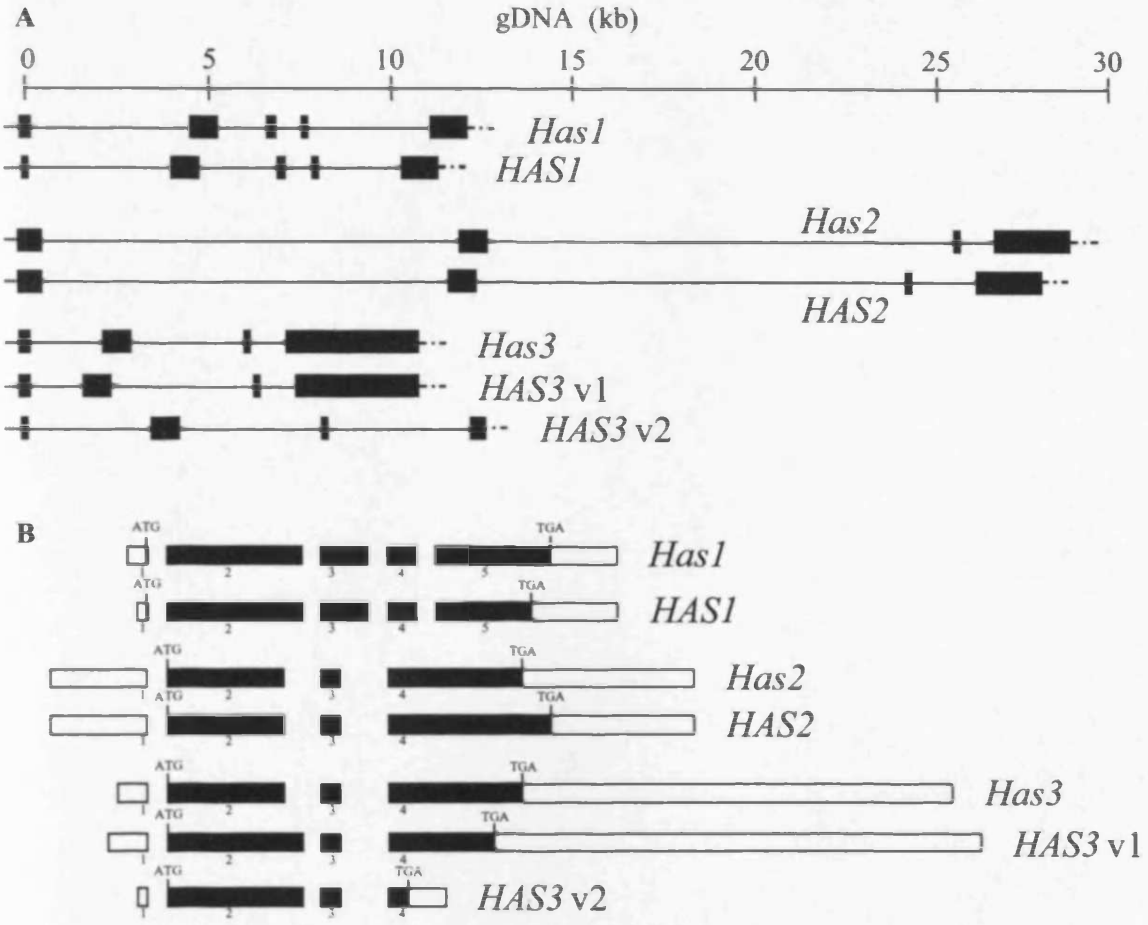

Figure 3.5. A. Genomic structures of the human (*HAS*) and murine (*Has*) hyaluronan synthase genes, drawn to scale in 5'-3' orientation. Exons are represented by filled boxes and are separated by introns (solid lines). Promoter regions are represented by dotted lines, and the downstream 3' regions by dotted and dashed lines. B. Alignment of the human *HAS* genes and their murine orthologues in 5'-3' orientation. Exons are represented by numbered boxes, with the coding regions filled and the 5'- and 3'-UTRs unfilled. Translation start sites (ATG) and termination codons (TGA) are labelled.

A comparison between the human HAS intron/exon boundaries and the corresponding regions in the murine *Has* genes [Spicer and McDonald, 1998] is shown in Figure 3.6. In each case, the predicted human sequences conformed to their corresponding consensus motifs [Krawczak et al, 1992]. A high level of nucleotide and amino acid sequence identity was observed between human and mouse orthologues for intron 2 for each *HAS* gene. There was also a high degree of similarity in intron 3 for HAS2

and HAS3v1. Indeed, high levels of amino acid identity were evident throughout, with the exception of HAS3v2. Furthermore, all intronic phases were identical in both species. HAS3v2 was distinct from both HAS3v1 and Has3, and could be distinguished clearly from the other human *HAS* gene transcripts at the cDNA and genomic level, together with variations at the intron/exon boundaries.

Gene:Intron		Intron / Exon Boundary Sequence	Intronic Phase
Has1	1	ACAGCCATGAAACAGgtgtgtgtgtgt.....ggtcacccacagGACATGCCAAAGCCC	0
		M K Q D M P K P	
HAS1	1	ACTGCGATGAGACAGgtgtgtgtgtgt.....cgctcccagcagGACGCGCCCAAGCCC	0
		M K Q D A P K P	
Has2	1	CAGGAGCTGAACAAGgtacgttatacaa.....attacatttcagATGCATTGTGAGAGG	0
		M H C E R	
HAS2	1	CAAGAGCTGAACAAGgtacgttacact.....attatattacagATGCATTGTGAGAGG	0
		M H C E R	
Has3	1	TAGCCCGTTTGCAGGgtgagtatgttt.....tcttgtttttagATGCCGGTGCAGCTG	0
		M P V Q L	
HAS3v1	1	GCGCCCCTTCAGCATgtaagctccgga.....ttctctcgccagATGCCGGTGCAGCTG	0
		M P V Q L	
HAS3v2	1	GCAGCCGGCGGCACGgtgagcgcgggc.....ttctctcgccagATGCCGGTGCAGCTG	0
		M P V Q L	
Has1	2	GTGGACTACGTGCAGgtgagtgatggg.....tcctcttcacagGTCTGTGACTCAGAC	0
		V D Y V Q V C D S D	
HAS1	2	GTGGACTACGTGCAGgtgagtagaggc.....tccaccttacagGTCTGTGACTCGGAC	0
		V D Y V Q V C D S D	
Has2	2	GTGGATTATGTACAGgtaggtctgaaa.....tctttcttgcagGTGTGTGACTCAGAT	0
		V D Y V Q V C D S D	
HAS2	2	GTGGATTATGTACAGgtaggtctccac.....gcttctttgcagGTTTGTGATTCAGAC	0
		V D Y V Q V C D S D	
Has3	2	GTGGACTACATCCAGgtaaggctgcct.....atcctcctgcagGTGTGTGACTCTGAC	0
		V D Y I Q V C D S D	
HAS3v1	2	GTGGACTACATCCAGgtaagggcgcct.....ctccctctgcagGTGTGCGACTCTGAC	0
		V D Y I Q V C D S D	
Has1	3	TCAGTGGTCCTCTGGgtgagtggaagc.....cactctacctagGTCTATACAGAAACA	1
		I S G P L G L Y R N	
HAS1	3	TCAGCGGTCCTCTAGgtaagcaggggc.....ccctccacccagGCCTATATAGGAATA	1
		I S G P L G L Y R N	
Has2	3	GGAGGAGATGTCCAGgtacatatggct.....ttctacttgcagATTTTAAACAAGTAT	0
		G G D V Q I L N K Y	
HAS2	3	GGGGGAGATGTCCAGgtacatggcttc.....ttcttcttgcagATTTTAAACAAGTAC	0
		G G D V Q I L N K Y	
Has3	3	GGAGGAGATGTCCAAgtaagaagtaac.....cttcccttacagATCCTCAACAAGTAT	0
		G G D V Q I L N K Y	
HAS3v1	3	GGGGGAGATGTCCAGgtaagatgagac.....attcccttgcagATCCTCAACAAGTAC	0
		G G D V Q I L N K Y	
HAS3v2	3	GGGGGAGATGTCCAGgtaagatgagac.....tctgtgttcaagCCCCCAGGGAAAGGT	0
		G G D V Q P P G K G	
Has1	4	GGGCTATGCTACCAAgtaagttaagag.....tctgcctgtcagGTATACCTCGCGCTC	2
		G Y A T K Y T S R S	
HAS1	4	GGGTTATGCTACCAAgtaagctgaggg.....gcccccgtgcagGTACACCTCCAGGTC	2
		G Y A T K Y T S R S	

Figure 3.6. Comparison of intron/exon boundary nucleotide and amino acid sequences in human *HAS* and murine *Has* genes. Exonic sequences are represented in upper case, with the intronic sequences in lower case. Amino acids are labelled using their single-letter abbreviations. Sequence variations are highlighted in red.

3.3.4 Luciferase analysis of HAS promoters

The sequences directly upstream of the transcription start site for each human *HAS* gene were amplified using PCR from genomic DNA. After cloning each promoter into the pGL3-Mod luciferase reporter vector (Figure 3.7), they were assayed for transcriptional activity.

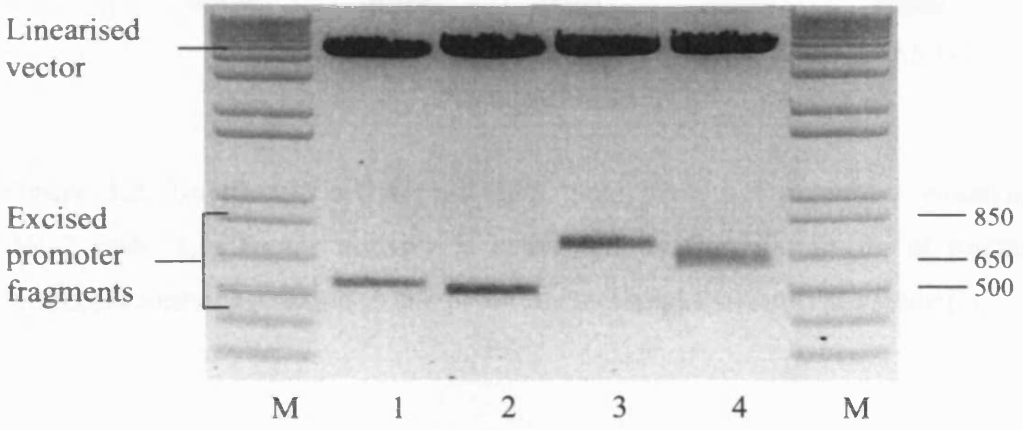

Figure 3.7. Enzymatic digestion of clones containing proximal promoters for the human *HAS* genes; 1 – HAS1; 2 – HAS2; 3 – HAS3 variant 1; 4 – HAS3 variant 2. Double-stranded DNA size markers (M) and their sizes in bp are also marked.

The luciferase activity for each of the HAS promoters in HK-2 cells is shown in Figure 3.8. Each promoter displayed an increase in luciferase activity over the promoterless control vector. The HAS1 and HAS3v2 promoters showed marked increases in luciferase activity, with 10 fold and 4 fold increases respectively. HAS2 and HAS3v1 gave much lower readings, with both promoters only displaying a 2 fold increase. In 3 repeat experiments, the variance readings for each promoter were low (HAS1, 0.15; HAS2, 0.01; HAS3v1 0.01; HAS3v2, 0.07) showing that the results were highly reproducible.

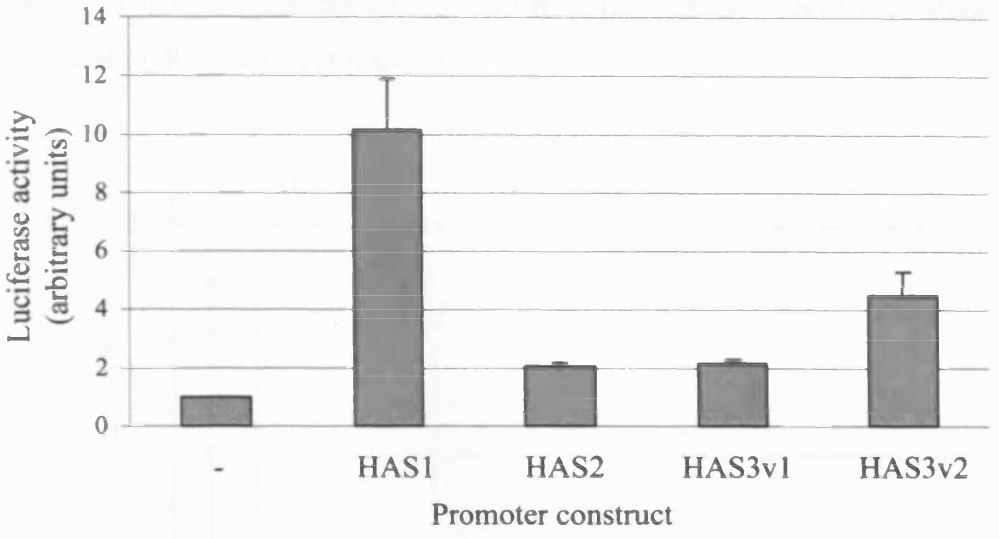

Figure 3.8. Luciferase activity of HAS gene proximal promoter constructs in HK-2 cells. Luciferase activity is expressed as the magnitude of normalized luciferase activity relative to the promoterless negative control vector (-).

A second, established luciferase reporter assay was therefore used to analyse the HAS promoter constructs. This system had been developed by Coleman et al (2002) to analyse DNA sequences for promoter activity. The luciferase activity was measured in two cell lines (HEK293t and TE671). If the analysed DNA sequence displayed a 10 fold increase in activity over the promoterless control in either cell line, then it could be classed as a true promoter. The luciferase data for the HAS promoter constructs in HEK293t and TE671 cells is shown in Figure 3.9. In eight replicates, low variance values for each HAS promoter construct were obtained, again showing that the results were highly reproducible. In the HEK293t cells these were 0.16 for HAS1, 0.30 for HAS2, 0.22 for HAS3v1 and 0.28 for HAS3v2. In the TE671 cell line the variance readings were 0.17 for HAS1, 0.29 for HAS2, 0.22 for HAS3v1, and 0.31 for HAS3v2. In both cell lines, the respective promoter activities were ranked HAS1 > HAS3v2 > HAS3v1 > HAS2. In HEK293t cells, the HAS1 promoter demonstrated a 152 fold increase in luciferase activity over the promoterless control. HAS3v2, HAS3v1 and HAS2 promoters demonstrated 44-, 4.5- and 3.9 fold increases respectively. In the TE671 cells, the HAS1 promoter construct had 48 times the

activity of the promoterless vector, with HAS3v2, HAS3v1 and HAS2 showing 33-, 11.6- and 10 fold increases respectively.

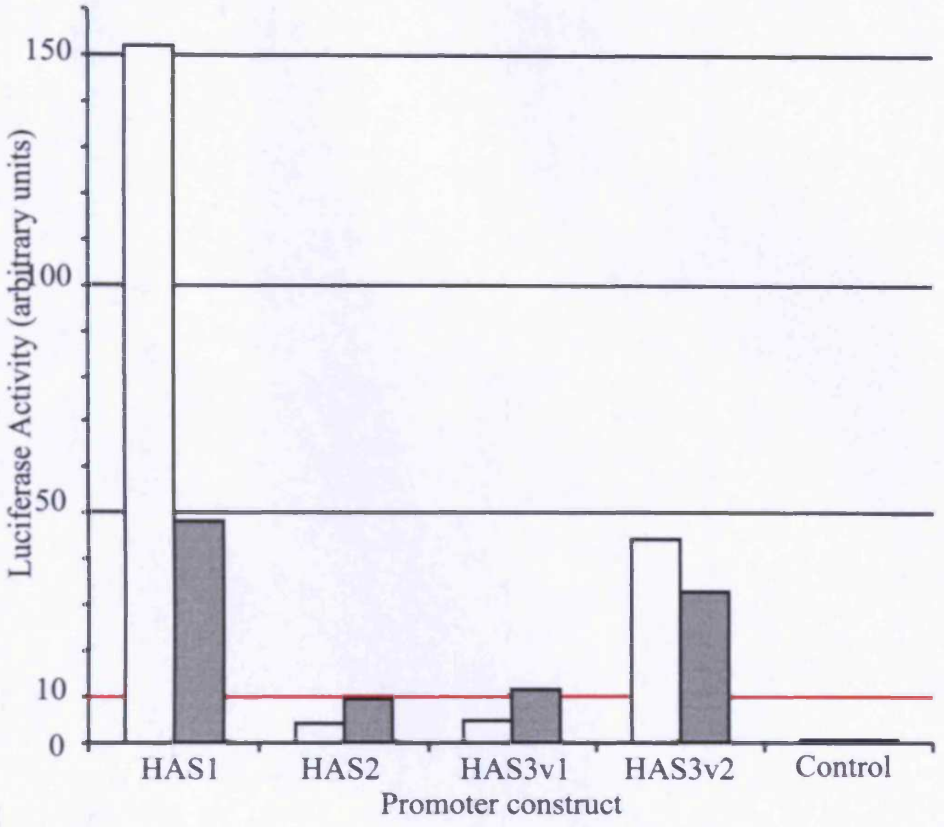

Figure 3.9. Luciferase activity of proximal promoter and control constructs for each *HAS* gene in HEK293t (white bars) and TE671 (shaded bars) cell lines. Luciferase activity is expressed as the magnitude of normalized luciferase activity relative to the promoterless negative control vector. The 10 fold threshold described in the text is indicated in red.

3.3.5 Identification of putative TFBSs

Using default parameters, the MatInspector program at the Genomatix database was used to analyse approximately 500 bp immediately upstream of the reported transcription start site for each *HAS* gene. Forty-six TFBSs were detected in the HAS1 proximal promoter, 54 for HAS2, 46 for HAS3v1 and 56 for HAS3v2. The Chip2Promoter analysis program was then used to identify TFBSs common to all the

HAS promoters. As shown in Figure 3.10, the analysis program identified E2FF, MZF1, ZBPF, CREB, E-BOX, EGRF, NF-κB and Sp1 binding sites common to each HAS proximal promoter. In addition, despite a number of shared TFBSs, there were no obvious similarities in the distribution of the sequences between the different promoters.

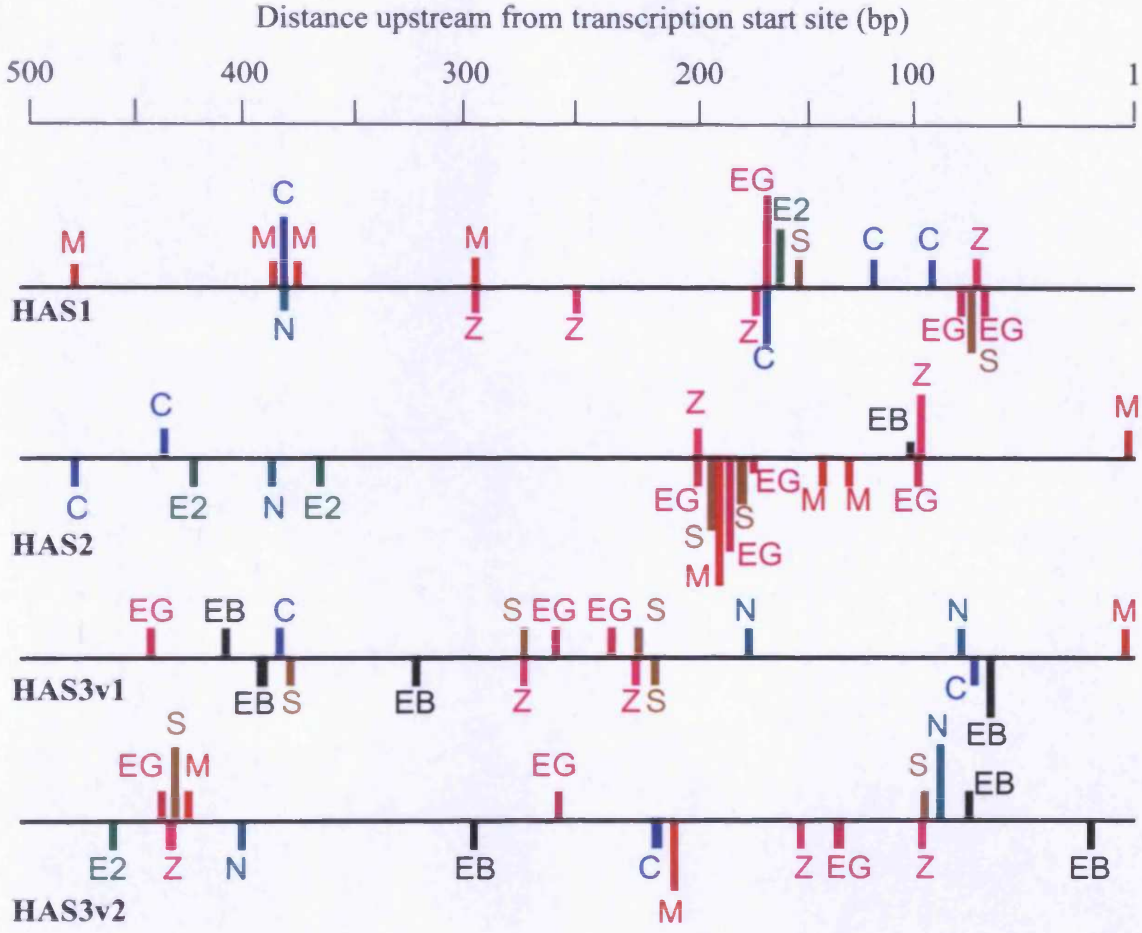

Figure 3.10. The TFBSs identified by the Chip2Promoter analysis program of the 500 bp immediately upstream of each HAS transcription initiation site. The horizontal line represents the proximal promoter in 5' to 3' orientation. Sites above the line are in sense orientation and those below in antisense orientation. Key: C – CREB or CAMP-responsive element binding proteins; E2 – E2FF or E2F-myc activator / cell cycle regulator; EB – EBOX binding factors; EG – EGRF or EGR / nerve growth factor induced protein C and related factors; M – MZF1 or myeloid zinc finger 1 factor; N – NF-κB or nuclear factor-κB / c-rel; S – Sp1 or GC-box factors Sp1 / GC; Z – ZBPF binding protein factor ZPB-89.

3.3.6 HAS isoform-specific polymorphic dinucleotide microsatellite markers

Visual inspection of the HAS genomic sequence data for tandem repetitive elements resulted in the identification of a $(GT)_n$ microsatellite at the 5' splice junction of HAS1 intron 1 in sequence AC018755, which was also shared by the murine *Has1* gene. Similarly, a repeat of sequence $(AC)_n$ was found 408 bp downstream of HAS2 exon 1, and a $(GT)_n$ array situated 3.214 kb upstream of exon 1 of HAS3v2, i.e. 4.497 kb upstream of exon 1 of HAS3v1. PCR electrophoretograms are shown in Figure 3.11. Each microsatellite was amplified from a pooled sample of 184 gDNAs. Each marker was found to be polymorphic and pedigree analysis confirmed stable Mendelian inheritance. Allele frequencies for each HAS isoform-specific microsatellite were then estimated using a sample of 48 gDNAs. Marker heterozygosity (H) values are also given and fall within the range used frequently for whole genome linkage analysis, suggesting that these markers are suitable for this purpose.

Since the translation start site for HAS1 is situated 9 bp upstream from the HAS1 microsatellite sequence, a repeat allele of size $(GT)_{3n+1}$ has the potential to create an in-frame insertion of valine / cysteine repeat(s) into the polypeptide sequence of HAS1 thus: MRQ-$(VC)_n$-HAS1 protein. The alleles shown in figure 3.11 were assigned tentatively to the peaks on the basis of their frequency and size. Assuming approximate equivalence between electrophoretic mobility units and size in bp, it is clear that repeats with the potential to affect HAS1 splicing and primary amino acid sequence in vivo were detected. However, there is no evidence proving this is the case, and its occurrence remains a theoretical possibility.

A

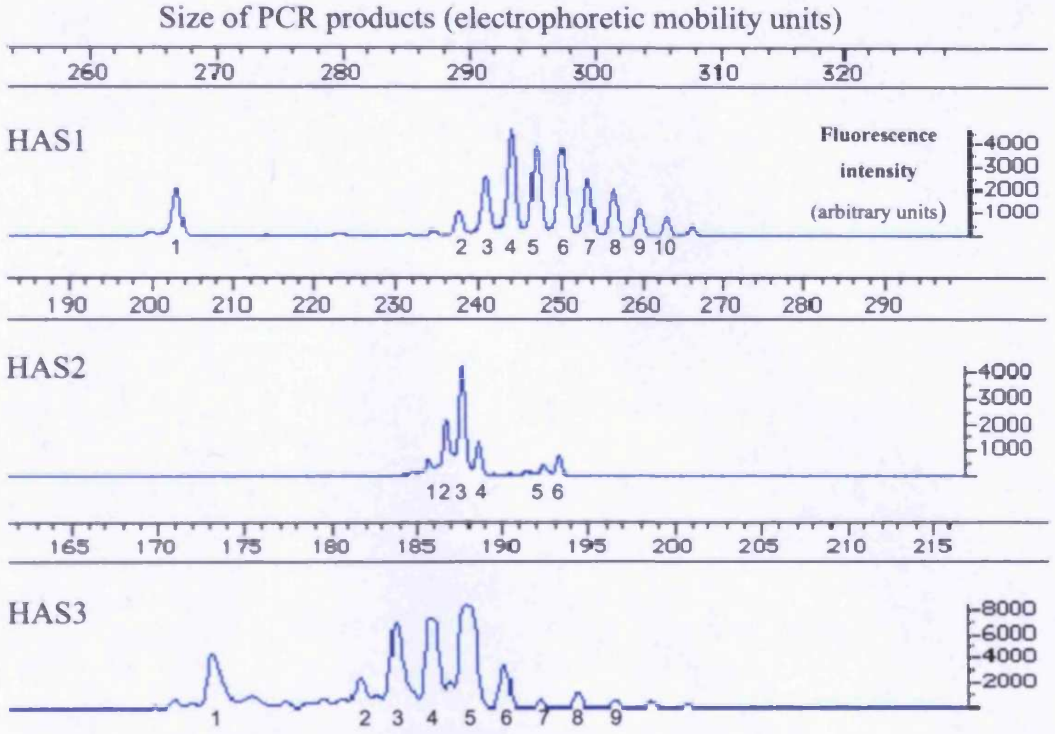

B

Marker	Number of genotypes	Allele number / [size (electrophoretic mobility units)] / estimated frequency (%)										H	Cloned size (bp) / repeat number
HAS1		1 [n]	2 [n+22]	3 [n+24]	4 [n+26]	5 [n+28]	6 [n+30]	7 [n+32]	8 [n+34]	9 [n+36]	10 [n+38]		
	38	4	9	11	27	13	8	8	11	8	1	0.86	293/19
HAS2		1 [n]	2 [n+2]	3 [n+4]	4 [n+10]	5 [n+14]	6 [n+16]						
	43	9	48	13	1	28	1					0.67	242/12
HAS3		1 [n]	2 [n+10]	3 [n+12]	4 [n+14]	5 [n+16]	6 [n+20]	7 [n+24]	8 [n+26]	9 [n+30]			
	42	6	7	1	61	11	6	6	1	1		0.60	188/19

Figure 3.11. A. Electrophoretograms of dinucleotide microsatellite alleles at each *HAS* locus in a sample of 184 individuals. Alleles are numbered, and electrophoretic mobility units are shown together with peak heights for each allele expressed as magnitude of fluorescence intensity. B. Predicted frequencies of alleles of each HAS-specific microsatellite. Allele sizes are given in electrophoretic mobility units relative to the smallest allele.

3.4 DISCUSSION

The genomic structures for the human *HAS* genes have here been elucidated for the first time. A combination of *in silico* and *in vitro* methodologies were used, as previously used for the analysis of the human glutamate receptor multigene family [Williams et al. 2002]. The cDNA sequences for the human *HAS* genes had already been characterised and deposited in the online database. These sequences were retrieved and used to find clones spanning each sequence in the high-throughput genomic sequences database. Putative genomic structures, together with the proximal promoters were then reconstructed for each *HAS* gene. Each HAS exon, along with its flanking sequences was then amplified and sequenced. The observed exonic PCR products were of the predicted size, and sequence analysis showed 99% identity with the respective gDNA sequences. Furthermore, the intron/exon boundaries conformed to the corresponding consensus motifs.

The genomic structures for the murine *Has* genes had been previously elucidated [Spicer and McDonald, 1998]. These could therefore be used as a useful tool to further confirm the structures of the human *HAS* genes. As has been found with many murine and human genes, the *HAS* and *Has* genes showed a high degree of similarity. The exonic breakdown for each isoform was identical (i.e. HAS1 and Has1 comprise five exons, and the others comprise four exons). In addition, the intronic sequences for each isoform were of similar length. Sequence analysis (both DNA and amino acid) also showed a high degree of similarity between the human and murine isoforms. The above evidence therefore pointed towards a high degree of evolutionary conservation.

The genomic sequence for HAS3v2 was an exception. Its genomic breakdown was indeed, identical to HAS3v1 (where it shares the same exon 2 and 3) and Has3, with it comprising of four exons. This was, however, where the similarities ended. The cDNA sequence for HAS3v2 was significantly shorter than that of HAS3v1 (Figure 3.1). As previously mentioned, its 3'-UTR was also devoid of any ATTTA mRNA decay signals and AATAAA polyadenylation signals. It also showed variation at its intron/exon boundaries. It is known that HAS3v1 generates much smaller hyaluronan

chains than HAS1 and HAS2 *in vitro*. Very little is however known about HAS3v2, and its functional significance remains a mystery [Sayo et al. 2002].

Microsatellites found by visual inspection of each *HAS* gene, were found to be polymorphic and confirmed stable Mendelian inheritance. The amplification procedures described here for each HAS exon and for their microsatellites, together with the SNP data deposited in internet databases, comprise a comprehensive resource for mutation detection screening of all exons and/or linkage analysis of microsatellite alleles for each *HAS* gene. The influence of SNPs on matrix interactions is implied by recent work identifying common and potentially functional polymorphisms in TSG-6, whose protein product interacts with HA in the matrix [Nentwich et al. 2002]. Further studies are now required to evaluate the clinical relevance of genetic variation at the *HAS* loci. Specific alleles at the HAS1 microsatellite were found to have the potential to cause in-frame insertions into the HAS1 peptide sequence, depending on the exact splice site at the HAS1 exon 1/intron 1 junction. Even though this is only a theoretical assumption, the same microsatellite was also found in the murine HAS1 gene, and may therefore be an area of future interest.

With the genomic structures of the human *HAS* genes now determined, analysis of their transcriptional control could be undertaken. The sequences directly upstream of the transcription start site for each *HAS* gene were amplified and analysed for transcriptional activity using two different luciferase reporter assay systems. The first system, was performed using HK-2 cells and showed that each promoter could drive transcription of the luciferase gene. The observed activities, however, particularly those observed for HAS2 and HAS3v1, were only just above those displayed by the promoterless control, and it was difficult to determine whether they could be classed as promoters. An established luciferase assay system, as described by Coleman et al. (2002), was therefore used. This high-throughput system had been optimised to look at DNA sequences of approximately 500 bp, which influenced the design of PCR primers for promoter amplification. All fragments showed significant promoter activity in at least one of the two cell lines tested. Both cell types gave a similar trend with the HAS1 promoter construct demonstrating the highest activity; 151- and 49-fold increase in activity over the promoterless control in the HEK293t and TE671 cell lines respectively. The second highest activity was shown by the HAS3v2 promoter

(45- and 33- fold), followed by HAS3v1 (5- and 11- fold), and finally the promoter region of HAS2 (4- and 10- fold). Interestingly, this trend corresponded to the data obtained using the HK-2 cell line, with the HAS1 promoter displaying the greatest activity (10 fold increase over the promoterless control), followed by HAS3v2 (4 fold), HAS3v1 (2.1 fold) and finally HAS2 (2.0 fold).

Due to a lack of consensus on the definition of promoter activity in reporter systems, Coleman et al. (2002) determined a conservative threshold of 10 times the activity of the promoterless control. Therefore, each of the HAS promoter fragments analysed could be categorised as 'true promoters' in the TE671 cell line. The values for HAS3v1 and HAS2 fell below this threshold (although demonstrated a similar trend to that shown in the TE671 cells) in HEK293t cells. It is therefore conceivable that the HAS2 and HAS3v1 promoters may be more sensitive to cell-specific effects than their counterparts for HAS1 and HAS3v2.

A number of studies have shown that HAS2 expression is induced in a variety of cellular functions. HAS2 is specifically upregulated in response to wound healing in a mesothelial cell model [Yung et al, 2000], and HAS2 overexpression in fibrosarcoma cells yields significantly larger subcutaneous tumours in nude mice [Kosaki et al, 1999]. HAS2 knockout mouse studies have been shown to have an embryonic lethal phenotype [Camenisch et al, 2000]. The *HAS2* gene may therefore be under tighter regulatory control than the other HAS isoforms. In addition, its lower activity may be because of an absence of sites, perhaps further upstream, that are required for true constitutive expression. Tissue specific upstream exons and alternative promoter regions may also facilitate increased HAS2 and/or HAS3v1 expression [Anney et al. 2002].

The MatInspector program identified a variety of transcription factor binding sites in the proximal promoter region for each HAS isoform. Interestingly, none of the promoters showed evidence of a TATA box. This site is commonly found in a large number of eukaryotic promoters, required for the binding of the RNA polymerase transcriptional machinery. A number of transcription factor binding sites were also identified that were common to all four promoter regions, when analysed using the Chip2promoter software. Due to the high similarity between the coding regions for

each gene, it is conceivable that their transcription may be controlled, in part, by the binding of common transcription factors. On the other hand, where there is differential tissue expression of the HAS isoforms, this may be due to the binding of transcription factors unique to each promoter region. These initial findings represent the first step in characterising the transcriptional mechanisms of each *HAS* gene.

In conclusion, the reconstructed human HAS genomic structures, along with amplification of their exons and microsatellites, will provide a useful tool in further studies of the *HAS* genes. Combined analysis of regulatory and genomic HAS sequences will provide a more detailed picture of the evolution of this multigene family and permit further investigation of the functional relationships of the different isoforms.

CHAPTER FOUR

RECONFIGURATION OF THE TRANSCRIPTION INITIATION SITE FOR THE HUMAN HYALYRONAN SYNTHASE 2 GENE

4.1 INTRODUCTION

Transcription of the *HAS2* gene does not occur as widely in the body as *HAS1*. Evidence for its transcription is seen in the heart and submucosa of the small intestine, and only in low levels in other tissues [Spicer and McDonald, 1998]. Nevertheless, *HAS2* transcription can be induced by a variety of different stimuli. Epidermal keratinocytes, for example, show an increase in HAS2 expression in response to epidermal growth factor [Pienimäki et al, 2001; Pasonen-Seppänen et al, 2003], and also to keratinocyte growth factor [Karvinen et al, 2003]. Other cytokines and growth factors reported to induce HAS2 expression include PDGF in both corneal endothelial cells [Usui et al, 2000] and mesothelial cells [Jacobson et al, 2000], TNF-α and IL-1β in periodontal ligament cells [Ijuin et al, 2001], FGF and insulin-like growth factor 1 (IGF-1) [Recklies et al, 2001]. TGF-β1, on the other hand, can stimulate, or suppress HAS2 expression, depending on the cell type [Usui et al, 2000; Jacobson et al, 2000; Recklies et al, 2001; Pasonen-Seppänen et al, 2003].

As discussed in chapter 3, reports from our and other laboratories have demonstrated the importance of HAS2 expression in HA metabolism in kidney disease. An increase in HA expression in the renal corticointerstitium is commonly associated with the progression of interstitial fibrosis leading to ESRD [Strutz, 2001; Jones et al, 2003; Nilsson et al, 2001]. In high glucose concentrations, which mimic diabetic nephropathy, renal proximal tubular epithelial cells synthesise high levels of HA, which is coincident with specific upregulation of transcription at the *HAS2* locus [Jones et al, 2001]. The following chapters therefore concentrate on characterising the HAS2 promoter.

Preliminary luciferase analysis of the sequence directly upstream of the HAS2 reference mRNA sequence demonstrated constitutive promoter activity. This sequence was the least active when compared to the corresponding regions in the other *HAS* genes, but still conformed to the criteria established for promoter activity [Coleman et al, 2002]. Preliminary analysis, as detailed in the beginning of the results section, suggested that the HAS2 TIS was located at a different position that had been previously reported. The work that followed therefore concentrated on 1) confirming the new location of the TIS for the *HAS2* gene, 2) investigating why the original

location of the HAS2 TIS appeared to be incorrect and 3) analysing the new proximal promoter region to pinpoint specific areas important for transcriptional control. The starting point for this work was NCBI database entry NM_005328 for HAS2.

4.2 METHODS

4.2.1 Primer extension

Primer extension was first used to identify the location of the TIS for the *HAS2* gene. The primers used for both experiments were the same, and their oligonucleotide sequences are given in table 4.1. For primer extension, the two primers were radiolabelled with γ-^{32}P ATP. The labelled primers were then used in an annealing reaction with purified mRNA from HK-2 cells, and the primer extension reaction was carried out as described in section 2.7.3.

Name	Antisense strand primer
RACE	GTCTTTCTGCCCCCGATAAC
RACE-N	GCCTGTGGAAGACTCAGCA

Table 4.1. Oligonucleotide sequences of the primers used to amplify the 5' end of the human HAS2 transcript.

4.2.2 5'-RACE

Purified mRNA from three human cell lines (TE671, HEK293t and HK-2) was reverse-transcribed using the SMART RACE kit as described in section 2.7.4. The 5'end of HAS2 was then amplified by PCR in a two stage reaction. The cDNA generated above was used as a template for the RACE primer (Table 4.1). An aliquot of the product from this reaction was then used as a template for a second reaction using the nested RACE-N primer.

RACE products were sized by agarose gel electrophoresis, gel extracted and cloned (sections 2.3.4, 2.4). Clones were subjected to enzymatic digestion with *Eco* RI to check for the presence of the RACE fragments and sent for sequencing using the M13 forward and reverse primers.

4.2.3 Generation of nested promoter fragments

A common antisense strand primer at position +22 to +43 bp downstream of the transcription start site of reference HAS2 mRNA sequence NM_005328 was tagged with a *Hin* dIII recognition site (Table 4.2). A series of sense strand primers tagged with *Kpn* I recognition sites (Table 4.2) was then designed to amplify a nested set of PCR fragments when used with the antisense strand primer, ranging in size from 117 bp up to 1171 bp (Figure 4.1).

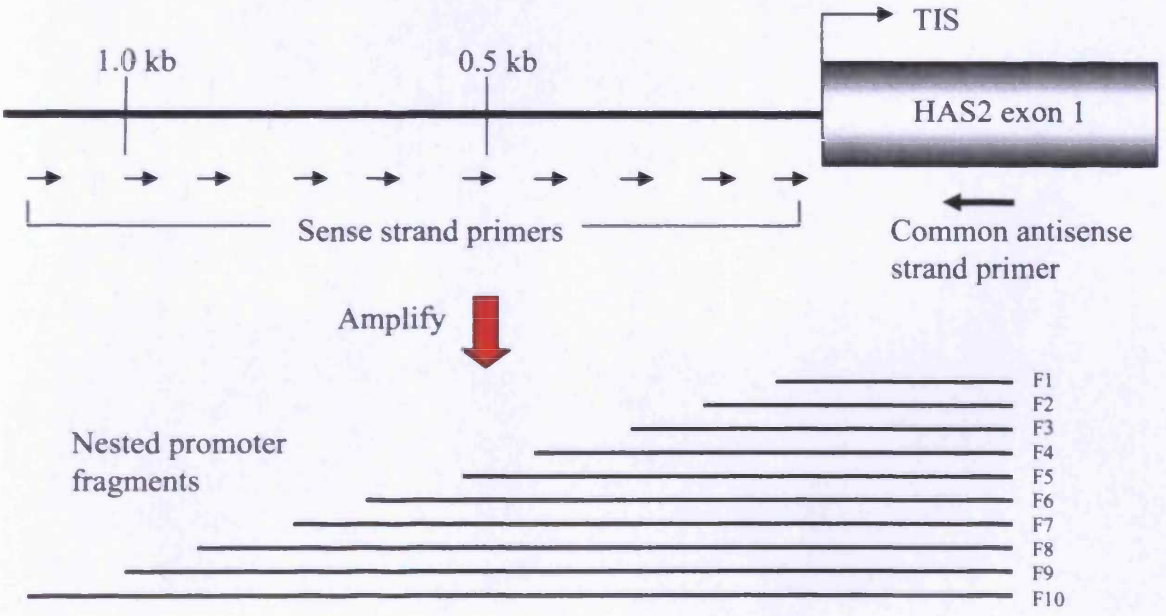

Figure 4.1. Schematic for the generation of HAS2 nested promoter fragments. Sense strand primers were individually used with the common antisense strand primer to amplify a set of HAS2 promoter fragments of increasing size (F1 – F10).

Name	Sense Strand Primer	Antisense Strand Primer	Predicted size
F1	CCGGTACCAAAACACCCACCAGCTCACTTG	CCAAGCTTCGAAGCCAGGACTGGGTAATTC	117
F2	CCGGTACCAGTCCACACCTCCCTCTCCACT	"	173
F3	CCGGTACCGAACCGGCCTGTAGCTCAGAG	"	294
F4	CCGGTACCGCCCCCTATGTGTCTTGCATT	"	362
F5	CCGGTACCCCACAGGGAGTTTATCGCTTG	"	473
F6	CCGGTACCCACACCCCTCCCAACTGTTCCTC	"	555
F7	CCGGTACCGAGTTGGCGGGAAGAAAGGGTTA	"	682
F8	CCGGTACCTGCGCGCTGTTTGAGTATGTTT	"	829
F9	CCGGTACCGAAAGGCCATCTCCAAGCAAGA	"	972
F10	CCGGTACCCGCAATCTCCCAAGACCAAGTT	"	1171

Table 4.2. Oligonucleotide sequences in 5'-3' orientation for the amplification of nested HAS2 promoter fragments. The tagged restriction endonuclease recognition sites for *Kpn* I (sense strand primers) and *Hind* III (antisense strand primer) are shown in red. Predicted sizes are also given in base pairs (bp).

4.2.4 Generation of HAS2 promoter constructs

Following restriction endonuclease digestion, the HAS2 promoter fragments were ligated into the *Kpn* I and *Hin* dIII sites of the pGL3-Mod luciferase reporter vector as described in section 2.4.2. Clones were then digested with the same two restriction enzymes to check for the presence of the promoter fragment by agarose gel electrophoresis. Constructs were then submitted for sequencing analysis to ensure fidelity of amplification of promoter fragments using sequencing primers RV3 and GL2 (section 2.4.6).

4.2.5 Luciferase analysis of HAS2 promoter constructs

Each promoter construct was assayed for luciferase activity in HEK293t and TE671 cell lines as described in section 2.5.2, with the following amendment to maximise luciferase output. The growth medium used was a 1:1 mixture of Dulbecco's modified Eagle's medium / Ham's F-12 nutrient mixture without L-glutamine supplemented with 20 mM HEPES, 2 mM L-glutamine, 5ng/ml sodium selenite, 5 µg/ml insulin, 5 µg/ml transferrin and 0.4 µg/ml of hydrocortisone. Data for each luciferase construct (8 replicates) were calculated and plotted graphically as the fold increase of luciferase

activity compared with the promoterless control. Statistical analysis was performed using Friedman's two-way analysis of variance test from SPSS for Windows (SPSS Inc., Chicago, IL).

4.2.6 RT-PCR to detect expression of the extended HAS2 exon 1

Total RNA was extracted from a range of human cells as described in section 2.7.1 and 1 μg was then reverse transcribed as described in section 2.7.5. RT-PCR primers were designed to amplify the extended 5'-UTR identified by 5'-RACE. Primer HAS2-Prom-h-RT-F was positioned within the 130 bp extended sequence and spanned positions 54-75 from the new transcription start site, amplifying 77 nucleotides of sequence upstream of the transcription start site described previously in NM_005328. Primer HAS2-Prom-h-RT-R was positioned within HAS2 exon 2. The sequences of these primers are given in table 4.3. Also described are the sequences of primers used routinely for HAS2 RT-PCR analysis in our laboratory. In addition, extended 5'-UTRs were amplified from total RNA from mouse and rat kidneys (Ambion Europe Ltd, Cambridgeshire, UK) using primers specific to the corresponding region of the mouse (m - Genebank accession number NM_008216) and rat (r - NM_013153) HAS2 mRNAs. All RT-PCR reactions were carried out as described in section 2.7.5, and products were sized by agarose gel electrophoresis. Where appropriate, products were cloned into vector pCR2.1/TOPO and sequenced using M13 forward and reverse primers.

Name	Sense strand primer	Antisense strand primer	Predicted size
HAS2-Prom-h-RT	AAAACACCCACCAGCTCAC	CAAGGAGGAGAGAGACTCCAAA	686
HAS2-Prom-m-RT	ATTAAAACACCCACCGGCTCAC	CGAGGAGGAGAGACACTCCAAA	645
HAS2-Prom-r-RT	TTTAAAACACCCACCGGCTCAC	CGAGGAGGAGAGACACTCCAAA	645
HAS2-h-RT	CATAAAGAAAGCTCGCAACACG	ACTGCTGAGGAATGAGATCCAG	282
HAS2-m-RT	CATAAAGAAAGTTCACAACATG	GCTGCTGAGGAAGGAGATCCAG	282
HAS2-r-RT	CATAAAGAAAGTTCGCAACATG	ACTGCTGAGGAAGGAGATCCAA	282

Table 4.3. Oligonucleotide sequences for the amplification of HAS2 message from human (h), mouse (m) and rat (r). 'Prom' primers were used to amplify the extended 5'-UTR. The remaining primers amplified part of the coding sequence of the HAS2 transcript and are used routinely in our laboratory for analysis of HAS2 mRNA expression. The predicted sizes of the products are also given.

4.2.7 RNA secondary structure analysis

Analysis of the secondary structure of the extended HAS2 5'-UTR was carried out using software at the MFOLD database (section 2.1.7), using default parameters.

4.2.8 DNA sequence alignment and EST database analysis

Alignments for the genomic sequences upstream of HAS2 from human, mouse, rat and horse were carried out using the ClustalW algorithm at the EBI web server (section 2.1.4). These were then compared with expressed data from a range of different organisms in the EST databases as described in section 2.1.6.

4.3 RESULTS

4.3.1 Primer extension

Primer extension was the first method used to determine the location of the HAS2 TIS. Purified mRNA from HK-2 cells was used as a template for the primer extension

reaction, and two different radiolabelled primers were used. However, repeated primer extension experiments gave negative results. No bands longer than those of the primers used were observed, and the only visible bands were those corresponding to the radiolabelled primers and the unincorporated radiolabelled nucleotide (Figure 4.2). Therefore, a different method to locate the HAS2 TIS was used (5'-RACE).

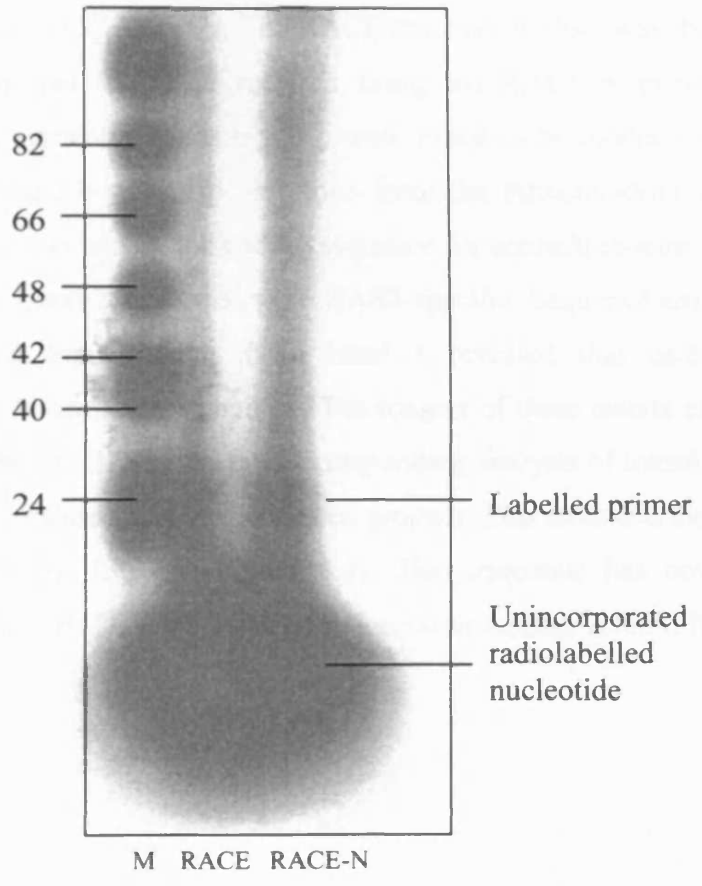

Figure 4.2. Primer extension using mRNA from HK-2 cells to identify the HAS2 TIS. Results using two different primers (RACE and RACE-N) are shown. Bands corresponding to the radiolabelled primers and unincorporated radiolabelled nucleotide are indicated. Size markers (M) are given in bp.

4.3.2 5'-RACE analysis of the *HAS2* gene using purified mRNA

Analysis by 5'-RACE was first carried out using purified mRNA from HK-2 cells. Figure 4.3 shows a typical RACE result obtained from reactions using the RACE primer, and then the nested RACE-N primer. In repeat reactions, a single (band a) or no product was produced in the first reaction using the RACE primer. Sequence analysis revealed that this was not from the HAS2 locus, but from the mitochondrial genome (accession number AY_275537). The RACE reaction product was then used as the template in a nested 5'-RACE reaction using the RACE-N primer, and produced a number of fragments. Bands b and c were found to be products of non-specific amplification. Band b was also amplified from the mitochondrial genome (AF_346988) and band c was part of the coding sequence for serine/threonine kinase-25 (BC_015793). Bands 1 and 2, however, were HAS2-specific. Sequence analysis of three randomly selected transformants from band 1 revealed that each insert terminated at a different 5'-terminal nucleotide. The longest of these inserts extended the HAS2 5'-UTR of NM_005328 by 49 bp. Corresponding analysis of transformants from the discrete band 2 resulted in a single cloned product. This extended the HAS2 5'-UTR of NM_005328 by 130 bp (Figure 4.4). This sequence has now been submitted to the GenBank/EBI Data Bank with the accession number AJ604570.

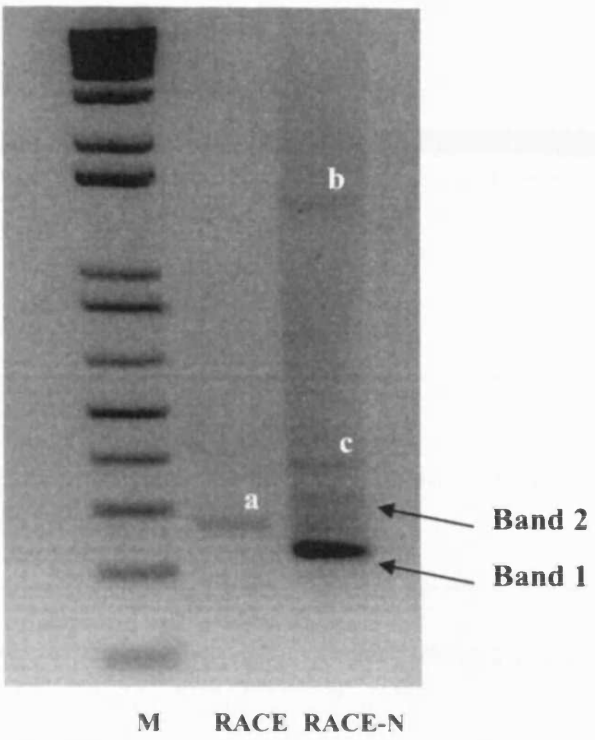

Figure 4.3. 5'-RACE analysis of the HAS2 transcript in HK-2 cells by agarose gel electrophoresis. Lanes for size marker (M) and HAS2 5'-RACE products from purified mRNA using primers RACE and RACE-N are shown. Bands labelled 1 and 2 were specific to the *HAS2* locus. Bands labelled a, b, and c were products of non-specific amplification and their origins are explained in the text.

Repeat 5'-RACE experiments using HK-2 mRNA always generated two HAS2 specific bands of the same size as shown for the experiment above. Sequencing analysis revealed further truncated products of varying lengths from band 1 that extended the HAS2 5'-UTR between 40 and 50 bp. Band 2 always elucidated a single product congruent with the findings above, that extended the HAS2 5-UTR by 130 bp. In no case, however, was band 2 observed in the absence of band 1.

A

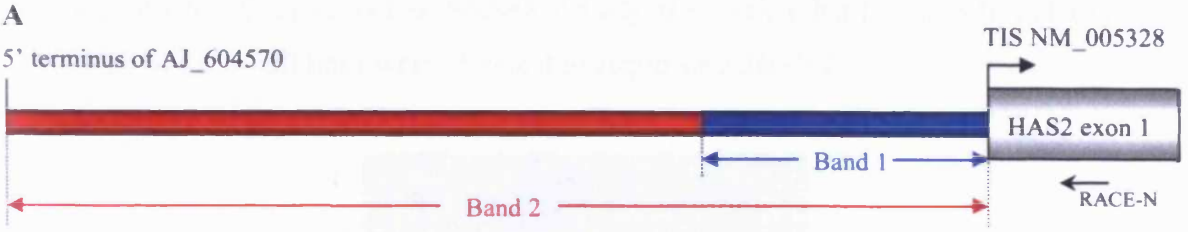

B

Band 2 (sequence AJ604570)

agtccacacctccctctccacttccctcacccccccactccctccgccgccctatta
aaacacccaccagctcacttgttaagacccccttaagttggaggaggcagaagggca
acaacggcggggaaggagaagtcaagacgtctggaaagaa

Band 1

agacccccttaagttggaggaggcagaagggcaacaacggcggggaaggagaagtca
agacgtctggaaagaa

Figure 4.4. A. Schematic of the genomic sequence directly upstream of the TIS for *HAS2* reference sequence NM_005328. The extended HAS2 exon 1 sequence from band 1 RACE products are shown in blue. The additional extended sequence from band 2 RACE products is shown in red. The 5' termination site for sequence AJ604570 is labelled. B. 5' termini of the sequences of band 1 and band 2 produced by 5'-RACE. Nucleotides shared with reference sequence NM_005328 are shown in black. The upstream sequence shared between the largest product from band 1 and products from band 2 are shown in blue. Additional upstream sequence from band 2 products is shown in red. The 5' terminal nucleotide from each band 1 reaction product is in blue and bold. The terminal adenine from the longest band 1 product is in blue, bold and underlined in both sequences.

5'-RACE analysis was then carried out using purified mRNA from HEK293t and TE671 cells. Figure 4.5 shows the products generated using the RACE-N primer for these two cell lines, when compared with those for HK-2. Two bands corresponding to the HAS2-specific bands observed for HK-2 cells (Figure 4.3) were also seen in the

HEK293t and TE671 cell lines. Sequence analysis revealed that products from band 2 for each of these cell lines were identical to sequence AJ604570.

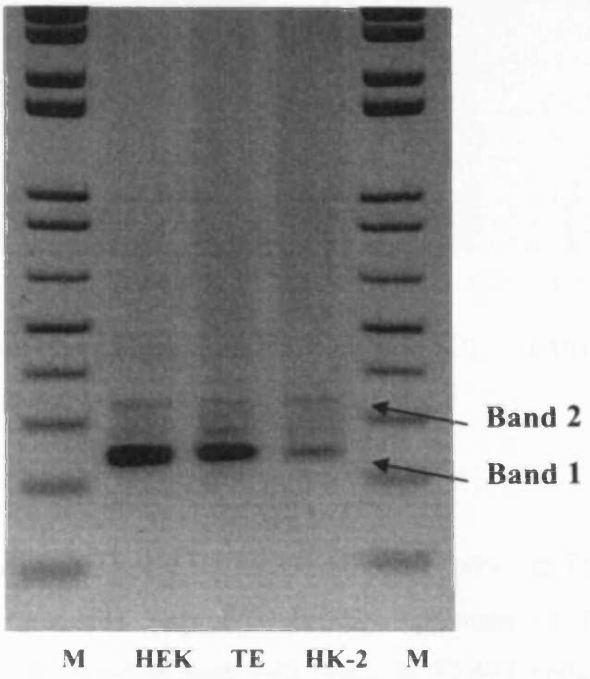

Figure 4.4. 5'-RACE of the HAS2 transcript in HEK293t (HEK), TE671 (TE) and HK-2 cell lines. Lanes for size marker (M) and 5'-RACE products using primer RACE-N are shown. Bands labelled 1 and 2 were specific to the *HAS2* locus.

4.3.3 Luciferase analysis of HAS2 nested promoter constructs

A nested set of HAS2 promoter fragments, with products ranging in size from 117 to 1171 bp, was amplified by PCR (Figure 4.5). Each fragment was then cloned into the pGL3-Mod reporter vector, and analysed for their ability to drive transcription using the established luciferase assay system as described by Coleman et al (2002).

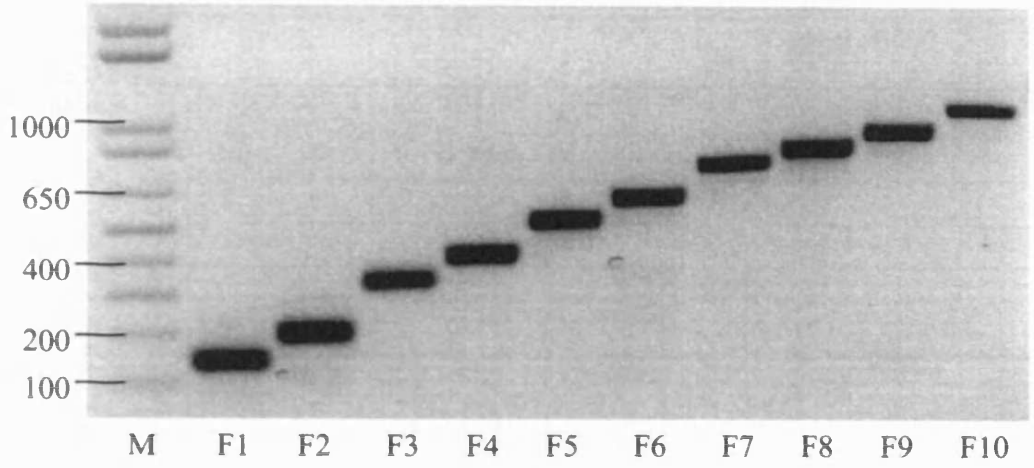

Figure 4.5. Nested set of HAS2 promoter fragments (F1 – F10) amplified by PCR. DNA size standard markers (M) are given in bp.

Luciferase assay data from TE671 and HEK293t cells are shown in Figure 4.6. From initial screening of the genomic sequence directly upstream of NM_005328, a bipartite distribution was observed in both cell lines. In TE671 cells, constructs F1 and F2 showed a very marginal increase in luciferase activity significant at the $p < 0.05$ level, compared to the promoterless control vector (C). A profound increase in activity was, however, displayed by the larger constructs F3-F10, and were found to be highly significant ($p < 0.001$). Constructs F3 and F4 demonstrated over a 30-fold increase in luciferase activity over the promoterless control in TE671 cells. The larger fragments (F5-F10) had lower activity, but were still significantly higher than the control vector. In the HEK293t cell line, constructs F1 and F2 demonstrated no luciferase activity compared to the promoterless control vector, significant at the $p < 0.01$ level. Constructs F3 and F4 exhibited over a 7- and 8-fold increase activity over the promoterless control respectively. This fold increase was then maintained in constructs F5-F10. Statistical analysis also showed that the difference between the low scoring constructs, C, F1 and F2 and the high readings for constructs F3-F10 in HEK293t cells, was highly significant ($p < 0.001$).

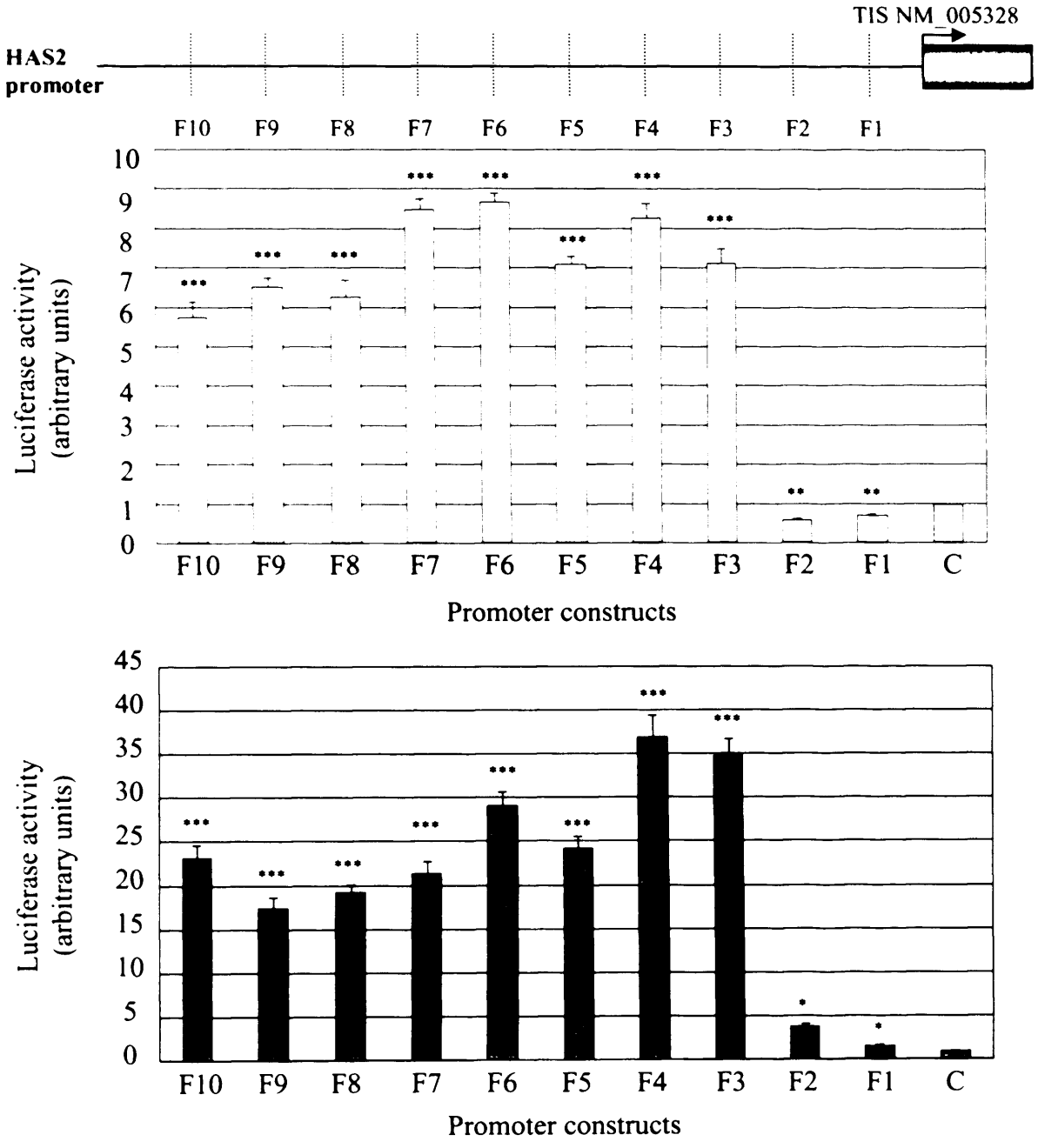

Figure 4.6. Luciferase activity of the genomic sequence directly upstream of HAS2 reference sequence NM_005328. Nested promoter fragments are identified by the sense strand primer designations given in Table 4.2. Data are displayed for HEK293t cells (white bars) and TE671 cells (shaded bars). Luciferase activity is expressed as the magnitude of normalised luciferase activity relative to the pGL3-Mod promoterless negative control vector (C). Significance values are indicated by asterisks: *, $p < 0.05$, **, $p < 0.01$, ***, $p < 0.001$.

4.3.4 RT-PCR to detect expression of the extended HAS2 exon 1

The results of RT-PCR analysis are shown in Figure 4.7. Despite differences in intensity, evidence of transcription of an AJ604570-specific extended HAS2 5'-UTR was detected in each of the cell types assayed. This included the two cell lines used for luciferase analysis (HEK293t and TE671), HK-2 (used for 5'-RACE), lung fibroblasts and also primary peritoneal mesothelial cells. HAS2-Prom-h-RT primers (Table 4.3) amplified the larger product spanning 686 bp, specific to sequence AJ604570 and comprising the 5'-UTR and the N-terminal amino acid codons of HAS2. The smaller band of 282 bp amplified codons from the glycosyltransferase domain of HAS2 using HAS2-h-RT primers (Table 4.3). To obviate the possibility of amplification from contaminating genomic DNA, both sets of primers amplified across one or more intron/exon boundaries spanning at least 11.5 kb of intronic sequence. Orthologous products from the total RNA from mouse and rat kidneys were also amplified. Mouse and rat specific HAS2-Prom-RT primers (Table 4.3) amplified the larger product spanning 645 bp of the corresponding HAS2 region in their respective species. The smaller product was also amplified using species-specific HAS2-RT primers (Table 4.3), and generated products of the same size as found in the human (282 bp). In no case was the message for either 5'-RACE Band 1 mRNA or NM_005328 detected in the absence of AJ604570.

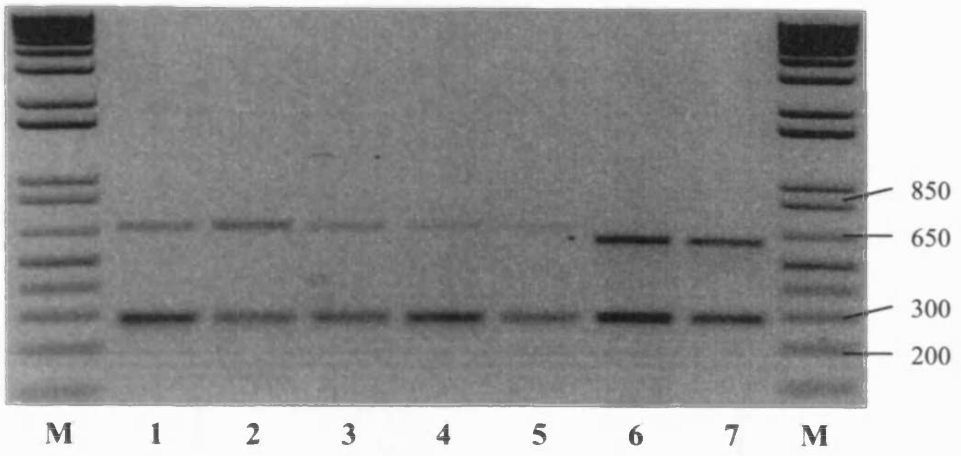

Figure 4.7. RT-PCR analysis of AJ604570 fragments. Upper band represents the extended HAS2 5'-UTR generated using HA2-Prom-RT primers. Lower band represents fragments generated using HAS2-RT primers. Size markers (M) are given in base pairs (bp). Lane 1 - HEK293t; lane 2 - TE671; lane 3 - HK-2; lane 4 - lung fibroblast (AG02222); lane 5 - primary peritoneal mesothelial; lane 6 - mouse kidney; lane 7 - rat kidney.

4.3.5 Analysis of extended HAS2 5'-UTR for secondary structure

The length of the HAS2 5'-UTR, together with the mononuclear repeat arrays of A and T residues in the NM_005328 sequence, and the additional G and C content of the extended HAS2 5'UTR, suggested that this structure might form stable secondary structures such as hairpin loops. The extended HAS2 5'UTR was therefore analysed using MFOLD for evidence of such folding. Using default parameters, 16 different structures were identified. Each structure demonstrated free energies of folding between -129.4 and -134.9 kcal/mol. The structures with the highest and lowest free energy values are shown in Figure 4.8. Numerous hairpin motifs were observed in both of these structures, and together with their high free energy values, provided evidence why there was premature termination of our 5'-RACE products retrieved from band 1 (figure 4.2).

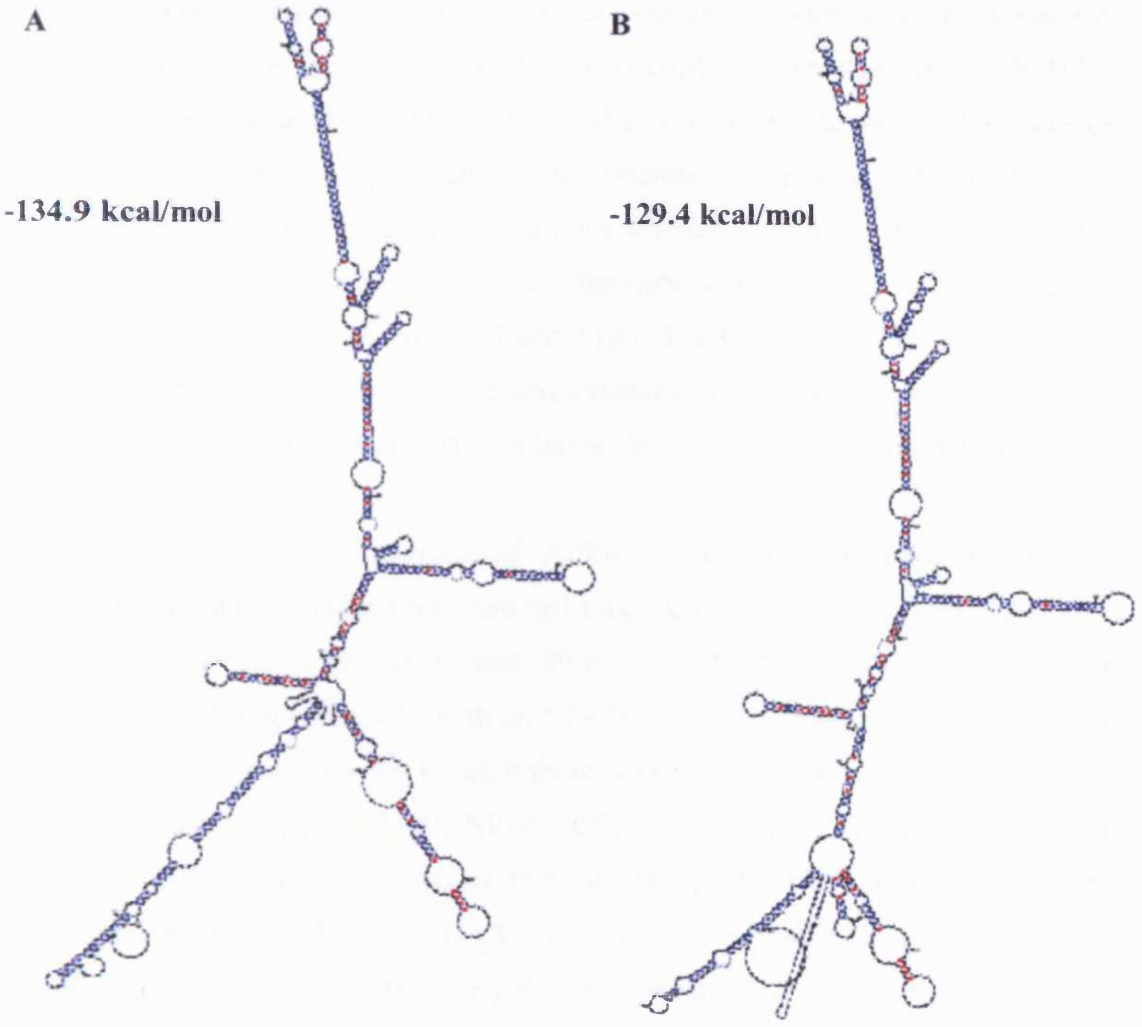

Figure 4.8. Predicted secondary structures of the extended HAS2 5'-UTR calculated using MFOLD. The structures giving the lowest (A) and highest (B) free energies of folding are presented. Hydrogen bonding between pyrimidine (red) and purine (blue) bases are indicated.

4.3.6 Sequence alignment, and EST database analysis of the HAS2 genes from different species

Sequences of the regions upstream of the reference sequences for the human (NM_005328), mouse (NM_008216), rat (NM_013153) and equine (AF_508308) *HAS2* genes were aligned using ClustalW alignment software (Figure 4.9). A total of 200 bp upstream of the 5' terminus of AJ604570 to 150 bp downstream was used as

the consensus sequence. Sequence variations were then highlighted in the mouse (m), rat (r) and equine (e) sequences. The transcription start sites for each HAS2 orthologue were located at different nucleotides. The mouse, rat and equine sequences terminated upstream of human *HAS2* reference sequence NM_005328, but downstream of the newly positioned site for reference sequence AJ604570. A high level of sequence similarity was evident throughout the majority of the alignment, most clearly between positions -100 and +100. The majority of the variations were base substitutions. In addition, there was evidence of base deletion in the three non-human sequences, particularly between bases -46 and -26 of sequence AJ604570.

The sequence directly upstream of AJ604570 was then scanned for putative transcription factor binding sites. Two Sp1 binding sites (Sp1-1 and Sp1-2; see Figure 4.9) were located at positions -60 and -40 respectively. An NF-Y / CCAAT element was observed 80 bp upstream, with an NF-κB site at position -150. The non-human sequences were then analysed to see if these sites were conserved. The mouse and rat sequences contained the NF-κB, NF-Y / CCAAT and Sp1-1 elements and the core motif of Sp1-2 (the remainder of this site being absent). The equine sequence contained the NF-κB, NF-Y / CCAAT and Sp1-1 sites. However, no Sp1-2 site was present as bases -8 to -51 surrounding this site were absent.

The EST database was then examined to see if there were any sequences present that contained part, or all of the extended HAS2 5'-UTR of reference sequence AJ604570. A number of sequences were found for a number of different species. The longest available ESTs from human (CD654109), mouse (BY110777) and bovine HAS2 (AW429456) are highlighted in Figure 4.9. Interestingly, each EST terminated upstream of their reference mRNA sequences.

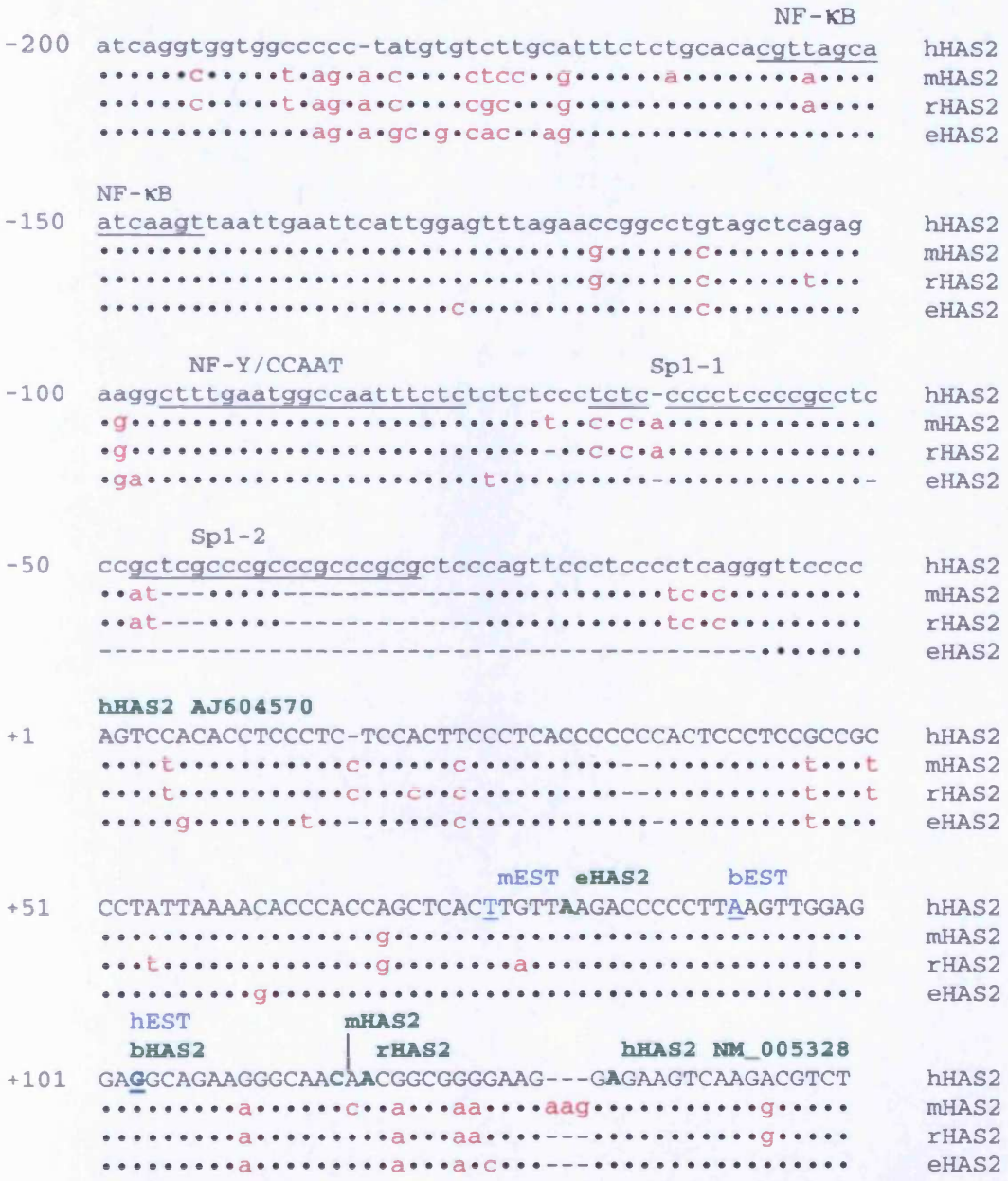

Figure 4.9. Alignment of the sequences upstream of the *HAS2* genes for human (h), mouse (m), rat (r) and horse (equine - e). The 5' terminus of sequence AJ604570 (uppercase) lies at nucleotide +1. The upstream human sequence is in lowercase. The 5' termini of the above reference HAS2 mRNAs, together with that for *Bos taurus* bovine HAS2 (b, NM_174079), are in bold and labelled in green. Sequence differences from human HAS2 are shown by a red lowercase nucleotide (a, c, g or t), and gaps are shown by a dash (-). Putative TFBSs are underlined and labelled. The 5' termini of three HAS2 ESTs are in blue and labelled; hEST, bEST and mEST.

4.4 DISCUSSION

The transcriptional regulation of HAS2 has potential significance in renal fibrosis, diabetic nephropathy and peritoneal inflammation. The genomic structures of the human *HAS* genes were described in Chapter 3, and in this chapter, work was carried out to investigate further the HAS2 promoter region. To identify the location of transcription for HAS2, primer extension analysis was used. Repeated experiments using primers binding at two different sites downstream of the reported HAS2 TIS produced negative results. 5'-RACE was therefore used as another means of locating the HAS2 TIS.

mRNA was purified from HK-2, HEK293t and TE671 cells and used as the template for 5'-RACE reactions. No products of the predicted size for NM_005328 were recovered, suggesting that this database entry was 5'-truncated. A significant number of similarly truncated sequences are deposited in the public databases because imperfect methodologies for creating libraries have generated incomplete cDNAs [Coleman et al, 2002]. The HAS2 specific products generated in the present study were visible as two discrete bands. Sequencing of the products from band 1 revealed that each one terminated at a different nucleotide between 45-50 bp upstream of NM_005328 and 80 bp downstream of the single 5' terminus of band 2. This also suggested that band 1 products were prematurely terminated, possibly due to a strong secondary structure in the HAS2 5'-UTR, as discussed later. Other products generated by 5'-RACE were due to non-specific amplification and were not from the *HAS2* locus. The bands labelled a and b in Figure 4.3 were of mitochondrial origin and band c was part of the coding sequence for serine/threonine kinase-25. These non-specific products were not generated consistently in replicate 5'-RACE reactions. The two HAS2-specific bands, however, were always present. An example of this can be seen in Figure 4.5. The two HAS2-specific bands are present in the three cell lines. No other distinct bands from non-specific amplification are observed.

There are a number of possible reasons why results were obtained using the 5'-RACE procedure and why no results were obtained by primer extension. Both methodologies are based on a reverse transcriptase (RT) reaction. The primer extension system used a different RT enzyme than that used in the 5'-RACE method, which may have not

been so well suited to the HAS2 template. In addition, primer extension does not contain a PCR amplification step after the RT reaction whereas 5'-RACE required a two-step PCR reaction following the RT step before any HAS2 specific bands were observed. Thus, the HAS2 transcript may have been present in low amounts to begin with, and may simply not have been detected in the primer extension experiment.

The high throughput luciferase assay system used had previously been shown to be sensitive, accurate and reproducible in analyses of a large number of human promoters, including naturally occurring polymorphic promoter variants [Coleman et al, 2002; Hoogendoorn et al, 2003]. Work presented in Chapter 3 demonstrated that 500 bp of gDNA immediately upstream of the mRNA reference sequence for each HAS isoform had basal promoter activity. In the present study, the system was used to analyse the ability of a set of nested HAS2 promoter constructs to drive luciferase transcription in HEK293t and TE671 cells. In addition, Friedman's two-way analysis of variance test was used to compare the significance of the variation of promoter activity with the previously established criterion of luciferase activity.

Luciferase analysis provided highly significant evidence that promoter function was only observed in constructs F3-F10 clustered approximately 250 bp upstream of the 5' terminus for NM_005328. In TE671 cells, these constructs also exceeded the 10 fold threshold for promoter activity [Coleman et al, 2002]. Constructs F1 and F2 in TE671 cells did show a marginal increase in luciferase activity, but this was contradicted by a decrease in activity for these constructs in HEK293t cells. Constructs F3-F10 in HEK293t cells demonstrated significant luciferase activities over the promoterless control, but their values were below the 10 fold threshold. It suggested that the HAS2 promoter may have been under tighter control in HEK293t cells than TE671 cells, therefore showing evidence for cell-specific control elements for the *HAS2* gene.

Luciferase analysis demonstrated that the sequence directly upstream of NM_005328 was not active in the luciferase assay. Basal promoter activity also appeared approximately consistent for constructs F3-F10. An overall decrease in activity in the larger vectors was observed, however the assay system had been optimised for 500 bp inserts. These constructs, however, still demonstrated a significant increase in luciferase activity over the promoterless control vector.

On comparing the luciferase data with the 5'-RACE data, constructs F1 and F2 contained inserts spanning 74 and 130 bp respectively of sequence upstream of NM_005328, and downstream of the 5' termination site for sequence AJ604570. If transcription could be initiated at either of these positions, each construct would contain sufficient upstream sequence to contain core promoter elements and the binding site for RNA polymerase II [Nikolov and Burley, 1997]. They would thus be expected to drive luciferase transcription as shown for the sequence upstream of AJ604570 (constructs F3-F10). Comparison of each putative TIS with the consensus sequence YYANWYY (where Y = pyrimidine; W = A or T; N = any nucleotide) described for transcription initiator elements between positions -2 and +5 [Smale, 1997] showed that only the 5' termination site for AJ604570 concurred fully with this or the key nucleotide consensus -2Y, +1A and +3W. The combined data therefore suggested very strongly that the TIS for the *HAS2* gene lay at the 5' terminus of sequence AJ604570, and that the promoter was upstream of this site.

RT-PCR showed that this extended sequence for exon 1 was expressed in two human renal cell lines and also in the mouse and rat kidney. Transcription of this sequence was also observed in human lung fibroblasts and peritoneal mesothelial cells. No evidence for variation in transcript length was found, as products specific for sequences AJ604570 and NM_005328 were detected throughout. There is evidence for a natural antisense mRNA synthesised from the opposite gDNA strand to HAS2 which includes the complementary sequence to the HAS2 TIS (HASNT) [Chao and Spicer, in press]. Because this is a potential confounder of molecular biological analysis of this locus, we designed primers to amplify trans-intronic HAS2-specific RT-PCR products.

Exon 1 of the human *HAS2* gene forms a discrete 5'-UTR, with its translation start site situated at the first base of exon 2. Sequence AJ604570 extends exon 1 (and therefore the 5'-UTR) from 538 to 668 bp. Approximately 10 % of mRNAs contain such complex 5'-UTRs and frequently encode regulatory proteins that may be subject to post-transcriptional regulation. Untranslated AUG motifs and/or secondary structure in excess of -50 kcal/mol in a complex 5'-UTR inhibit significantly the process of cap-dependent ribosomal scanning prior to the initiation of translation [Grobe and Esko, 2002; van der Velden and Thomas, 1999]. Our extended HAS2 5'-

UTR contains one untranslated AUG motif at +650 bp, 20 bp upstream of the predicted translation initiation site and not within a Kozak consensus signal [Kozak, 1987]. Its functional effect may therefore be limited. Analysis of the extended HAS2 5'-UTR for secondary structure showed a propensity for hairpin formation. The free energies of folding for these predicted structures were between -129.4 and 134.9 kcal/mol, much greater than the stated threshold value of -50 kcal/mol. Evidence for post-transcriptional control of the *HAS2* gene was therefore apparent, also giving a possible mechanism for premature termination of our 5'-RACE products from band 1 downstream of the HAS2 TIS.

Alignment of the gDNA sequences surrounding the 5' terminus for sequence AJ604570 for human, mouse, rat and equine *HAS2* loci demonstrated a high degree of similarity, particularly in the extended human HAS2 5'-UTR. Figure 4.9 also provided evidence for the evolutionary conservation of putative TFBSs, in particular Sp1-1, NF-Y/CCAAT and NF-κB. This was not, however, true for Sp1-2. The EST data suggested that the HAS2 reference mRNA sequences deposited in the NCBI database for human, mouse and bovine are 5'-truncated. This may also yet to prove true for the horse and rat orthologues.

In summary, the human HAS2 TIS was relocated 130 bp further upstream than had been previously reported. Evidence also suggested that the reference HAS2 mRNA sequences for mouse and bovine may not be complete. Certain TFBSs were also conserved in the promoter regions between the different species, and it is these that were analysed first in the next set of experiments.

CHAPTER FIVE

CONSTITUTIVE TRANSCRIPTIONAL REGULATION OF THE HUMAN HYALURONAN SYNTHASE 2 GENE

5.1 INTRODUCTION

Specific transcription initiation at class II gene promoters (of which HAS2 is a member) requires the assembly of a precisely positioned RNA polymerase II-containing pre-initiation complex over the core promoter DNA region. This core promoter region is approximately the first 100 bp upstream of the TIS. Most mammalian core promoter regions contain a TATA box at position -25 to -30 bp and/or an initiator element located at the TIS. Each of these can independently specify the location and direction of transcription initiation [Breathnach and Chambon, 1981; O'Shea-Greenfield and Smale, 1992]. On closer inspection of the HAS2 promoter region, no TATA box was identified at the specified location. The initiator element, however, was present at the HAS2 TIS. When present, the TATA box binds the transcription factor TFIID that is essential for the transcription of all mRNA. In the absence of a TATA box, transcription depends more heavily on other sites, including the initiator, in order to recruit TFIID [Crawford et al, 1999].

The core promoter region for the *HAS2* gene contained 2 stimulating protein-1 (Sp1) sites and a CCAAT box as well as a number of other putative TFBSs. The CCAAT box motif is found in 25-30% of all characterised promoters, including housekeeping genes, cell-cycle-regulated genes and tissue-specific and developmentally regulated genes [Bucher, 1990]. It is commonly positioned approximately -75 bp upstream of the TIS and able to initiate transcription with or without a TATA box present. A number of proteins can bind to the CCAAT box, including nuclear factor-Y (NF-Y), CCAAT-enhancer binding protein (C/EBP), nuclear factor-1 (NF-1) and CCAAT-displacement protein [Mantovani, 1998]. Expression of the ephrin-A4 gene, for example, is regulated by NF-Y through a CCAAT box, in the absence of a TATA box [Munthe and Aashiem, 2002].

Sp1 is a common transcription factor that binds to GC-rich regions. It is able to drive constitutive transcription of a number of mammalian genes without the presence of a TATA box, including human α_{1a}-adrenergic receptor [Razik et al, 1997], leukotriene C_4 synthase [Serio et al, 2000] and vascular endothelial growth factor [Brenneisen et al, 2003]. Sp1 can also cooperate with other factors to drive transcription including MAZ [Parks and Shenk, 1996] and NF-Y that binds to the CCAAT box [Pérez-

Gómez et al, 2003; Croager et al, 2000; Facchinetti et al, 2000]. In addition, Sp1 has been implicated to induce and repress the expression of certain genes in response to external stimuli, including the dynamin 1 [Yoo et al, 2002] and macrophage lipoprotein lipase [Hughes et al, 2002] genes respectively. It has also been implicated in repressing the expression of the murine C/EBPα gene in the mouse, yet activating the same gene in *Xenopus laevis* [Kockar et al, 2001].

The Sp1 sites and the CCAAT box in the human HAS2 core promoter region were conserved in the corresponding regions in the mouse and rat (see chapter 4), as was the initiator sequence. Taking this and the evidence from the literature, these sites were investigated to determine their importance in the constitutive expression of the human *HAS2* gene. A second set of promoter constructs were made, deleting each of these putative sites in sequence. These were then assayed for luciferase activity as previously described. DNA probes for each of the HAS2-specific sites were designed and used in EMSA experiments to distinguish if there were proteins binding in these regions. In addition, a specific Sp1 inhibitor was used to see if transcription of the *HAS2* gene could be inhibited. A promoter construct containing mutations at each of the binding sites was also generated to see if promoter activity could be diminished.

5.2 METHODS

5.2.1 Generation of nested promoter constructs for TFBSs and luciferase analysis

Sense strand primers (Table 5.1) were designed to increase the size of core promoter region by approximately 25 bp at a time, corresponding to the addition of a new transcription factor binding site in each case. Using the common antisense strand primer used in chapter 4, four new PCR core promoter fragments were generated (Figure 5.1). Each sense-strand primer was again tailed with a *Kpn* I restriction site, which along with the *Hin* dIII-tailed antisense strand primer, allowed them to be cloned in to the luciferase reporter vector as described previously (section 2.4.2). Constructs were then sequenced to ensure fidelity of amplification.

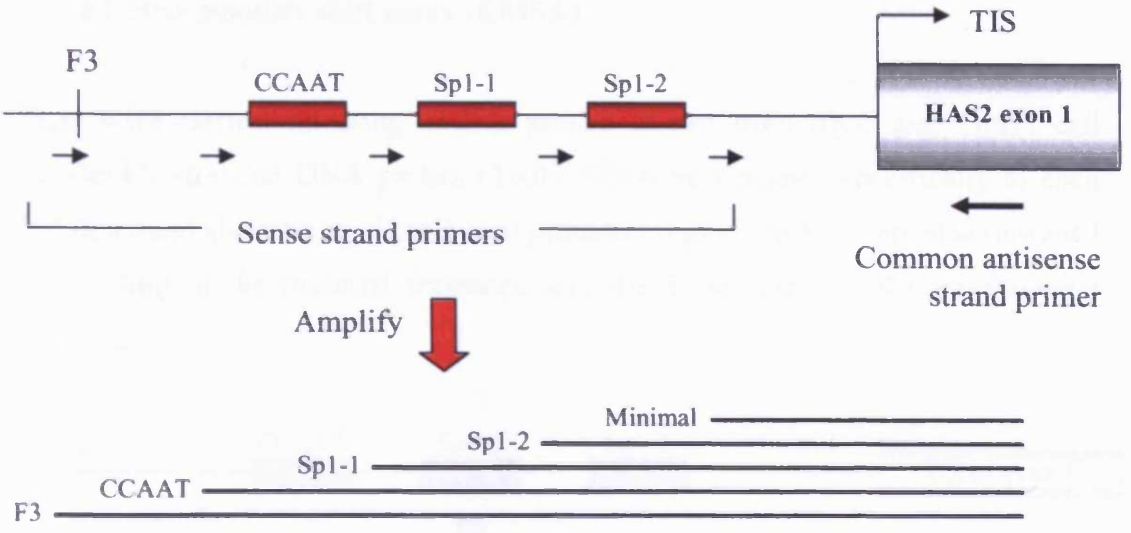

Figure 5.1. Schematic for the generation of nested PCR fragments for the HAS2 core promoter region. Four nested PCR fragments were generated; minimal – minimal promoter region directly upstream of HAS2 TIS; Sp1-2 – furthest 3' Sp1 binding site; Sp1-1 – furthest 5' Sp1 site; CCAAT – CCAAT box / NF-Y binding site. Primer binding sites are illustrated using arrows.

Name	Sense Strand Primer	Antisense Strand Primer	Predicted Size
Minimal	CCGGTACCTCCCAGTTCCCTCCCCTCA	CCAAGCTTCGAAGCCAGGACTGGGTAATTC	209
Sp1-2	CCGGTACCGCTCGCCCGCCCGCCCGCTCCCA	"	229
Sp1-1	CCGGTACCTCTCCCCCTCCCCGCCTCCCGCT	"	249
CCAAT	CCGGTACCTTTGAATGGCCAATTTCTC	"	276

Table 5.1. Oligonucleotide sequences in 5'-3' orientation for the amplification of the nested HAS2 core promoter fragments. The tagged restriction endonuclease recognition sites for *Kpn* I (sense strand primers) and *Hind* III (antisense strand primer) are shown in red. Predicted sizes are also given in base pairs (bp).

The luciferase activity of each of the constructs was then measured in the TE671 and HEK293t cells as described in section 2.5.2, with the modifications to the growth medium as described in section 4.2.5.

5.2.2 Electro-mobility shift assay (EMSA)

EMSAs were carried out using nuclear protein extract from HK-2 and TE671 cell lines. Double-stranded DNA probes (Table 5.2) were designed specifically to each TFBS described above in the HAS2 core promoter region. Probes were also designed corresponding to the minimal fragment, and the 5' terminus of the F3 fragment (Figure 5.2).

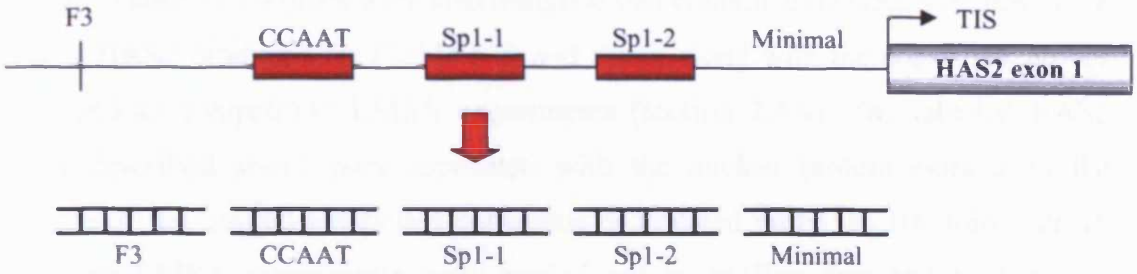

Figure 5.2. Schematic showing DNA probes used in EMSA analysis of the HAS2 core promoter region. 5 probes were designed covering the DNA sequence directly upstream of the HAS2 TIS to the 5' terminus of construct F3.

Probe	Sense Oligonucleotide	Antisense Oligonucleotide
Minimal	CGACCAGTTCCCTCCCCTCAGGGTTCCC	CGAGGGAACCCTGAGGGGAGGGAACTGG
Sp1-2	CGACCGCTCGCCCGCCCCCGCCCCGCTC	CGAGAGCGCGGGCGGCGGGCGAGCGG
Sp1-1	CGACTCCCTCTCCCCCTCCCCGCCTC	CGAGAGGCGGGGAGGGGGAGAGGGAG
CCAAT	CGAAGGCTTTGAATGGCCAATTTCTCTCT	CGAAGAGAGAAATTGGCCATTCAAAGCCT
F3	CGAGAACCGGCCTCTAGCTCAGAGA	CGATCTCTGAGCTACAGGCCGGTTC
mut-minimal	CGACCAGTTCCATACCCTCAGGGTTCCC	CGAGGGAACCCTGAGGGTATGGAACTGG
mut-Sp1-2	CGACCGCTCTACCAACCTACCGCGCTC	CGAGAGCGCGGTAGGTTGGTAGAGCGG
mut-Sp1-1	CGACTCCTTCTCCACTAACCCGACTC	CGAGAGTCGGGTTAGTGGAGAAGGAG
mut-CCAAT	CGAAGGCTTTGAATGGAGTATTTCTCTCT	CGAAGAGAGAAATACTCCATTCAAAGCCT
con-Sp1	CGAATTCGATCGGGGCGGGGCGAGC	CGAGCTCGCCCCGCCCCGATCGAAT
con-NF-Y	CGAAGACCGTACGTGATTGGTGAATCTCTT	CGAAAGAGATTAACCAATCACGTACGGTCT

Table 5.2. Oligonucleotide sequences of the DNA probes used in EMSA experiments. Each oligonucleotide was tailed with a 'cga' motif, indicated in blue. The bases that were changed to generate the mutated probes are indicated in red.

The probes were made and labelled as described in section 2.8.2. The EMSA experiments were then carried out using nuclear protein extract from HK-2 and TE671 cells, as described in section 2.8.3.

5.2.3 Competition and Supershift EMSAs for HAS2 core promoter region

In addition, probes were designed containing the consensus binding sites for NF-Y and Sp1 (Table 5.2). Probes were also designed that contained mutated versions of the specific HAS2 binding sites (Table 5.2) and these, along with the consensus probes were used in competition EMSA experiments (section 2.8.4). The labelled HAS2 probes described above were incubated with the nuclear protein extracts in the presence of the desired unlabelled consensus or mutated probe (in 100-fold excess). Supershift EMSA experiments were carried out to confirm that Sp1 protein was binding to the HAS2-specific DNA probes (section 2.8.5), using an antibody specific to the PEP-2 subunit of the Sp1 complex. Pre-immune serum was also added to one sample in each case to prove that the shifts observed using the PEP-2 antibody were specific.

5.2.4 Inhibition of HAS2 gene expression using mithramycin detected by RT-PCR

The Sp1-specific inhibitor, mithramycin was used in an attempt to inhibit HAS2 expression. Mithramycin (plicamycin®) belongs to the aureolic acid family isolated from *Streptomyces griseus* [Slavik and Carter, 1975]. It is a DNA-binding anti-tumour agent, which has been used clinically in several cancer therapies and Paget's disease [Kennedy, 1972; Du Priest and Fletcher, 1973; Elias and Evans, 1972]. It is known to specifically inhibit the binding of the transcription factor Sp1 to its cognate site in DNA by modifying the CG sequences, e.g., in the dihydrofolate reductase gene [Blume et al, 1991]. To determine if HAS2 gene expression could be inhibited using this drug, growth arrested HK-2 cells were treated for 24 h in the presence of increasing doses of mithramycin prior to RNA extraction. 1 μg of RNA from each sample was then reverse transcribed, followed by PCR using human HAS2-specific (table 4.3), β-actin-specific (table 5.3) and dihydrofolate reductase-specific (DHFR -

table 5.3) primers as described in section 2.7.5. PCR products were then analysed by gel electrophoresis.

Name	Sense oligonucleotide	Antisense oligonucleotide	Predcited size
Beta-actin	GGAGCAATGATCTTGATCTT	CCTTCCTGGGCATGGAGTCCT	204
DHFR	TAAACTGCATCGTCGCTGTG	GTTTAAGATGGCCTGGGTGA	387

Table 5.3. Oligonucleotide sequences of the primers used to detect expression of the housekeeping gene, β-actin and the dihydrofolate reductase (DHFR) gene by RT-PCR. The predicted sizes of the products are given in bp.

5.2.5 Inhibition of luciferase activity using the Sp1 inhibitor, mithramycin

HK-2 cells transfected with the F3 HAS2 promoter construct (section 2.5.1 with modifications as described in section 4.2.5) were incubated with or without 5 μM mithramycin for 24 hours prior to luciferase analysis. Statistical analysis was carried out using the non-parametric Wilcoxon signed rank test from SPSS for Windows.

5.2.6 Generation of mutated promoter construct

To further confirm the importance of the Sp1 sites in the constitutive expression of HAS2, a promoter construct containing these sites mutated was generated in which key residues in these sites were changed as described in section 2.9. A wildtype construct of the same length was also produced to use as a direct comparison. The luciferase activity of both constructs was then tested in HK-2 cells. Statistical analysis was carried out using the non-parametric Wilcoxon signed rank test from SPSS for Windows.

5.3 RESULTS

5.3.1 Luciferase analysis of HAS2 core promoter region

Luciferase activity of the nested constructs of the HAS2 core promoter region is shown in Figure 5.3. The activity of each construct is represented as a percentage of the activity recorded for construct F3. In TE671 cells, there was a gradual increase in activity as the size of the promoter fragment increased. The 'minimal' construct contained approximately 20% of the activity shown by F3; this then increased along with the size of the insert, with the Sp1-2, Sp1-1 and CCAAT-box constructs showing luciferase activity of 50%, 60% and 80% of construct F3 respectively. A different pattern was seen in HEK293t cells. No activity was detected with the 'minimal' and Sp1-2 constructs. A 30% activity was then observed by the Sp1-1 fragment, with the CCAAT box construct demonstrating 50% of the activity shown by F3.

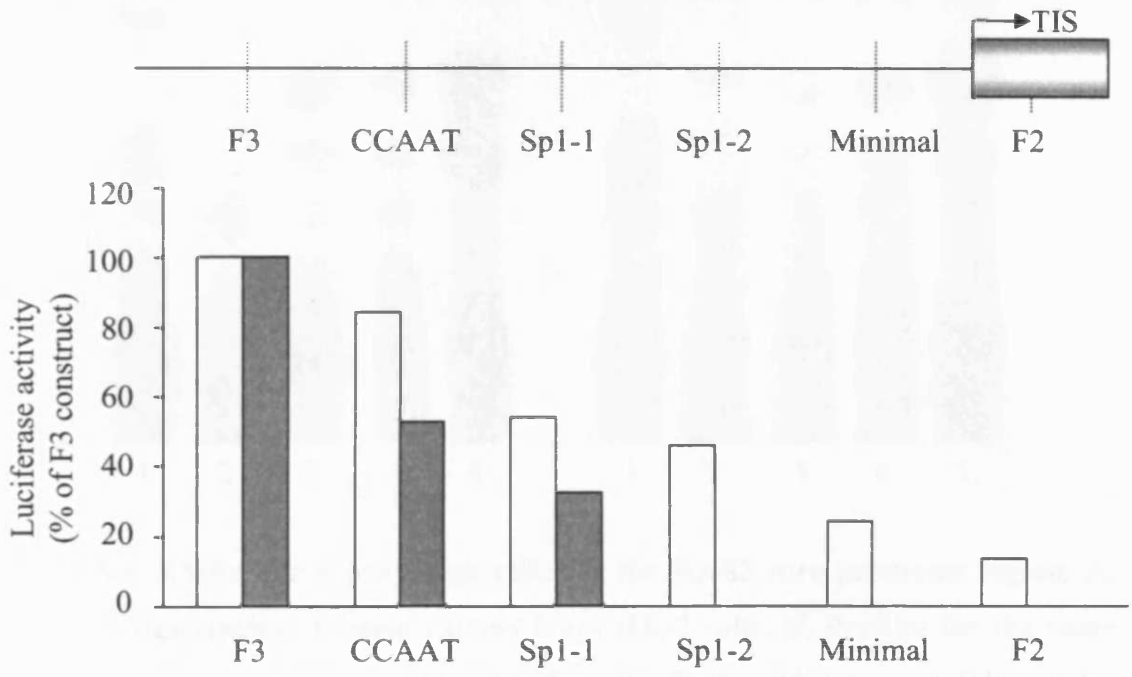

Figure 5.3. Luciferase activity of the nested constructs of HAS2 core promoter region. Data is displayed for TE671 cells (white bars) and HEK293t cells (shaded bars). Luciferase activity is expressed as the magnitude of normalised luciferase activity relative to construct F3.

5.3.2 Identification of proteins binding to the HAS2 core promoter region by EMSA

Gel shift assays were used to identify the proteins binding to the HAS2 core promoter region (the DNA sequence between constructs F2 and F3). Figure 5.4 demonstrated that in both HK-2 and TE671 cells, there was evidence of DNA-protein interaction for each of the HAS2 probes. HK-2 cells showed evidence of protein binding with the minimal, Sp1-2, Sp1-1 and F3 probes, whereas TE671 cells demonstrated binding with the minimal, Sp1-2, CCAAT box and F3 probes. The strongest association was seen for the 'minimal' probe in both cell lines. Interestingly, the profile observed for the minimal probe was identical to those profiles observed for Sp1-2 and Sp1-1. It therefore suggested that there was a Sp1 binding site in this region. Analysis of the F3 probe sequence revealed no specific TFBSs using default parameters.

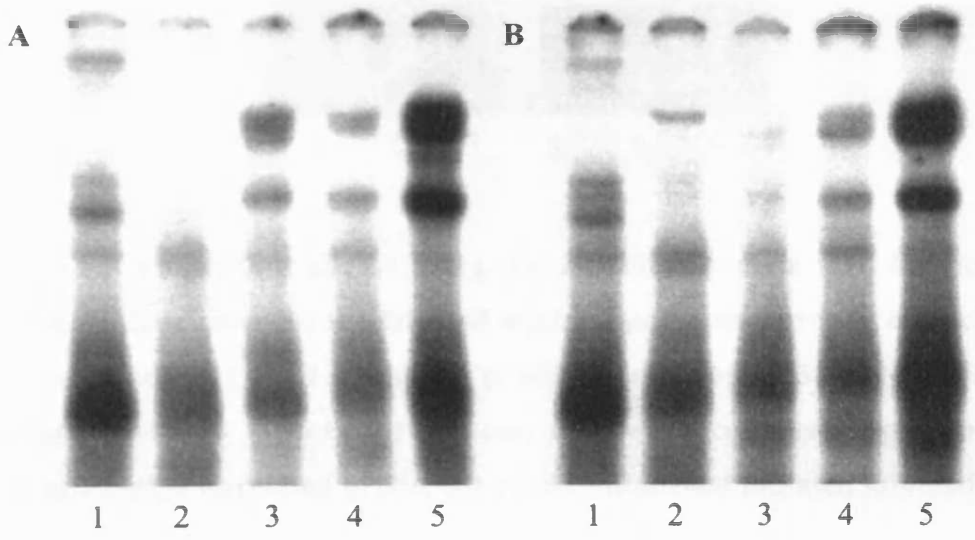

Figure 5.4. EMSA for 5 probes specific for the HAS2 core promoter region. A. Profiles using nuclear protein extract from HK-2 cells. B. Profiles for the same probes using nuclear protein from TE671 cells. Probes used were as follows; 1 – F3; 2 – CCAAT; 3 – Sp1-1; 4 – Sp1-2; 5 – Minimal.

Each of the DNA probes for the minimal, Sp1-2, Sp1-1 and CCAAT box regions were then analysed individually. Binding of the minimal, Sp1-2 and Sp1-1 probes was abrogated using an excess of the corresponding unlabelled probes. In addition,

analogues of each probe with key residues mutated were designed in order to compete for protein binding with the wildtype versions. An unlabelled consensus Sp1 probe was also used in excess, to determine which of the bands observed on the gel were specific for Sp1. An unrelated unlabelled probe, STAT1, was also used as a negative control.

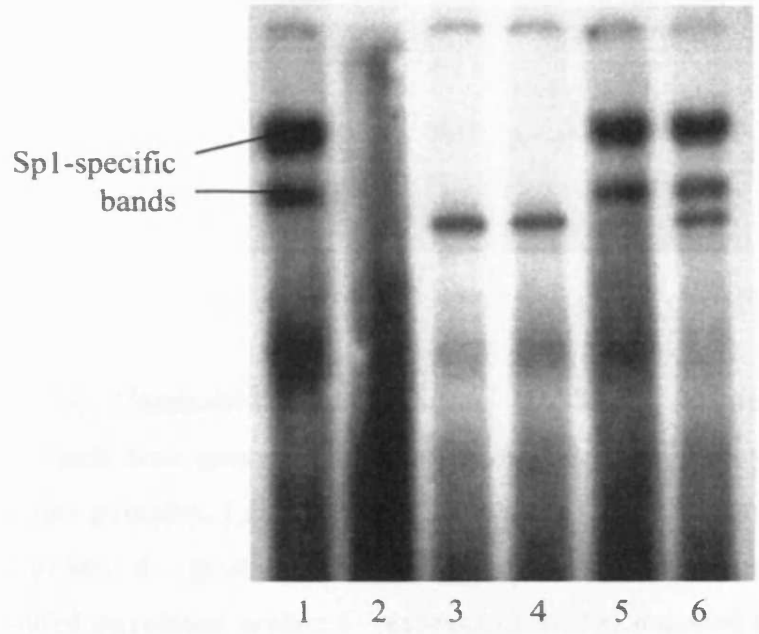

Figure 5.5. Competition EMSA using HK-2 nuclear protein with the 'minimal' probe. Each lane contains the labelled minimal probe and protein extract except lane 2 (no protein). Lane 1 – minimal probe; 2 – no protein; 3 – excess unlabelled 'minimal' probe; 4 – probe with excess unlabelled consensus Sp1 probe; 5 – excess unlabelled unrelated probe; 6 – excess unlabelled mutated minimal probe.

Figure 5.5 shows the results from the competition EMSAs for the 'minimal' probe using HK-2 nuclear protein extract. The bands labelled in lane 1 (probe and labelled probe only) disappeared when the reactions were treated with an unlabelled version of the minimal probe in excess, suggesting that they were specific for HAS2. Upon treatment with the unlabelled Sp1 consensus probe, the bands were undetectable, suggesting that they were specific for Sp1. The mutated minimal probe and the unrelated probe had little effect on the formation of the Sp1 complexes.

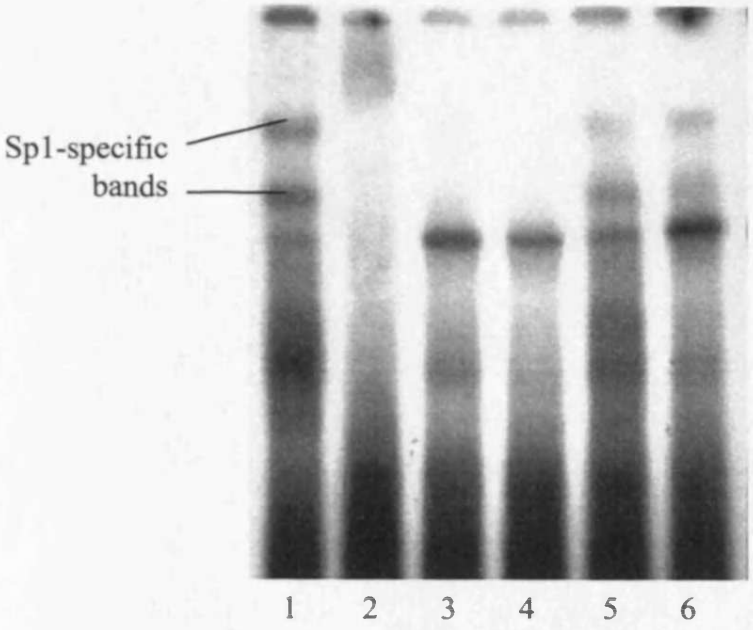

Figure 5.6. Competition EMSA using HK-2 nuclear protein with the Sp1-2 probe. Each lane contains the labelled Sp1-2 probe and protein extract except lane 2 (no protein). Lane 1 – Sp1-2 probe; 2 – no protein; 3 – excess unlabelled Sp1-2 probe; 4 – probe with excess unlabelled consensus Sp1 probe; 5 – excess unlabelled unrelated probe; 6 – excess unlabelled mutated Sp1-2 probe.

Figure 5.6 shows the competition EMSA using the Sp1-2 probe. A similar profile was observed as shown when using the 'minimal' probe, with however, much less intensity. Upon treatment with the unlabelled Sp1 probes (Sp1-2 and consensus Sp1; lanes 3 and 4 respectively) in excess, the bands labelled in lane 1 disappeared, suggesting specificity for Sp1. Treatment with unlabelled mutated Sp1-2 (lane 7) and unrelated (lane 6) probes in excess had minimal effects on protein binding with the labelled Sp1-2 probe.

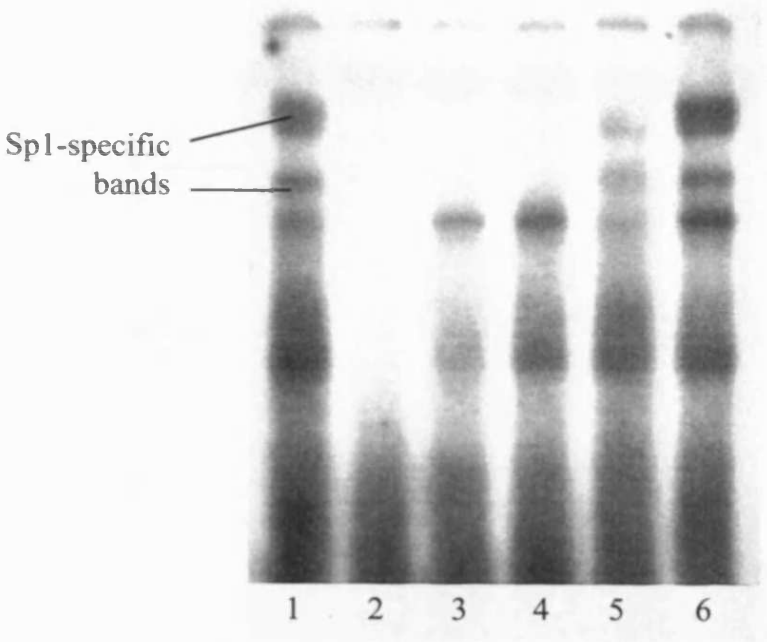

Figure 5.7. Competition EMSA using HK-2 nuclear protein with the Sp1-1probe. Each lane contains the labelled Sp1-1 probe and protein extract except lane 2 (no protein). Lane 1 – Sp1-1 probe; 2 – no protein; 3 – excess unlabelled Sp1-1 probe; 4 – probe with excess unlabelled consensus Sp1 probe; 5 – excess unlabelled unrelated probe; 6 – excess unlabelled mutated Sp1-1 probe.

Figure 5.7 shows the competition EMSA for HK-2 cells using the Sp1-1 probe. Upon treatment with unlabelled Sp1-1 (lane 3) and consensus Sp1 (lane 4) probes in excess, the bands labelled in lane 1 (labelled Sp1-1 probe with protein only) were not observed, again suggesting their specificity for Sp1. The unrelated unlabelled probe appeared to have an inhibitory effect on binding when added in excess (lane 6). In contrast, the mutated unlabelled Sp1-1 probe showed no effect on protein binding to the labelled Sp1-1 probe (lane 7).

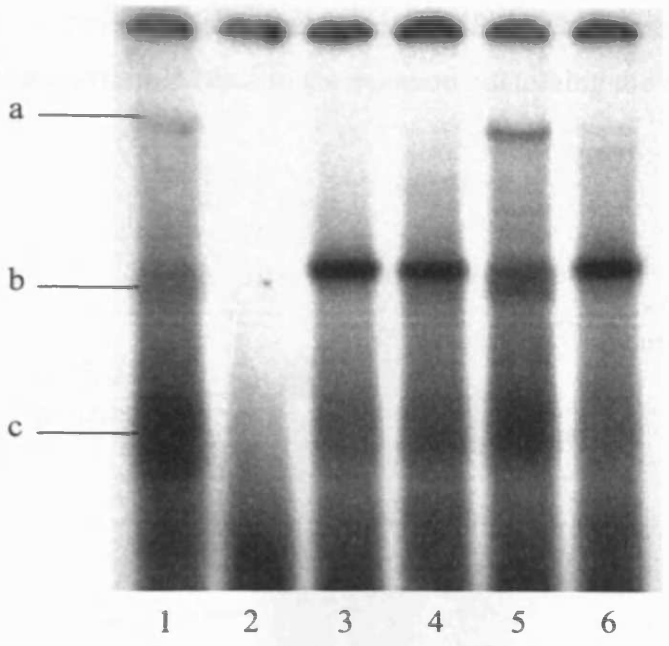

Figure 5.8. Competition EMSA using HK-2 nuclear protein with the CCAAT probe. Each lane contains the labelled CCAAT probe and protein extract except lane 2 (no protein). Lane 1 – CCAAT probe; 2 – no protein; 3 – excess unlabelled CCAAT probe; 4 – probe with excess unlabelled consensus NF-Y probe; 5 – excess unlabelled unrelated probe; 6 – excess unlabelled mutated CCAAT probe. Bands labelled a, b and c were a product of non-specific binding.

Figure 5.8 shows the competition EMSA for HK-2 cells using the CCAAT box probe. Upon treatment with unlabelled CCAAT (lane 3) and consensus NF-Y (lane 4) probes in excess bands a and b were absent. Band c was present, but a lower intensity. This suggested that one or all of these complexes were specifically binding to the CCAAT box. In addition, a new band was observed, probably as a result of non-specific binding. Treatment with an unlabelled unrelated probe in excess (lane 5) had no effect on the binding, compared to lane 1. In contrast, the addition of an unlabelled mutated CCAAT probe in excess (lane 6) inhibited protein binding to the labelled CCAAT probe. This suggested that the bands seen in lane 1 were not CCAAT-specific.

The above data suggested a strong role for Sp1 in the constitutive transcription of HAS2. It was therefore necessary to confirm the direct binding of Sp1 to the HAS2 specific probes. Using the Sp1 binding antibody PEP-2, supershift EMSAs were

carried out by incubating the nuclear protein extract with the radiolabelled 'minimal', Sp1-2 and Sp1-1 probes in the presence of PEP-2. The presence of Sp1 would be shown by a greater retarded band in the reaction containing the antibody.

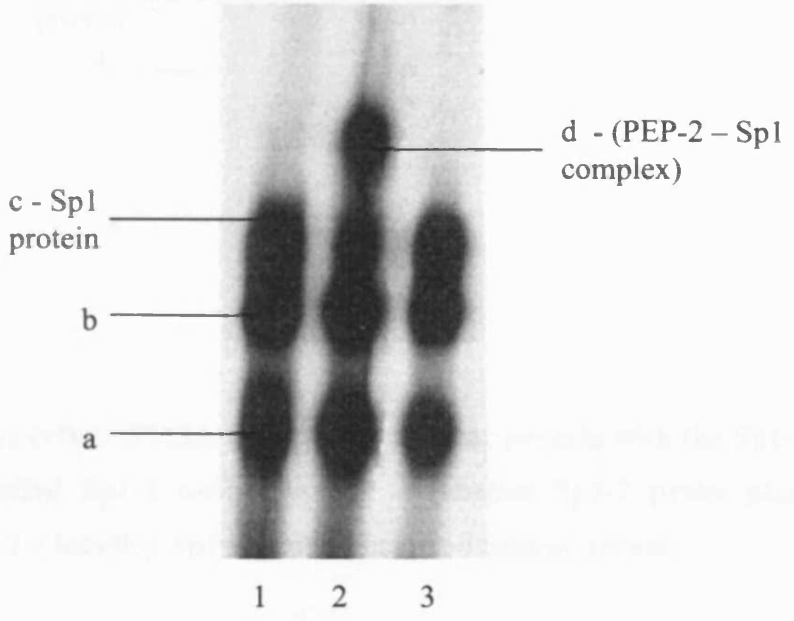

Figure 5.9. Supershift EMSA using HK-2 nuclear protein with the 'minimal' probe. Lane 1 – labelled 'minimal' probe; lane 2 – labelled 'minimal' probe plus PEP-2 antibody; lane 3 – labelled 'minimal' probe plus pre-immune serum.

Figure 5.9 shows the supershift EMSA using the 'minimal' probe. Addition of the PEP-2 antibody (lane 2) showed evidence of a new protein complex (band d) that was absent in the sample containing no antibody (lane 1). In addition, band c in lane 2 was less intense than the same band in lane 1, suggesting that the same protein was present in the complex represented by bands c and d. The absence of band d in the pre-immune serum control sample (lane 3) proved that band d was specific for the PEP-2 antibody, thereby confirming the presence of Sp1. There was no difference in intensity of bands a and b between lanes 1 and 2, suggesting that neither band contained Sp1.

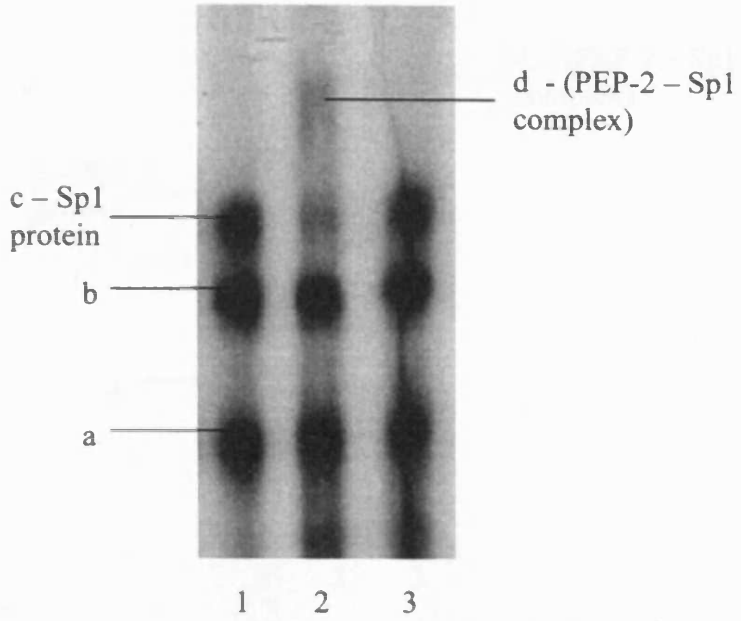

Figure 5.10. Supershift EMSA using HK-2 nuclear protein with the Sp1-2 probe. Lane 1 – labelled Sp1-2 probe; lane 2 – labelled Sp1-2 probe plus PEP-2 antibody; lane 3 – labelled Sp1-2 probe plus pre-immune serum.

Figure 5.10 shows the supershift EMSA for HK-2 nuclear protein with the Sp1-2 probe. This showed a similar profile to that obtained using the 'minimal' probe. The intensity of the bands however, was lower. A fourth discrete band (band d) could be observed when the protein was incubated in the presence of PEP-2 (lane 2). This band was not present when the antibody was absent (lane 1), or in the sample containing the pre-immune serum control (lane 3), confirming that this band was again a PEP-2/Sp1 complex. The intensity of band c in lane 2 was significantly less intense than the same band in lane 1, confirming that band c represented the Sp1 protein. As for the minimal probe, no difference in intensity was observed for bands a and b in all three lanes.

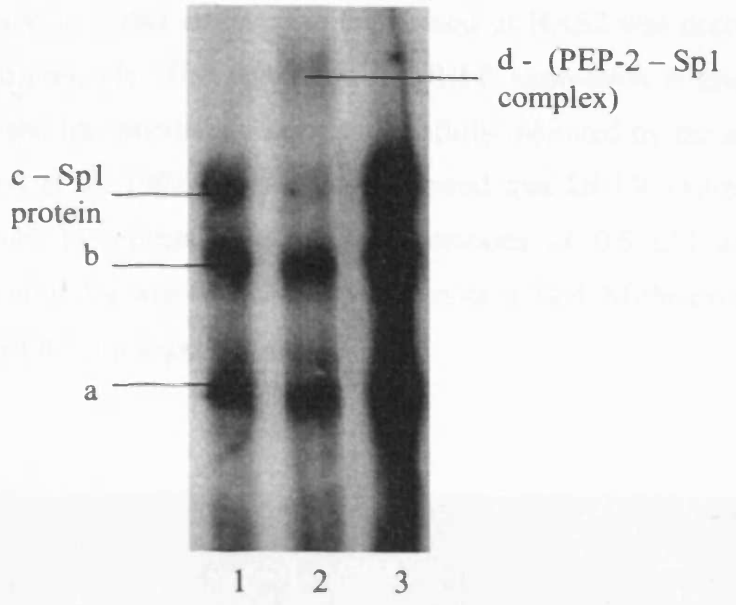

Figure 5.11. Supershift EMSA using HK-2 nuclear protein with the Sp1-1 probe. Lane 1 – labelled Sp1-1 probe; lane 2 – labelled Sp1-1 probe plus PEP-2 antibody; lane 3 – labelled Sp1-1 probe plus pre-immune serum.

Figure 5.11 shows the supershift EMSA for HK-2 cells using the Sp1-1 probe. As for the 'minimal' and Sp1-2 probes, a protein complex was observed (band d) unique to the sample containing the PEP-2 antibody (lane 2). This band was not present when the antibody was absent (lane 1), or in the sample containing the pre-immune serum control (lane 3), confirming that this band was a PEP-2/Sp1 complex. The intensity of band c in lane 2 was again significantly decreased in the presence of the PEP-2 antibody, confirming it represented the Sp1 protein. As for the minimal probe, no difference in intensity was observed for bands a and b between lanes 1 and 2, suggesting that these bands did not contain any Sp1 protein.

5.3.3 Inhibition of *HAS2* gene expression using mithramycin

Mithramycin is a compound that directly competes the binding of Sp1 proteins to its DNA recognition sequences. Figure 5.12 shows the effect of increasing doses of mithramycin on the constitutive expression of the HAS2, dihydrofolate reductase (DHFR) and the β-actin genes in HK-2 cells,. At moderate concentrations (0.2, 0.5 and 1 μM) it had no effect on the expression levels of HAS2. As the concentration of

the inhibitor increased to 5 and 10 μM, the expression of HAS2 was decreased, but was not inhibited completely. The regulation of DHFR expression is known to be controlled by Sp1, and has previously been successfully inhibited by the addition of mithramycin [Blume et al, 1991]. Figure 5.12 showed that DHFR expression was successfully inhibited by mithramycin at concentrations of 0.5 μM and above, confirming that the inhibitor was functioning in the system used. Mithramycin had no effect on the levels of β-actin expression.

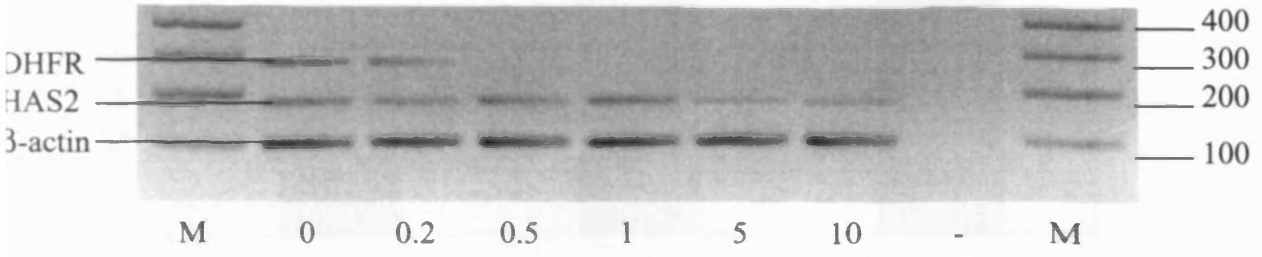

Figure 5.12. Effect of mithramycin on the expression of HAS2 in HK-2 cells. HK-2 cells were treated with increasing concentrations of mithramycin (0.2 – 10 μM) or without the inhibitor (0) and the mRNA levels of DHFR, HAS2 and the housekeeping gene β-actin were measured. DNA size standard markers (M) are given in bp.

This provided further evidence that Sp1 was important for the constitutive expression of HAS2, however, only high concentrations of mithramycin had an inhibitory effect on the basal expression levels. Furthermore, it did not completely eradicate HAS2 expression. To determine if mithramycin could inhibit the binding of Sp1 to the core promoter region, the F3 HAS2 promoter construct was examined for its ability to drive transcription of the luciferase gene in the presence of the inhibitor. After transfection with the F3 construct, HK-2 cells were treated with 5 μM mithramycin for 24 hours prior to the luciferase assay. Figure 5.13 shows one of three repeat experiments using the inhibitor. Mithramycin was able to inhibit the transcriptional activity of the F3 construct, but not eradicate the activity completely. In the absence of the inhibitor, the F3 construct demonstrated almost a 7 fold increase in luciferase activity over the promoterless control, which was found to be highly significant ($p <$

0.05). This was decreased to a 5.6 fold increase in the presence of mithramycin, but was still significantly higher than the promoterless control ($p < 0.05$).

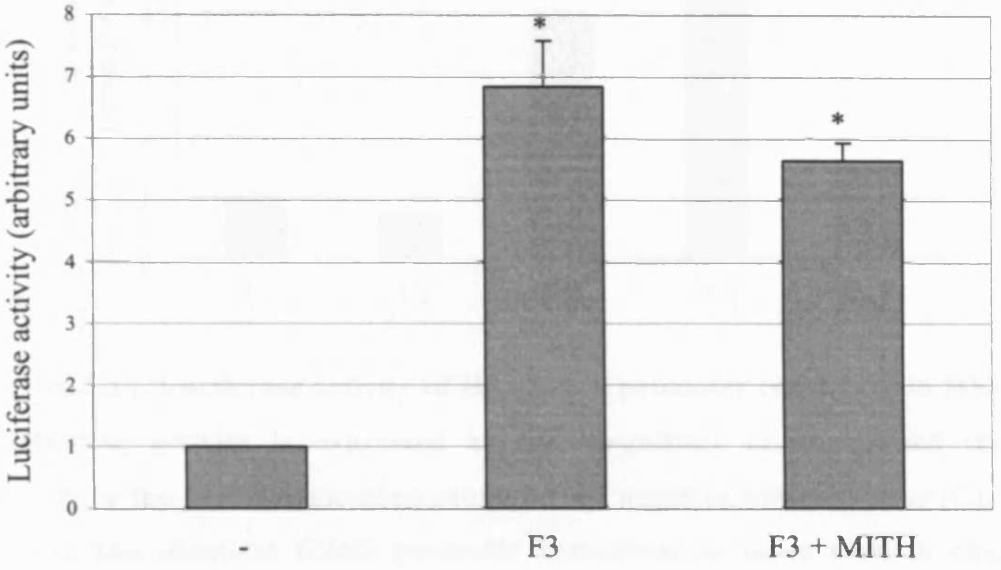

Figure 5.13. Effect of mithramycin on the luciferase activity of the F3 HAS2 promoter construct in HK-2 cells. Transfected cells were incubated in the absence (F3) or presence (F3 + MITH) of 5 μM mithramycin. Luciferase activity is expressed as the magnitude of normalised luciferase activity to the promoterless control vector (-). Asterisks represent statistical significance ($p < 0.05$).

5.3.4 Luciferase analysis of promoter constructs containing mutated Sp1 binding sites

EMSA analysis had suggested a role for Sp1 in the constitutive expression of HAS2. Two luciferase promoter constructs were therefore designed containing the HAS2 core promoter region; the first with the wildtype promoter sequence, the second containing mutations (in the form of base substitutions) of the Sp1 binding sites in the Sp1-1, Sp1-2 and minimal regions. These were then tested for luciferase activity in HK-2 cells and compared to the activity of the constructs used in chapter 4.

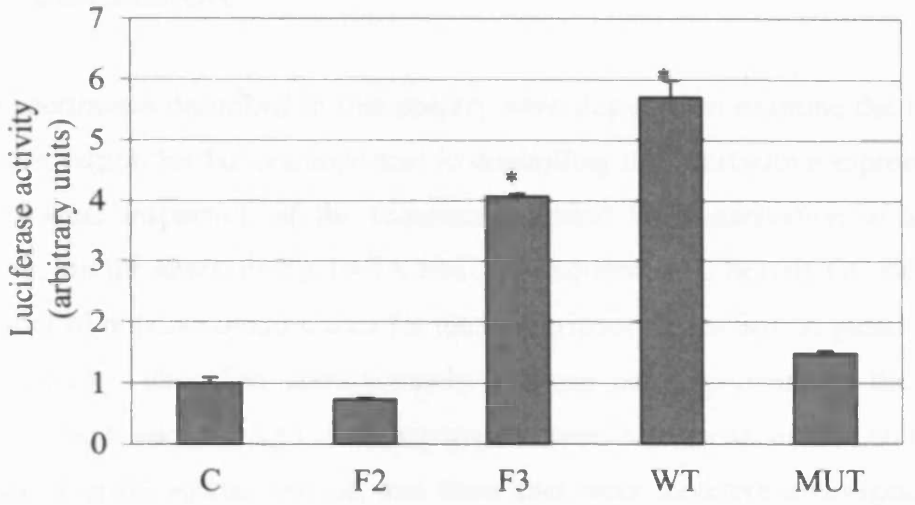

Figure 5.14. Luciferase activity of HAS2 core promoter constructs in HK-2 cells. Luciferase activity is expressed as the magnitude of normalised luciferase activity to the pGL3-Basic-Mod promoterless negative control vector (C). F2 and F3 are the identical HAS2 promoter constructs to those used in chapter 4. Luciferase activity for the new wildtype (WT) and mutated (MUT) HAS2 core promoter constructs are also given. Asterisks represent statistical significance ($p < 0.05$).

The luciferase activity of these constructs in the HK-2 cell line is shown in Figure 5.14. As was seen in the TE671 and HEK293t cell lines, construct F2 demonstrated no activity when compared to the negative control (C). Construct F3 showed significant luciferase activity ($p < 0.05$), with a 4-fold increase over the promoterless vector. Significant luciferase activity was also demonstrated by the wildtype (WT) HAS2 promoter construct, showing nearly a 6-fold increase ($p < 0.05$). This activity was almost abolished in the mutated promoter construct (MUT), displaying only a 1.5-fold increase over the negative control.

5.4 DISCUSSION

The experiments described in this chapter were designed to examine the HAS2 core promoter region for factors important in controlling the constitutive expression of the gene. Visual inspection of the sequence revealed the conservation of an initiator element, but the absence of a TATA box. The sequence was heavily GC-rich, creating a number of putative binding sites for the transcription factor Sp1. A putative CCAAT box was also identified approximately 80 base pairs upstream of the TIS. The initiator, Sp1 and CCAAT box sequences were conserved in the corresponding sequences in the mouse and rat, and these sites were therefore investigated in more detail.

A set of nested promoter constructs for the HAS2 core promoter region were designed and tested for their ability to drive transcription of the luciferase gene. In each cell line, there was an incremental rise in luciferase activity as the insert size increased, confirming that this sequence was functionally active as a promoter. The smaller constructs were unable to drive transcription in HEK293t cells unlike in TE671 cells. The larger constructs (CCAAT and Sp1-1) did demonstrate constitutive promoter activity.

EMSA identified DNA/protein complexes forming at common areas of the HAS2 core promoter in both TE671 and HK-2 cells. Interestingly, identical complexes were observed using the Sp1-1, Sp1-2 and 'minimal' probes. Complexes were also observed that were unique for the CCAAT box and F3 probes, but these were far less prominent than those seen using the Sp1-1, Sp1-2 and 'minimal' sequences. This suggested that the key factors required for constitutive *HAS2* transcription were binding in the Sp1-1, Sp1-2 and minimal regions of the core promoter.

The complexes binding to the 'minimal' probe appeared identical to those binding to the two Sp1 probes. This suggested that the 'minimal' probe contained a putative Sp1 site not identified by the MatInspector software, but which was apparent after visual inspection. Using a different transcription factor binding site identification program called TFSearch (http://www.cbrc.jp/research/db/TFSEARCH.html) with a threshold cut-off value of 75.0, a putative Sp1 site was identified between positions –14 and –23

bp. This showed that Sp1 was now able to bind to three possible areas within the HAS2 core promoter region.

Competition studies were carried out on the CCAAT box and the three putative Sp1 sites. A DNA probe containing the consensus Sp1 sequence was used to determine if any of the complexes observed using the Sp1-1, Sp1-2 and 'minimal' probes were specific for Sp1. The observed complexes were successfully inhibited from binding with all three probes, suggesting that one or more of these may represent Sp1. In addition, it was the same complexes that were inhibited for each of the probes tested. This further supported evidence that Sp1 was successfully binding to the 'minimal' probe. Mutated Sp1-1, Sp1-2 and 'minimal' probes were also designed and used in competition studies. No effect on binding to the wildtype Sp1-1 and 'minimal' probes was observed in the presence of their mutated counterparts, however inhibition was seen for the Sp1-2 sequence. This suggested that the Sp1-2 sequence in the HAS2 promoter was less specific for binding Sp1 than the Sp1-1 and minimal sequences. Indeed, Figure 5.4 (A) showed that the bands obtained using the Sp1-2 probe were less prominent than those bands observed using the Sp1-1 and minimal probes, providing further support for a lower degree of specificity of the Sp1-2 sequence for the Sp1 protein.

Three complexes observed using the CCAAT box probe were successfully inhibited using a consensus NF-Y probe in excess. However, the same three complexes were also successfully inhibited using its mutated counterpart. This suggested that the CCAAT site in the HAS2 promoter was capable of protein binding, but that it was not specific for *HAS2* transcription. Putative CCAAT box sequences have been investigated thoroughly for their ability to aid transcription of a number of different genes. The HAS2 core promoter CCAAT sequence correlated with those CCAAT sequences that were found to be inactive [Mantovani, 1999]. This further suggested that it did not play a role in the constitutive expression of HAS2.

Supershift analysis revealed that the larger complex binding to the Sp1-1, Sp1-2 and 'minimal' was indeed Sp1. No shift of the smaller complexes was observed. Previous reports have observed similar binding profiles to those identified here for HAS2. In many cases, the smaller complexes have been identified as the transcription factor

Sp3. Sp3 is of the same family of proteins as Sp1, and has been shown to be involved in transcriptional regulation, in particular in co-operation with Sp1 [Hughes et al, 2002; Serio et al, 2000]. Its role in the regulation of HAS2 expression is yet to be determined.

To further confirm the role of Sp1 in the constitutive expression of the *HAS2* gene, the Sp1-specific inhibitor mithramycin was used to try and repress *HAS2* transcription. RT-PCR analysis showed that moderate doses (up to 1 μM) of the inhibitor had no effect on the expression levels of HAS2. Doses of 5 and 10 μM mithramycin did lower *HAS2* transcription, but did not inhibit it completely. Analysis of the effect of the inhibitor by luciferase assay on the HAS2 core promoter directly gave similar results. Five μM mithramycin inhibited the transcriptional activity of the F3 promoter construct, but not to such an extent as to stop transcriptional activity completely. The mithramycin did successfully inhibit the expression of DHFR, a gene that has previously been shown to be controlled by Sp1 [Blume et al, 1991]. Indeed, it may be that the mithramycin has no effect on HAS2 transcription, as has been observed for other Sp1-controlled genes (Dipak Ramji – personal communication). Mutation of the Sp1 sites in unison was shown to almost completely abrogate the core promoters' ability to express the luciferase gene. This confirmed that the Sp1 sites, as well as binding of the Sp1 protein played a key role in the constitutive expression of the *HAS2* gene. It also confirmed that the CCAAT box located at position -80 bp had a very minor role in HAS2 expression in this system.

The degree of importance of each individual Sp1 site in the constitutive expression of HAS2 is yet to be determined and is an area for further research. The data only confirmed that mutating all three Sp1 sites in unison stopped transcription. Previous reports have shown that much smaller doses of mithramycin (200 nM) can significantly inhibit expression of other genes where Sp1 is involved [Yoo et al, 2002]. It is clear that Sp1 is a key factor in the constitutive expression of the HAS2 gene. However, the small inhibitory effect of high doses of mithramycin on the levels of *HAS2* transcription suggests that there may be other factors involved that stop mithramycin from directly competing for the Sp1 binding sites. It is possible that Sp1 is part of a larger complex of proteins (one of which could be Sp3) that are all required for constitutive HAS2 expression. Whether Sp1 alone is capable of recruiting

the transcription factors for RNA polymerase II binding (e.g. TFIID) remains to be investigated. It is also possible that the conserved initiator sequence at the TIS may be important in this process.

CHAPTER SIX

TRANSCRIPTIONAL REGULATION OF THE HUMAN HYALURONAN SYNTHASE 2 GENE IN RESPONSE TO IL-1β

6.1 INTRODUCTION

The cytokine interleukin 1 beta (IL-1β) has been implicated in a number of different diseases and is a commonly produced during the inflammatory response. IL-1β can directly influence the expression of many genes, including the *HAS* gene family [Ijuin et al, 2001; Kennedy et al, 2000; Yamada et al, 2004]. IL-1β has been shown to specifically induce HAS2 expression in a number of different cellular systems, including in HK-2 cells [Jones et al, 2001], and periodontal ligament cells [Ijuin et al, 2001].

Two of the common ways by which IL-1β can directly influence gene expression is via the nuclear factor kappa-B (NF-κB) and activating protein-1 (Ap1) signalling pathways. Analysis of 3 kb of gDNA sequence directly upstream of the HAS2 TIS revealed an NF-κB site at approximately -250 bp. The first Ap1 site, however, was situated approximately 1100 bp upstream. The NF-κB site was found to be conserved in the corresponding murine and equine HAS2 sequences and was investigated for its involvement in the IL-1β-dependent increase in HAS2 expression.

RT-PCR showed upregulation of HAS2 mRNA in response to stimulation with IL-1β. Luciferase assays were then carried out to determine if changes in promoter activity could be observed when the cells were treated with the same cytokine. DNA probes specific to the HAS2 NF-κB site, and for the consensus NF-κB sequence, were designed to detect evidence of protein binding using EMSA. Competition EMSAs and supershift analysis was used to determine the role of the HAS2 NF-κB site in the IL-1β mediated response, and a specific NF-κB inhibitor was used to block any IL-1β-stimulated response at this site.

6.2 METHODS

6.2.1 Effect of IL-1β on the expression of HAS2 by RT-PCR

RT-PCR analysis was used to confirm reports that HAS2 expression is increased after stimulation with IL-1β. Growth-arrested HK-2 cells were treated with 10 ng/ml IL-1 β for 3, 6, 9, 12 and 24 hours. 1 μg of RNA from each sample was then used for RT-PCR as described in section 2.7.5. Expression levels of the housekeeping gene β-actin were also measured and used as a control. The primers used for the expression of HAS2 are described in Table 4.3 and the primers and expected product size for β-actin were described in Table 5.3.

6.2.2 Effect of IL-1β on promoter activity of the *HAS2* gene

Luciferase analysis was used to determine the effect of IL-1β stimulation on the activity of the HAS2 promoter constructs containing the NF-κB site. Constructs devoid of (F3) and containing this site (F5 and F8) were transfected into HK-2 cells as described previously (section 2.5.1). Prior to luciferase assay, cells were treated with IL-1β (10 ng/ml or 50 ng/ml) for 24 hours, or left untreated. Assays were performed as previously described (section 2.5.1). The effect of adding FCS (10%) to the cells for the duration of the incubation period between transfection and luciferase analysis was also investigated. Statistical analysis was performed using the non-parametric Wilcoxon signed rank test from SPSS for Windows.

6.2.3 Role of the HAS2 NF-κB site after IL-1β treatment by EMSA

A DNA probe identical to the HAS2 NF-κB site was designed along with a probe containing the NF-κB consensus sequence (Table 6.1). Nuclear protein was extracted from HK-2 cells after treatment with IL-1β at time points 5, 10, 20, 30, 45, 60, 90 and 120 minutes. 5 μg of extract was then incubated separately with each probe. The EMSA was then carried out as described in section 2.8.3.

Probe	Sense Oligonucleotide	Antisense Oligonucleotide
HAS2-NF-kB	CGAGAGTTCAGGGAAATCCAAGAGGCG	CGACGCCTCTTGGATTTCCCTGAACTC
con-NF-kB	CGAAGTTGAGGGGACTTTCCCAGGC	CGAGCCTGGGAAAGTCCCCTCAACT

Table 6.1 Oligonucleotide sequences of the HAS2 specific (HAS2) and consensus (con) NF-κB probes used for the EMSA experiments. Each oligonucleotide was tailed with a 'cga' motif, indicated in blue.

6.2.4 Competition EMSA and supershift for HAS2 NF-κB

The labelled consensus NF-κB probe was incubated with HK-2 protein extract in the presence of the unlabelled HAS2 NF-κB probe or unlabelled consensus NF-κB probe in excess in the competition studies. In addition, supershifts were carried out using antibodies for the different subunits that can bind to NF-κB including p50, p65, p52, c-Rel and Rel-B. Experiments were carried out as described in sections 2.8.4 and 2.8.5.

6.2.5 Effect of an NF-κB inhibitor on the IL-1β-induced expression of HAS2 by RT-PCR

SN-50 is a specific NF-κB cell permeable inhibitor peptide. It contains the nuclear localisation sequence (NLS) of the transcription factor NF-κB p50 linked to the hydrophobic region of the signal peptide of Kaposi fibroblast growth factor (K-FGF). The peptide N-terminal K-FGF region confers cell-permeability, while the NLS inhibits translocation of the NF-κB active complex into the nucleus [Lin et al, 1995].

The effect of the NF-κB signalling inhibitor SN-50 on IL-1β-induced expression of the HAS2 gene was then investigated. Growth arrested HK-2 cells were treated in the presence or absence of 10 ng/ml IL-1β, with or without increasing doses of SN-50 for 6 h prior to RNA extraction. Reverse transcription and PCR was then performed using HAS2-specific primers as described previously (section 2.7.5). The transcription of β-actin mRNA was also analysed as a positive control.

6.2.6 Effect of an NF-κB inhibitor on the IL-1β-induced expression of HAS2 by EMSA

Growth arrested HK-2 cells were treated in the presence or absence of 10 ng/ml IL-1β, with or without 5 μM SN-50. Nuclear protein was extracted from samples after 10 seconds, and 30 minutes of stimulation. The effect of the inhibitor on total NF-κB signalling in HK-2 cells was then analysed using the radiolabelled consensus NF-κB probe described in section 6.2.3. In addition, the effect of SN-50 on signalling via the putative NF-κB site in the HAS2 promoter was also investigated using the radiolabelled HAS2 specific NF-κB probe also described in section 6.2.3. To confirm the specificity of the interactions using the HAS2 specific NF-κB probe, a competition EMSA was also carried out using an excess of unlabelled consensus NF-κB probe in each sample.

6.3 RESULTS

6.3.1 Effect of IL-1β stimulation on HAS2 expression in HK-2 cells

RT-PCR was used to determine the effect of IL-1β on HAS2 expression (Figure 6.1). The expression level of the housekeeping gene β-actin was used as a positive control at each time point. An increase in HAS2 expression was observed after 3 hours of treatment, reaching a maximal level after 6 hours. HAS2 expression then returned to a basal level 24 hours after the addition of the cytokine. No increase in the expression of β-actin was detected.

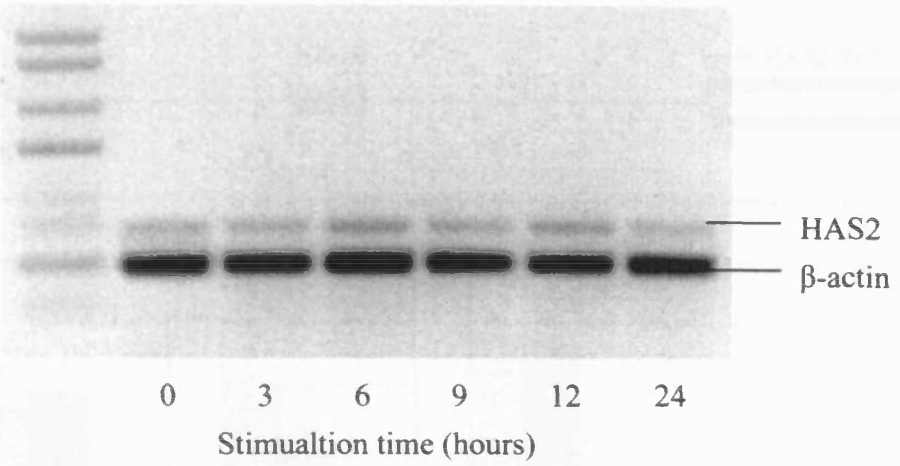

Figure 6.1. Effect of IL-1β on HAS2 expression in HK-2 cells. The levels of HAS2 and β-actin were measured by RT-PCR after treatment with 10 ng/ml IL-1β for 0, 3, 6, 9, 12 and 24 hours.

6.3.2 Effect of IL-1β stimulation on the promoter activity of the HAS2 gene

Analysis of the HAS2 promoter sequence identified a single putative NF-κB site approximately 250 bp upstream of the transcription start site. To determine if the above increase in HAS2 transcription in response to IL-1β stimulation was mediated by this site, promoter constructs F3, F5 and F8 (see chapter 4) were analysed for luciferase activity in the presence or absence of IL-1β.

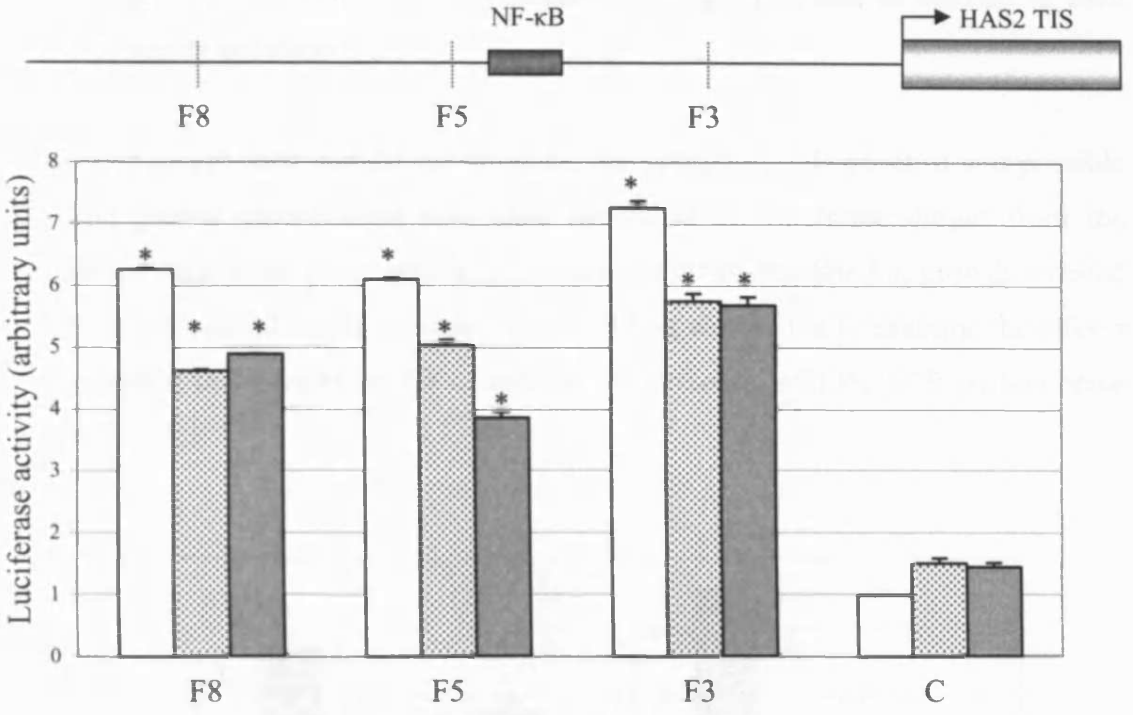

Figure 6.2. Luciferase activity of HAS2 promoter constructs after stimulation with IL-1β in HK-2 cells. Promoter fragments are identified by the sense primer designations given in chapter 4. Data are displayed for no cytokine stimulation (white bars), 10 ng/ml of IL-1β for 6 hours (stippled bars) and 50 ng/ml of IL-1β for 6 hours (shaded bars). Luciferase activity is expressed as the magnitude of normalised luciferase activity relative to the pGL3-Mod promoterless negative control vector (C). Asterisks represent statistical significance ($p < 0.05$).

Figure 6.2 shows the luciferase analysis (n=3) of the constructs F3, F5 and F8 with and without treatment with IL-1β. Construct F3 contained only 130 bp of HAS2 promoter and therefore did not contain the putative NF-κB site. Constructs F5 and F8 both contained the NF-κB site. In the absence of IL-1β, all three constructs displayed significant ($p < 0.05$) constitutive promoter activity in HK-2 cells. F3 demonstrated over a 7-fold increase in activity over the promoterless control (C), whereas constructs F5 and F8 both showed a 6-fold rise in activity. Treatment of constructs F3, F5 and F8 with either 10 ng/ml or 50 ng/ml IL-1β did not increase luciferase activity when compared to the levels shown in the absence of IL-1β, however luciferase output was still significantly higher ($p < 0.05$) than the promoterless control.

Interestingly, the addition of IL-1β resulted in a slight decrease in activity of each HAS2 promoter construct.

The above assays were carried out in serum free conditions. However, it was possible that this growth environment may have decreased the luciferase output from the transfected cells since many cellular processes are down-regulated in growth-arrested conditions. A second luciferase assay was therefore carried out to examine the effects of incubating the transfected HK-2 cells in the presence of 10% FCS on luciferase output.

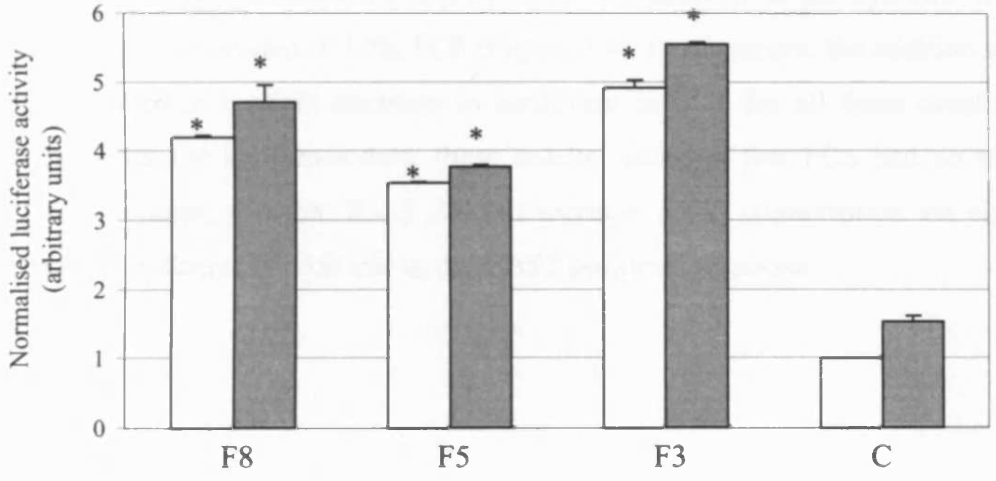

Figure 6.3. Effect of FCS on the luciferase activity of HAS2 promoter constructs in HK-2 cells. Prior to luciferase assay, cells were either incubated in the absence (white bars) or presence (shaded bars) of 10% FCS. Luciferase activity is expressed as the magnitude of normalised luciferase activity relative to the promoterless control vector (C). Asterisks represent statistical significance ($p < 0.05$).

Figure 6.3 shows the luciferase results (n=3) of the effect of treating the cells in the presence or absence of FCS. Each of the HAS2 promoter constructs showed a significant increase ($p < 0.05$) in luciferase activity over the promoterless control (C) in either the presence or absence of FCS. Each construct displayed a marginal increase in luciferase output in the presence of FCS, however these changes were not statistically significant. These data suggested that incubation of transfected HK-2 cells

in 10% FCS for the duration of the experiment had no effect on the luciferase activity of the HAS2 promoter constructs.

To further analyse the effect of FCS on luciferase output in the assay system used, transfected cells incubated in the presence of 10% FCS were then stimulated with two separate doses of IL-1β (10 ng/ml and 50 ng/ml). Luciferase analysis (n=3) of the three HAS2 promoter constructs gave results that mirrored those obtained for the same experiment in the absence of FCS (Figure 6.2). Each construct demonstrated a significant increase in luciferase activity ($p < 0.05$) over the promoterless control (C), with or without IL-1β stimulation. However, no further increase in luciferase output was observed for constructs F5 and F8 upon the addition of the cytokine when the cells had been incubated in 10% FCS (Figure 6.4). Furthermore, the addition of IL-1β again resulted in a slight decrease in luciferase activity for all three constructs. In keeping with the luciferase data, these results indicated that FCS had no effect on luciferase output, and that IL-1β did not increase *HAS2* transcription via signalling through the putative NF-κB site in the HAS2 proximal promoter.

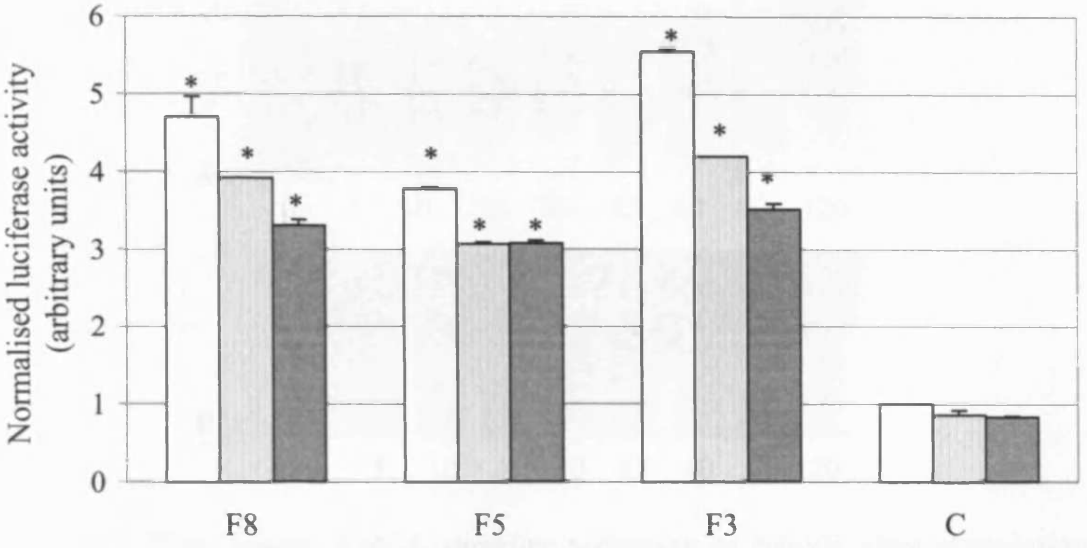

Figure 6.4. Luciferase activity of HAS2 promoter constructs after stimulation with IL-1β in HK-2 cells, with 10% FCS present in all incubation steps. Promoter fragments are identified by the sense primer designations given in chapter 4. Data are displayed for no cytokine stimulation (white bars), 10 ng/ml of IL-1β for 6 hours (stippled bars) and 50 ng/ml of IL-1β for 6 hours (shaded bars). Luciferase activity is expressed as the magnitude of normalised luciferase activity relative to the pGL3-Basic-Mod promoterless negative control vector (C). Asterisks represent statistical significance ($p < 0.05$).

6.3.3 Determination of the involvement of the putative NF-κB site in the IL-1β mediated response

The role of the putative NF-κB site in the HAS2 promoter in the IL-1β-activated expression of HAS2 was then investigated further by other experimental methods. A double stranded DNA probe was designed to span the putative NF-κB binding site within the HAS2 promoter. This probe and a commercially available NF-κB consensus probe were analysed for their involvement in the IL-1β-induced expression of HAS2 by EMSA.

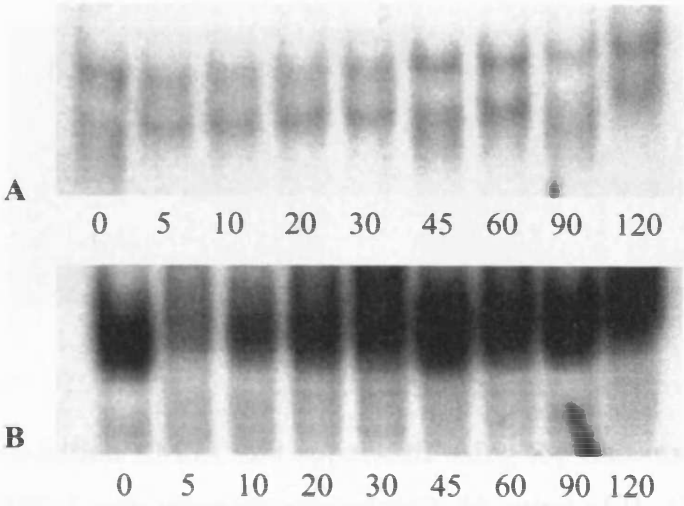

Figure 6.5. Time course EMSA showing activation of NF-κB after stimulation with IL-1β (10 ng/ml) in HK-2 cells. A. Time course using the HAS2-specific NF-κB probe. B. Time course using the consensus NF-κB probe. The period of IL-1β stimulation prior to protein extraction is given in minutes.

Figure 6.5 shows a time course for IL-1β stimulation in HK-2 cells. Prior to stimulation (zero minutes), binding was observed when using the HAS2 specific NF-κB probe. On the addition of IL-1β, an increase in binding was observed at 30, 45 and 60 minutes. In contrast, much stronger binding was observed prior to stimulation when using the consensus NF-κB probe. The addition of IL-1β caused this band to disappear, in parallel with the appearance of a slightly more retarded band after 5 minutes. The intensity of this band then increased following a normal distribution, with maximal binding observed after 45 minutes stimulation.

From the above data, it was apparent that NF-κB was active in cellular responses to IL-1β in HK-2 cells, including via the putative NF-κB site in the HAS2 proximal promoter. The HAS2-specific NF-κB probe was tested to see if it could directly compete for binding of complexes to the consensus NF-κB probe. Supershifts were also carried out to prove that the bands observed using the consensus probe were specific for NF-κB binding proteins (Figure 6.6).

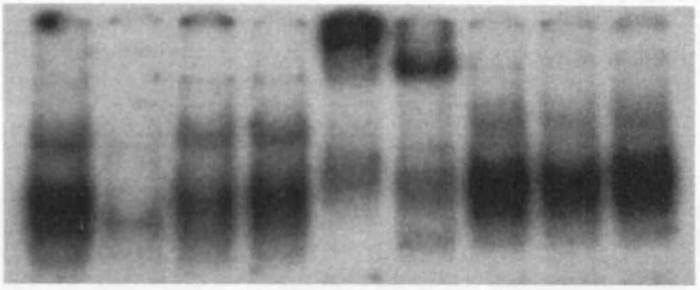

Figure 6.6. Competition EMSA and supershift using the consensus NF-κB probe for HK-2 cells. HK-2 cells were stimulated with 10 ng/ml of IL-1β for 30 minutes prior to nuclear protein extraction. Each lane contains 5 μg protein and the radiolabelled consensus NF-κB probe plus the following; lane 2 – excess unlabelled consensus NF-κB probe; lane 3 – excess unlabelled HAS2-specific NF-κB probe; lane 4 – excess unlabelled unrelated probe; lane 5 – antibody for p65; lane 6 – antibody for p50; lane 7 – antibody for p52; lane 8 -antibody for c-Rel; lane 9 – antibody for Rel-B.

Competition studies using the unlabelled consensus NF-κB probe in excess (lane 2) confirmed that the bands observed were specific for the NF-κB consensus probe. When the unlabelled HAS2-specific NF-κB probe was added in excess (lane 3), binding to the labelled probe was slightly inhibited confirming that this site in the HAS2 promoter was indeed specific for NF-κB. Competition with an unrelated unlabelled probe (lane 4) had no effect on protein binding. Antibodies to the protein subunits p65 and p50 confirmed the binding of these proteins to the consensus NF-κB probe (lanes 5 and 6). The NF-κB binding proteins p52, c-Rel and Rel-b (lanes 7, 8 and 9 respectively) were not present.

6.3.4 Inhibition of the IL-1β-induced HAS2 expression by SN-50

The above data proved that HAS2 mRNA was upregulated in response to IL-1β. EMSA analysis suggested that the putative NF-κB site in the HAS2 promoter was able to bind NF-κB signalling proteins, however luciferase analysis suggested that in the context of the HAS2 promoter, it was not involved in the upregulation of *HAS2* by

IL-1β. SN-50 was therefore used to determine whether the IL-1β-induced expression could be inhibited.

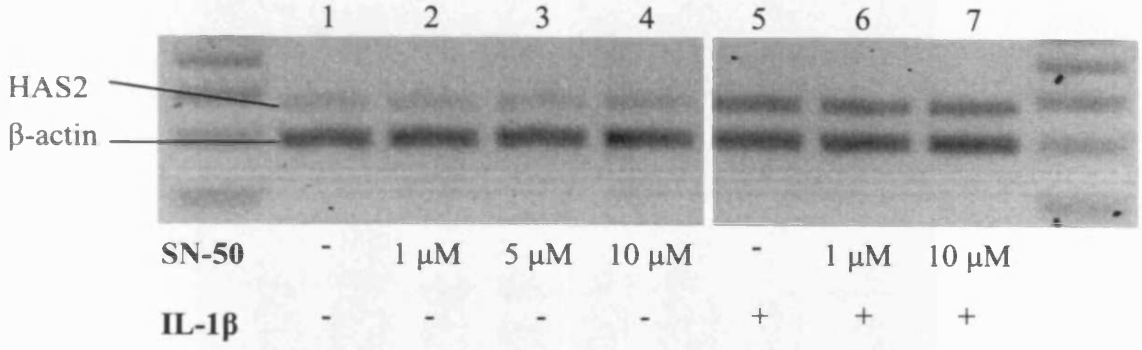

Figure 6.7. Effect of the NF-κB inhibitor SN-50 on the IL-1β-induced expression of HAS2. HK-2 cells were incubated with either 1, 5 or 10 μM SN-50 in the presence or absence of 10 ng/ml IL-1β for 3 hours. Expression levels of β-actin were also measured.

Figure 6.7 shows the effect of SN-50 on the expression of HAS2 mRNA by RT-PCR. The presence of SN-50 at a concentration of 1, 5, or 10 μM did not inhibit the constitutive expression of HAS2, in samples where IL-1β was absent (lanes 1 – 4). The addition of IL-1β in the absence of SN-50 (lane 5) increased HAS2 expression, as described previously. However, addition of either 1 μM or 10 μM SN-50 (lanes 6 and 7 respectively) did not inhibit the IL-1β-induced expression of HAS2 at the mRNA level.

SN-50 was then analysed for its ability to inhibit binding of the NF-κB proteins to the NF-κB consensus and HAS2-specific probes by EMSA (Figure 6.8). An increase in binding to the labelled NF-κB consensus probe (A) was observed after stimulation with 10 ng/ml IL-1β for 10 seconds (lane 2) compared to the unstimulated sample (lane 1). This binding was further increased after a stimulation time of 30 minutes (lane 6). The addition of 5 μM SN-50 (lanes 3 and 7) showed no changes in binding when compared to the control samples (lanes 1 and 5) in the absence of IL-1β. However, in the presence of IL-1β for both 10 seconds and 30 minutes (lanes 4 and 8

respectively), binding of NF-κB proteins to the consensus probe was clearly decreased.

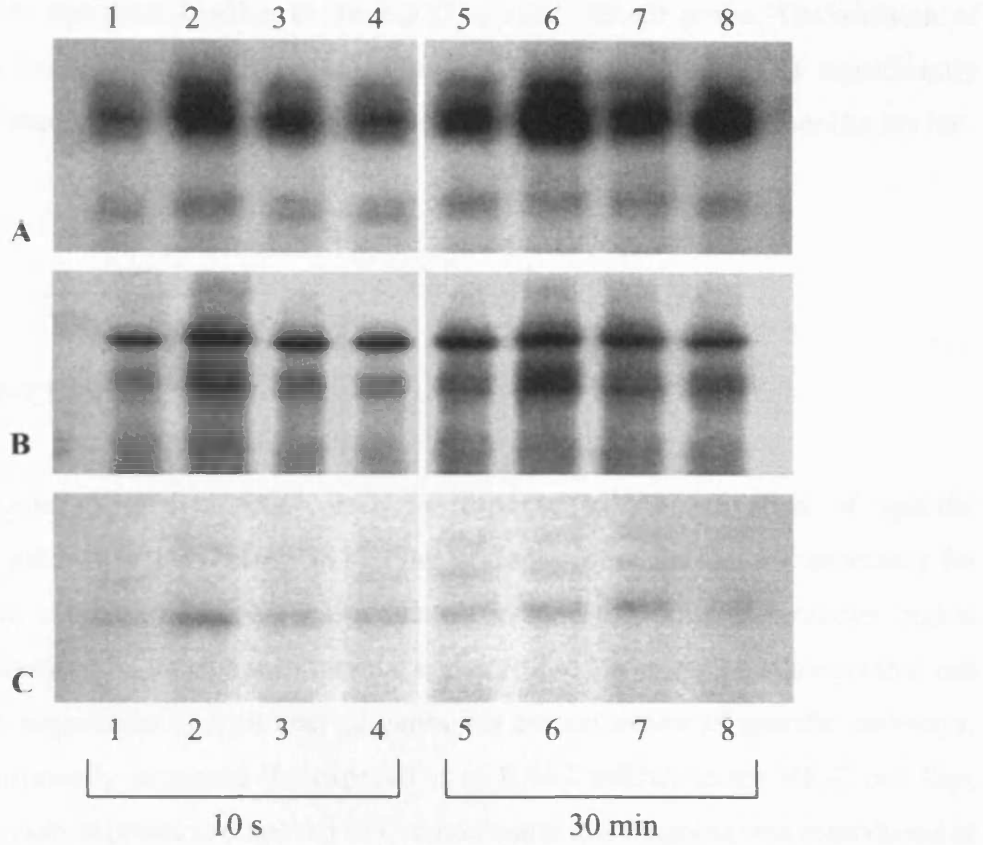

Figure 6.8. Effect of SN-50 on IL-1β-induced NF-κB signalling in HK-2 cells at time points of 10 seconds (lanes 1-4) and 30 minutes (lanes 5-8). SN-50 was tested for its ability to inhibit binding to a radiolabelled NF-κB consensus probe (A), a radiolabelled HAS2 specific NF-κB probe (B) and a radiolabelled HAS2-specific NF-κB probe in the presence of excess unlabelled consensus NF-κB probe (C). Lanes 1 and 5 – negative control (no IL-1β or SN-50); lanes 2 and 6 - 10 ng/ml IL-1β; lanes 3 and 7 – 5 μM SN-50; lanes 4 and 8 – 10 ng/ml IL-1β and 5 μM SN-50.

A similar trend in binding was observed when using the radiolabelled HAS2 specific NF-κB probe (B). An increase in bound protein was observed upon the addition of IL-1β (lane 2) for 10 seconds when compared to the negative control (lane 1). Binding was then further increased after IL-1β stimulation for 30 minutes (lane 6). In the absence of IL-1β, SN-50 had no effect on binding (lanes 3 and 7) compared to the

negative control samples (lanes 1 and 5). However, the addition of IL-1β in the presence of SN-50 for both 10 seconds and 30 minutes (lanes 4 and 8 respectively), significantly decreased binding to the HAS2-specific NF-κB probe. The addition of unlabelled consensus NF-κB probe in excess to these samples (C) significantly decreased binding, confirming that all the observed interactions were specific for NF-κB.

6.4 DISCUSSION

Induced gene expression takes place in response to the activation of specific signalling pathways. This results in binding of transcription factors not necessary for constitutive expression of the gene of interest to bind to the target promoter region and an increase in induced transcriptional activity. IL-1β is one such stimulus that can induce the expression of a number of genes via the activation of specific pathways. IL-1β significantly increased the expression of HAS2 mRNA in the HK-2 cell line, with maximum expression observed after 6 hours and this response was reproduced in the TE671 cell line (data not shown). A crucial regulator of many IL-1β responsive genes is the NF-κB family of transcription factors and the consensus pathway for NF-κB activation has been extensively characterised [Karin and Ben-Neriah, 2000]. The MCP-1 gene, for example is upregulated by IL-1β via activation of NF-κB in mesangial cells. In addition, the constitutive expression of MCP-1 in this cell line is controlled by Sp1 [Stylianou et al, 1999]. The HAS2 promoter contained a putative NF-κB site approximately 250 bp upstream of the TIS, and was analysed for activity in response to IL-1β stimulation.

The addition of IL-1β to HK-2 cells transfected with the HAS2 promoter constructs displayed no further increase in luciferase activity compared to constitutive levels. It was first thought that this may be because of the growth arrested condition of the transfected cells that had been incubated in the absence of FCS for the duration of the experiment. It was possible that the signalling pathways had become inactivated, in the serum free conditions, and therefore IL-1β treatment was having no effect. Luciferase assays carried out using samples incubated in the presence of FCS slightly

increased the luciferase activity of the HAS2 promoter constructs. Indeed, FCS has been known to increase HAS2 expression in certain cell types [Jacobson et al, 2000]. However, assays carried out on samples incubated in the presence of FCS which were then stimulated with IL-1β showed no further increase in luciferase activity compared to the reported constitutive levels. Taken together, these results suggested that the IL-1β-induced expression of HAS2 was not occurring through the putative NF-κB site in the HAS2 proximal promoter.

The possibility that the IL-1β-induced increase of HAS2 mRNA by RT-PCR could not be detected by the luciferase assay system was investigated by EMSA using probes containing the HAS2-specific NF-κB site and the consensus NF-κB sequence. Supershift assays using the consensus NF-κB probe confirmed the presence of the NF-κB subunits p65 and p50 in the HK-2 nucleus following IL-1β stimulation. The putative NF-κB site in the HAS2 promoter also displayed binding capabilities, and to a limited extent was able to compete with the binding of proteins to the consensus probe. It therefore appeared that the putative NF-κB site was able to interact weakly with NF-κB factors, but was not important in the IL-1β-induced expression of HAS2 mRNA. Experiments using the NF-κB signalling inhibitor SN-50 supported these findings. RT-PCR analysis demonstrated that the IL-1β-induced upregulation of HAS2 mRNA could not be blocked using the inhibitor. However, EMSA analysis using the consensus and HAS2 specific NF-κB probes revealed that 1) SN-50 was able to decrease total IL-1β-induced NF-κB signalling in HK-2 cells and 2) it could decrease binding of NF-κB proteins to the HAS2-specific NF-κB probe. This confirmed that the putative NF-κB sequence in the HAS2 promoter was able to bind NF-κB signalling complexes, and show an increase in binding following stimulation with IL-1β. However, in the context of the HAS2 promoter, this interaction was not involved in the upregulation of HAS2 mRNA after IL-1β stimulation.

Previous reports have shown that the IL-1β-induced expression of HAS2 in HK-2 cells occurs via an NF-κB dependent process [Jones et al, 2001]. Analysis of the HAS2 promoter revealed no other putative NF-κB sites within 3000 bp of the TIS. One recent investigation has demonstrated that epidermal growth factor (EGF) induces *HAS2* transcription via a signal transducer and activator of transcription (STAT) binding site within the HAS2 promoter [Saavalainen et al, 2005].

Furthermore, the STAT binding site overlaps the putative NF-κB site. This may explain why this NF-κB site is not activated during the induced transcription of *HAS2* by IL-1β. A second recent report has demonstrated that IL-1β can induce HAS2 expression via the p38 and ERK1/2 mitogen activated protein (MAP) kinase pathways [Ducale et al, 2005]. Ap-1 is a known downstream target of this signalling cascade, and with two putative Ap-1 binding sites in the HAS2 promoter, suggests a possible alternative mechanism by which IL-1β is increasing *HAS2* transcription. In contrast, other reports have suggested a role for the MAP kinase pathways, specifically p38, in IL-1β-induced mRNA stability [Winzen et al, 1999]. HAS2 contains adenosine- and uridine-rich elements that are known to confer message instability [Gou et al, 1998]. Taken together, these findings highlight new areas for future investigations in unravelling the mechanisms by which IL-1β can induce *HAS2* gene expression.

CHAPTER SEVEN

GENERAL DISCUSSION

HA is an ubiquitous molecule that is present under normal conditions in many organ systems. Significant quantitative changes in HA levels in many of these systems are however observed during the onset of disease. Understanding the mechanisms involved in HA synthesis and turnover therefore has important implications for many aspects of human health. HA is involved in a variety of cellular processes, including cell adhesion, proliferation, migration, differentiation and tissue remodelling. It has also been implicated in various pathological processes and diseases, including cancer, rheumatoid arthritis, atherosclerosis, embryonic development wound healing and tissue fibrosis, however its precise role remains unclear. Reports have demonstrated that HA can facilitate, and/or attenuate the progression of various disease processes, and therefore it is only by understanding precisely how HA production and degradation is controlled will it become possible to augment or reduce its activity in one or more of these areas.

The completion of the Human Genome Project generated an avalanche of sequence data, but the even bigger task of interpreting and analysing this data beyond mere sequence comparisons and gene finding has become just as important. During transcriptional initiation, a variety of transcription factors interact with the promoter regions that lie upstream of gene sequences and mediate their transcriptional regulation in sophisticated ways. To understand how genetic information is processed, promoter identification becomes a necessary step, and will allow insights into the control of expression of those genes involved in developmental control, morphogenesis, cell differentiation, tissue specificity cell communication and cellular stress responses. Extensive data concerning transcriptional initiation and promoter structure has been defined in detail for a relatively small number of genes, and the majority still need to be analysed thoroughly. One of the main problems is the limited understanding of underlying molecular recognition mechanisms of transcription initiation.

The work presented in this thesis has focused on the mechanisms involved in the transcriptional regulation of the *HAS* genes. The investigations have concentrated on determining the factors required for the expression of the *HAS2* gene, since its upregulation had previously been implicated, along with increased HA production, during the early inflammatory stages preceding kidney fibrosis.

At the beginning of the project, little work had been carried out on the human *HAS* genes. The cDNA and gDNA sequences for the murine *Has* genes had been reported and work had begun on characterising the murine *Has1* promoter. However, the identification and cloning of the cDNA sequences was the only work that had been completed for the human isoforms. The genomic DNA structures of each of the human *HAS* genes were therefore reconstructed *in silico*, and the results were confirmed using experimental methods [Monslow et al, 2003]. The proximal promoter region for each *HAS* gene was analysed, and it was shown that each was functionally active *in vitro*. In addition, microsatellites were identified specific for each HAS isoform providing polymorphic markers for each *HAS* locus.

HAS2 transcription can be induced in a number of cellular systems and by a variety of stimuli. Evidence to date indicates that it is the most inducible of all the *HAS* genes. For example, the upregulation of HA synthesis seen in an *in vitro* model of diabetic nephropathy using proximal tubular cells is coincident with a specific upregulation of transcription at the *HAS2* locus [Jones et al, 2001]. Studies were therefore carried out to determine the mechanisms involved in the transcriptional regulation of the *HAS2* gene on two levels; 1) to identify the factors required for constitutive expression of the gene, and 2) to identify the additional factors required for the induction of HAS2 expression by the inflammatory cytokine IL-1β.

Before investigations could begin on the HAS2 promoter region, the location of the HAS2 transcription initiation site (TIS) needed to be confirmed. 5'-RACE analysis repositioned the HAS2 TIS a further 130 bp upstream than the site reported in the HAS2 reference sequence NM_005328, suggesting that this database entry was truncated at the 5'-end and incomplete [Monslow et al, 2004]. Improved and reliable experimental methodologies are now available to characterise full gene transcripts. These methods, together with the computational-based programs and the increasing number of sequences deposited in the Expressed Sequence Tag (EST) database, now allow the TISs and full length cDNAs of many genes to be elucidated much more accurately [Ma et al, 2004; Das et al, 2001]. Sequences were thus identified in the EST database specific to the *HAS2* locus that extended further upstream than the original HAS2 TIS (NM_005328). Analysis of the HAS2 5'-UTR also showed the potential for formation of a tightly folded secondary structure [Monslow et al, 2004].

Taken together, these results provided further evidence to explain the truncation of HAS2 reference sequence NM_005328. Sequences were also identified in the EST database that extended upstream of the TISs for the HAS2 reference sequences in the bovine and the mouse. Further investigations will need to be carried out to determine whether these entries are also incomplete.

Analysis of the promoter region directly upstream of the new HAS2 TIS showed that it was functionally active and able to initiate transcription. Maximal constitutive activity was attained by the first 120 bp of the proximal promoter. The HAS2 core promoter region contained a large GC-rich region which was found to have a prominent role in the transcription of HAS2. Analysis of this region identified three sites that specifically bound the transcription factor Sp1. Furthermore, mutation of these three sites inhibited Sp1 binding and more importantly, significantly inhibited transcription.

IL-1β has been reported to induce HAS2 expression in a number of cellular systems, including in proximal tubular cells within the kidney. A common mechanism by which IL-1β can influence gene expression is via the NF-κB pathway. The HAS2 promoter contained a putative NF-κB site approximately 250 bp upstream of the TIS. This site was therefore investigated for its potential role in the IL-1β-induced expression of the *HAS2* gene. The NF-κB site was able to bind NF-κB proteins on its own, but in the context of the HAS2 promoter was not involved in the upregulation of HAS2 mRNA by the cytokine IL-1β. Other factors may be required that were not detectable in the system used. On the other hand, IL-1β may be acting via a different mechanism (e.g. the Ap-1 pathway) or via a novel mechanism that is, as yet, undetermined.

The role of HA simply acting as a 'space filling molecule in the ECM' has been long since forgotten, and it is now clear that it has many biological roles, both in normal and pathological conditions. In a similar way, HA metabolism was first predominantly thought to be controlled at the enzymatic level of the HAS and HYAL enzymes that synthesise and degrade HA respectively. However, with a steady increase in publications reporting changes in HAS expression levels in certain

pathological conditions, it appears that essential mechanisms for the control of HA production lie at the level of HAS transcription.

In the present study, HAS2 regulation was investigated predominantly in the renal proximal tubular epithelial cell line HK-2, a cell type with a potentially highly significant role in controlling HA production during the onset of kidney fibrosis. As previously discussed, the accumulation of HA in the corticointerstitium (in the form of HA cables) also has anti-inflammatory effects. Monocytes bind to these cable structures via CD-44, which stops them interacting with the resident cells and attenuates the inflammatory response [Hascall et al, 2004; Selbi et al, 2004]. Treatment of HK-2 cells with BMP-7 increases HA cable formation and monocyte binding. Interestingly, BMP-7 also increases HAS2 expression, and simultaneously down-regulates the expression of HYAL1 and HYAL2 [Selbi et al, 2004]. This suggests that the increase in HA cable formation by BMP-7 is directly linked with an upregulation of HAS2 mRNA. The interaction of HAS2 and HA cable formation therefore provides another avenue of investigation.

Recently, increased HAS2 expression and an associated increase in HA synthesis has also been reported in the progression of breast cancer [Udabage et al, 2005], and also in wound healing in epidermal keratinocytes [Tammi et al, 2005]. In the latter example, changes in HA production are observed during cell proliferation and differentiation in response to wounding of the epidermis and coincide with variations in HAS2 and HYAL2 expression. Research is currently underway investigating the importance of these enzymes in this wound healing mechanism [Mack et al, 2003]. The work outlined in this thesis may therefore help to determine the transcriptional mechanisms important in HAS2 expression in the process of wound healing in the epidermis.

A number of reports suggest that the different HAS genes may respond differently to a common stimulus. Treatment of articular chondrocytes with FGF increases HAS2 expression, but simultaneously down-regulates HAS1 mRNA [Recklies et al, 2001]. Conversely, treatment of normal human mesothelial cells with TGF-β1 attenuates HAS2 expression, but increases the expression of HAS1 [Jacobson et al, 2000]. In addition, the three HAS genes from *Xenopus leavis* show different temporal

expression patterns during embryonic development [Nardini et al, 2004]. It is thus conceivable that the different HAS enzymes and/or genes may directly interact with one another. These interactions, may then contribute to the different HAS expression patterns that are seen in response to common stimuli, during successive stages of development or perhaps during different pathological conditions. To date, the control of HA production by these means has not been investigated, and may therefore develop in importance.

Understanding the transcriptional control of the HAS genes may in the future provide new avenues of therapeutic research via the control of HA synthesis. A combination of methods for both transcriptional and enzymatic control of the HAS enzymes however, may prove to be the most effective strategy. The evidence strongly suggests that in many systems, important control mechanisms are still situated at the levels of HA (rather than HAS) synthesis and degradation. Indeed, a recent report has identified latent HAS enzymes within the ER-golgi pathway that can be rapidly mobilised and inserted into the plasma membrane to generate more HA [Rilla et al, 2005]. The lack of antibodies for the detection of functioning HAS enzymes still remains a problem, and the successful production of HAS-specific antibodies would be seen as a major breakthrough in HA research.

At present, there are no known splice variants of the HAS2 gene, and therefore no knowledge of correlations between any HAS2 variants and different disease conditions where increased HA production is observed. HAS3 is known to have 2 different splice variants (HAS3v1 and HAS3v2). One recent study investigated HAS2 allele expression in nephropathic versus non nephropathic diabetic patients, but no correlation was found (Nair et al, unpublished observation). It is known that HAS3v1 generates shorter HA chains than HAS1 and HAS2. The functional significance of this, however, is not known. One recent report has demonstrated, for the first time, splice variation of the HAS1 gene in multiple myeloma, and showed that one of the variants correlated with reduced survival [Adamia et al, 2005]. It is possible that there may also be splice variants for HAS2. Indeed, if they exist, they also have the potential to act as specific markers for different diseases, thereby providing another interesting area of therapeutic investigation.

APPENDIX

APPENDIX I - REAGENT LIST

All reagents were purchased from Fischer Scientific (Loughborough, Leicestershire, UK) unless stated.

Buffer A

10 mM HEPES-KOH (pH 7.9) (Gibco)
1.5 mM $MgCl_2$
10 mM KCl
0.5 mM DTT* (Invitrogen)
0.2 mM Phenylmethylsulphonyl fluoride (PMSF)* (Sigma)
*added immediately before use

Buffer C

20 mM HEPES-KOH (pH 7.9)
25% Glycerol
420 nM NaCl
1.5 mM $MgCl_2$
0.2 mM EDTA
0.3 mM DTT*
0.2 mM PMSF*
*added immediately before use

EMSA binding buffer (10 x)

340 mM KCl
50 mM $MgCl_2$
1 mM DTT

EMSA dilution buffer

40 mM KCl
0.1 mM EDTA

TBE buffer (5 x)

54g TRIS base

27.5 g Boric acid

0.5 M EDTA

Made up to 1 L with H_2O

TENS buffer

10 mM TRIS-Cl

1 mM EDTA

0.1 M NaOH

0.5% SDS

YT agar (per litre)

16 g Bacto-tryptone (Oxoid, Ltd, Basingstoke, Hampshire, UK)

10 g Yeast extract (Oxoid)

5 g NaCl

20 g Agar (Oxoid)

YT broth (per litre)

16 g Bact-tryptone

10 g Yeast extract

5 g NaCl

APPENDIX II - VECTOR MAPS

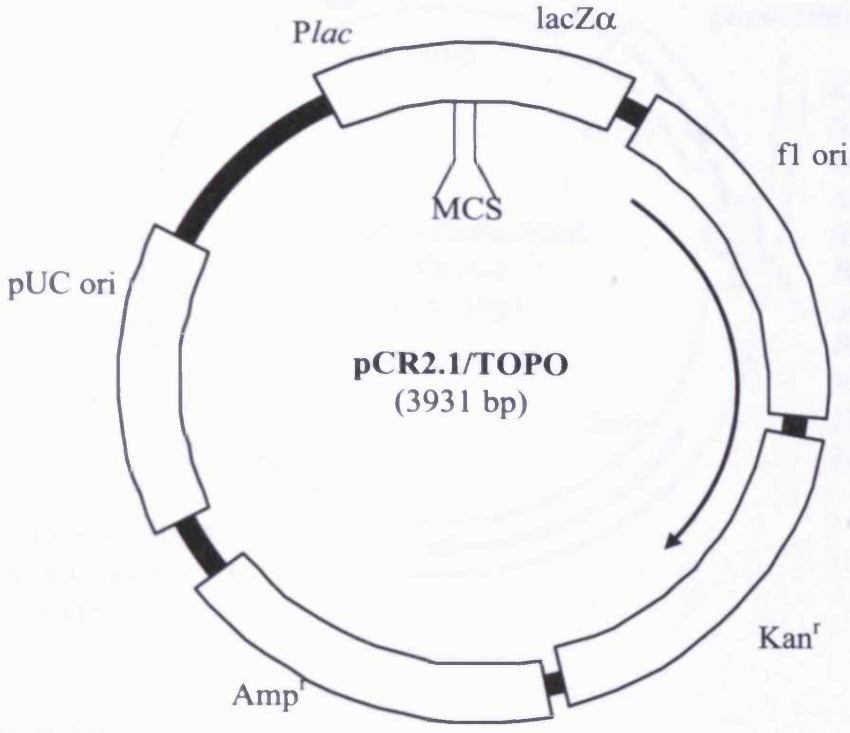

PCR2.1/TOPO MCS

*lacZ*αATG *Hin* dIII *Kpn* I *Sac* I *Bam* HI *Spe* I

CAG GAA ACA GCT ATG ACC ATG ATT ACG CCA AGC TTG GTA CCG AGC TCG GAT CCA CTA

M13-R

Bst XI *Eco* RI *Eco* RI

PCR PRODUCT

GTA ACG GCC GCC AGT GTG CTG GAA TTC GCC CTT----------AAG GGC GAA TTC TGC

Eco RV *Bst* XI *Not* I *Xho* I *Nsi* I *Xba* I *Apa* I

AGA TAT CCA TCA CAC TGG CGG CCG CTC GAG CAT GCA TCT AGA GGG CCC AAT TCG CCC

TAT AGT GAG TCG TAT TAC AAT TCA CTG GCC GTC GTT TTA CAA CGT CGT GAC TGG GAA

T7 Promoter M13-F

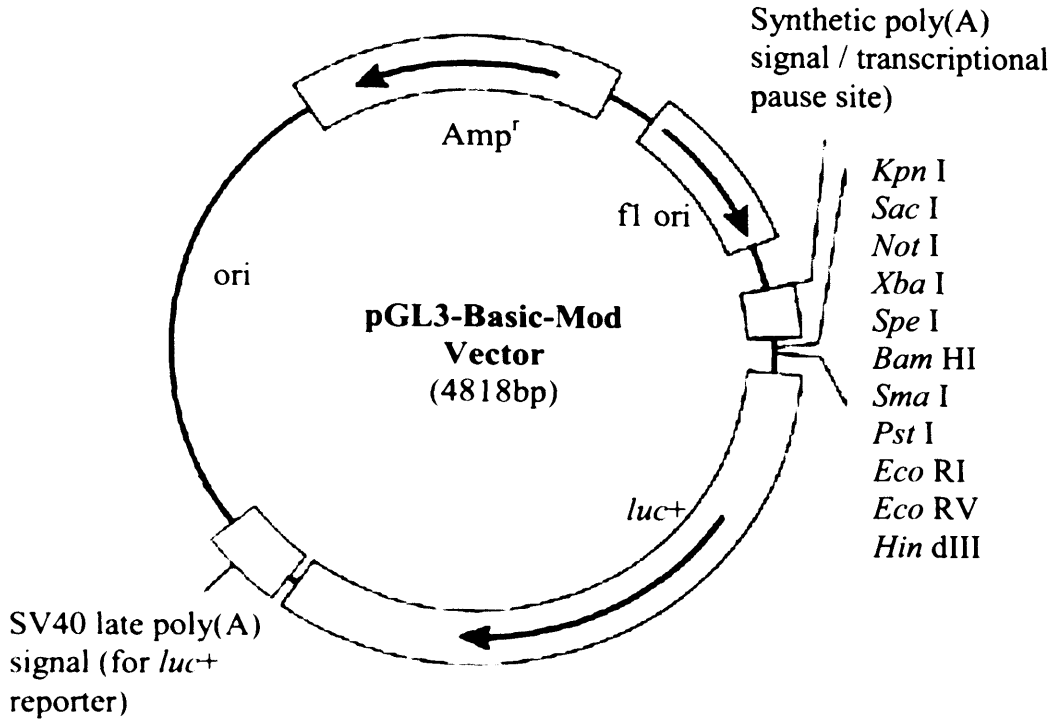

pGL3-Basic MCS

Kpn I *Sac* I *Mlu* I *Nhe* I *Sma* I *Xho* I *Bgl* II *Hin* dIII

GGT ACC GAG CTC TTA CGC GTG CTA GCC CGG GCT CGA GAT CTG CGA TCT AAG TAA GCT

pGL3-Mod MCS

Kpn I *Sac* I *Not* I *Xba* I *Spe* I *Bam* HI *Sma* I

GGT ACC GAG CTC CAC CGC GGT GGC GGC CGC TCT AGA ACT AGT GGA TCC CCC GGG CTG

Pst I *Eco* RI *Eco* RV *Hin* dIII

CAG GAA TTC GAT ATC AAG CTT

REFERENCES

Abrass, C.K., Berfield, A.K., Stehman-Breen, C., Alpers, C.E. and Davis, C.L., 1999. Unique changes in interstitial extracellular matrix composition are associated with rejection and cyclosporine toxicity in human renal allograft biopsies. *Am J Kidney Dis*, **33,** 11-20.

Acevedo, M.L. and Kraus, W.L., 2004. Transcriptional activation by nuclear receptors. *Essays Biochem*, **40,** 73-88.

Adamia, S., Reiman, T., Crainie, M., Mant, M.J., Belch, A.R. and Pilarski, L.M., 2005. Intronic splicing of hyaluronan synthase 1 (HAS1): a biologically relevant indicator of poor outcome in multiple myeloma. *Blood*, **105,** 4836-44.

Alpers, C.E., Hudkins, K.L., Floege, J. and Johnson, R.J., 1994. Human renal cortical interstitial cells with some features of smooth muscle cells participate in tubulointerstitial and crescentic glomerular injury. *J Am Soc Nephrol*, **5,** 201-9.

Altschul, S.F., Madden, T.L., Schaffer, A.A., Zhang, J., Zhang, Z., Miller, W. and Lipman, D.J., 1997. Gapped BLAST and PSI-BLAST: a new generation of protein database search programs. *Nucleic Acids Res*, **25,** 3389-402.

Anney, R.J., Rees, M.I., Bryan, E., Spurlock, G., Williams, N., Norton, N., Williams, H., Cardno, A., Zammit, S., Jones, S., Jones, G., Hoogendoorn, B., Smith, K., Hamshere, M.L., Coleman, S., Guy, C., O'Donovan, M.C., Owen, M.J. and Buckland, P.R., 2002. Characterisation, mutation detection, and association analysis of alternative promoters and 5' UTRs of the human dopamine D3 receptor gene in schizophrenia. *Mol Psychiatry*, **7,** 493-502.

Aruffo, A., Stamenkovic, I., Melnick, M., Underhill, C.B. and Seed, B., 1990. CD44 is the principal cell surface receptor for hyaluronate. *Cell*, **61,** 1303-13.

Assmann, V., Jenkinson, D., Marshall, J.F. and Hart, I.R., 1999. The intracellular hyaluronan receptor RHAMM/IHABP interacts with microtubules and actin filaments. *J Cell Sci*, **112 (Pt 22),** 3943-54.

Assmann, V., Marshall, J.F., Fieber, C., Hofmann, M. and Hart, I.R., 1998. The human hyaluronan receptor RHAMM is expressed as an intracellular protein in breast cancer cells. *J Cell Sci*, **111 (Pt 12),** 1685-94.

Beck-Schimmer, B., Oertli, B., Pasch, T. and Wuthrich, R.P., 1998. Hyaluronan induces monocyte chemoattractant protein-1 expression in renal tubular epithelial cells. *J Am Soc Nephrol*, **9,** 2283-90.

Beech, D.J., Madan, A.K. and Deng, N., 2002. Expression of PH-20 in normal and neoplastic breast tissue. *J Surg Res*, **103,** 203-7.

Benz, P.S., Fan, X. and Wuthrich, R.P., 1996. Enhanced tubular epithelial CD44 expression in MRL-lpr lupus nephritis. *Kidney Int*, **50,** 156-63.

Biancone, L., David, S., Della Pietra, V., Montrucchio, G., Cambi, V. and Camussi, G., 1994. Alternative pathway activation of complement by cultured human proximal tubular epithelial cells. *Kidney Int*, **45,** 451-60.

Blume, S.W., Snyder, R.C., Ray, R., Thomas, S., Koller, C.A. and Miller, D.M., 1991. Mithramycin inhibits SP1 binding and selectively inhibits transcriptional activity of the dihydrofolate reductase gene in vitro and in vivo. *J Clin Invest*, **88,** 1613-21.

Bohle, A., Mackensen-Haen, S. and Wehrmann, M., 1996. Significance of postglomerular capillaries in the pathogenesis of chronic renal failure. *Kidney Blood Press Res*, **19,** 191-5.

Bourguignon, L.Y., Gunja-Smith, Z., Iida, N., Zhu, H.B., Young, L.J., Muller, W.J. and Cardiff, R.D., 1998. CD44v(3,8-10) is involved in cytoskeleton-mediated tumor cell migration and matrix metalloproteinase (MMP-9) association in metastatic breast cancer cells. *J Cell Physiol*, **176,** 206-15.

Bourguignon, L.Y., Lokeshwar, V.B., He, J., Chen, X. and Bourguignon, G.J., 1992. A CD44-like endothelial cell transmembrane glycoprotein (GP116) interacts with extracellular matrix and ankyrin. *Mol Cell Biol*, **12,** 4464-71.

Bourguignon, L.Y., Zhu, H., Chu, A., Iida, N., Zhang, L. and Hung, M.C., 1997. Interaction between the adhesion receptor, CD44, and the oncogene product, p185HER2, promotes human ovarian tumor cell activation. *J Biol Chem*, **272,** 27913-8.

Bourguignon, L.Y., Zhu, H., Shao, L. and Chen, Y.W., 2000. CD44 interaction with tiam1 promotes Rac1 signaling and hyaluronic acid-mediated breast tumor cell migration. *J Biol Chem*, **275,** 1829-38.

Bourguignon, L. Y., Zhu, H., Shao, L., and Chen, Y. W., 2001. CD44 interaction with c- Src kinase promotes cortactin-mediated cytoskeleton function and hyaluronic acid-dependent ovarian tumor cell migration. *J Biol Chem*, **276,** 7327-36.

Breathnach, R. and Chambon, P., 1981. Organization and expression of eucaryotic split genes coding for proteins. *Annu Rev Biochem*, **50,** 349-83.

Brecht, M., Mayer, U., Schlosser, E. and Prehm, P., 1986. Increased hyaluronate synthesis is required for fibroblast detachment and mitosis. *Biochem J*, **239,** 445-50.

Brenneisen, P., Blaudschun, R., Gille, J., Schneider, L., Hinrichs, R., Wlaschek, M., Eming, S. and Scharffetter-Kochanek, K., 2003. Essential role of an activator protein-2 (AP-2)/specificity protein 1 (Sp1) cluster in the UVB-mediated induction of the human vascular endothelial growth factor in HaCaT keratinocytes. *Biochem J*, **369,** 341-9.

Brito, P.L., Fioretto, P., Drummond, K., Kim, Y., Steffes, M.W., Basgen, J.M., Sisson-Ross, S. and Mauer, M., 1998. Proximal tubular basement membrane width in insulin-dependent diabetes mellitus. *Kidney Int*, **53,** 754-61.

Bucher, P., 1990. Weight matrix descriptions of four eukaryotic RNA polymerase II promoter elements derived from 502 unrelated promoter sequences. *J Mol Biol*, **212,** 563-78.

Burke, T.W. and Kadonaga, J.T., 1996. Drosophila TFIID binds to a conserved downstream basal promoter element that is present in many TATA-box-deficient promoters. *Genes Dev*, **10,** 711-24.

Camenisch, T.D. and McDonald, J.A., 2000. Hyaluronan: is bigger better? *Am J Respir Cell Mol Biol*, **23,** 431-3.

Camenisch, T.D., Spicer, A.P., Brehm-Gibson, T., Biesterfeldt, J., Augustine, M.L., Calabro, A., Jr., Kubalak, S., Klewer, S.E. and McDonald, J.A., 2000. Disruption of hyaluronan synthase-2 abrogates normal cardiac morphogenesis and hyaluronan-mediated transformation of epithelium to mesenchyme. *J Clin Invest*, **106,** 349-60.

Catterall, J.B., Gardner, M.J., Jones, L.M. and Turner, G.A., 1997. Binding of ovarian cancer cells to immobilized hyaluronic acid. *Glycoconj J*, **14,** 867-9.

Chatziantoniou, C., Boffa, J.J., Tharaux, P.L., Flamant, M., Ronco, P. and Dussaule, J.C., 2004. Progression and regression in renal vascular and glomerular fibrosis. *Int J Exp Pathol*, **85,** 1-11.

Cherr, G.N., Yudin, A.I. and Overstreet, J.W., 2001. The dual functions of GPI-anchored PH-20: hyaluronidase and intracellular signaling. *Matrix Biol*, **20,** 515-25.

Clouthier, D.E., Comerford, S.A. and Hammer, R.E., 1997. Hepatic fibrosis, glomerulosclerosis, and a lipodystrophy-like syndrome in PEPCK-TGF-beta1 transgenic mice. *J Clin Invest*, **100,** 2697-713.

Coleman, S.L., Hoogendoorn, B., Guy, C., Smith, S.K., O'Donovan, M.C. and Buckland, P.R., 2002. Streamlined approach to functional analysis of promoter-region polymorphisms. *Biotechniques*, **33,** 412, 414, 416 passim.

Collis, L., Hall, C., Lange, L., Ziebell, M., Prestwich, R. and Turley, E.A., 1998. Rapid hyaluronan uptake is associated with enhanced motility: implications for an intracellular mode of action. *FEBS Lett*, **440,** 444-9.

Comper, W.D. and Laurent, T.C., 1978. Physiological function of connective tissue polysaccharides. *Physiol Rev*, **58,** 255-315.

Crawford, D.L., Segal, J.A. and Barnett, J.L., 1999. Evolutionary analysis of TATA-less proximal promoter function. *Mol Biol Evol*, **16,** 194-207.

Crawford, S.E., Stellmach, V., Murphy-Ullrich, J.E., Ribeiro, S.M., Lawler, J., Hynes, R.O., Boivin, G.P. and Bouck, N., 1998. Thrombospondin-1 is a major activator of TGF-beta1 in vivo. *Cell*, **93,** 1159-70.

Croager, E.J., Gout, A.M. and Abraham, L.J., 2000. Involvement of Sp1 and microsatellite repressor sequences in the transcriptional control of the human CD30 gene. *Am J Pathol*, **156,** 1723-31.

Cruz, C.I., Ruiz-Torres, P., del Moral, R.G., Rodriguez-Puyol, M. and Rodriguez-Puyol, D., 2000. Age-related progressive renal fibrosis in rats and its prevention with ACE inhibitors and taurine. *Am J Physiol Renal Physiol*, **278,** F122-9.

Csoka, A.B., Frost, G.I. and Stern, R., 2001. The six hyaluronidase-like genes in the human and mouse genomes. *Matrix Biol*, **20,** 499-508.

Csoka, A.B., Scherer, S.W. and Stern, R., 1999. Expression analysis of six paralogous human hyaluronidase genes clustered on chromosomes 3p21 and 7q31. *Genomics*, **60,** 356-61.

Das, M., Harvey, I., Chu, L.L., Sinha, M. and Pelletier, J., 2001. Full-length cDNAs: more than just reaching the ends. *Physiol Genomics*, **6,** 57-80.

Day, A.J., 1999. The structure and regulation of hyaluronan-binding proteins. *Biochem Soc Trans*, **27,** 115-21.

Day, A.J. and Prestwich, G.D., 2002. Hyaluronan-binding proteins: tying up the giant. *J Biol Chem*, **277,** 4585-8.

de la Motte, C.A., Hascall, V.C., Drazba, J., Bandyopadhyay, S.K. and Strong, S.A., 2003. Mononuclear leukocytes bind to specific hyaluronan structures on colon mucosal smooth muscle cells treated with polyinosinic acid:polycytidylic acid: inter-alpha-trypsin inhibitor is crucial to structure and function. *Am J Pathol*, **163,** 121-33.

DeAngelis, P.L., 1996. Enzymological characterization of the Pasteurella multocida hyaluronic acid synthase. *Biochemistry*, **35,** 9768-71.

DeAngelis, P.L., 1999. Hyaluronan synthases: fascinating glycosyltransferases from vertebrates, bacterial pathogens, and algal viruses. *Cell Mol Life Sci*, **56,** 670-82.

DeAngelis, P.L., Jing, W., Drake, R.R. and Achyuthan, A.M., 1998. Identification and molecular cloning of a unique hyaluronan synthase from Pasteurella multocida. *J Biol Chem*, **273,** 8454-8.

DeAngelis, P.L., Jing, W., Graves, M.V., Burbank, D.E. and Van Etten, J.L., 1997. Hyaluronan synthase of chlorella virus PBCV-1. *Science*, **278,** 1800-3.

DeAngelis, P.L., Papaconstantinou, J. and Weigel, P.H., 1993. Molecular cloning, identification, and sequence of the hyaluronan synthase gene from group A Streptococcus pyogenes. *J Biol Chem*, **268,** 19181-4.

DeAngelis, P.L. and Weigel, P.H., 1994. Immunochemical confirmation of the primary structure of streptococcal hyaluronan synthase and synthesis of high molecular weight product by the recombinant enzyme. *Biochemistry*, **33,** 9033-9.

Diamond, J.R., Levinson, M., Kreisberg, R. and Ricardo, S.D., 1997. Increased expression of decorin in experimental hydronephrosis. *Kidney Int*, **51,** 1133-9.

Ducale, A.E., Ward, S.I., Dechert, T. and Yager, D.R., 2005. Regulation of hyaluronan synthase-2 expression in human intestinal mesenchymal cells: mechanisms of interleukin-1{beta} mediated induction. *Am J Physiol Gastrointest Liver Physiol.* (Epub ahead of print)

Du Priest, R.W., Jr. and Fletcher, W.S., 1973. Chemotherapy of testicular germinal tumors. *Oncology*, **28,** 147-63.

Eddy, A.A., 2000. Molecular basis of renal fibrosis. *Pediatr Nephrol*, **15,** 290-301.

Eisen, A. and Lucchesi, J.C., 1998. Unraveling the role of helicases in transcription. *Bioessays*, **20,** 634-41.

Elias, E.G. and Evans, J.T., 1972. Mithramycin in the treatment of Paget's disease of bone. *J Bone Joint Surg Am*, **54,** 1730-6.

Entwistle, J., Hall, C.L. and Turley, E.A., 1996. HA receptors: regulators of signalling to the cytoskeleton. *J Cell Biochem*, **61,** 569-77.

Evanko, S.P. and Wight, T.N., 1999. Intracellular localization of hyaluronan in proliferating cells. *J Histochem Cytochem*, **47,** 1331-42.

Facchinetti, V., Lopa, R., Spreafico, F., Bolognese, F., Mantovani, R., Tavner, F., Watson, R., Introna, M. and Golay, J., 2000. Isolation and characterization of the human A-myb promoter: regulation by NF-Y and Sp1. *Oncogene*, **19,** 3931-40.

Fan, J.M., Ng, Y.Y., Hill, P.A., Nikolic-Paterson, D.J., Mu, W., Atkins, R.C. and Lan, H.Y., 1999. Transforming growth factor-beta regulates tubular epithelial-myofibroblast transdifferentiation in vitro. *Kidney Int*, **56,** 1455-67.

Fellstrom, B., Klareskog, L., Heldin, C.H., Larsson, E., Ronnstrand, L., Terracio, L., Tufveson, G., Wahlberg, J. and Rubin, K., 1989. Platelet-derived growth factor receptors in the kidney--upregulated expression in inflammation. *Kidney Int*, **36,** 1099-102.

Felsenfeld, G. and Groudine, M., 2003. Controlling the double helix. *Nature*, **421,** 448-53.

Feusi, E., Sun, L., Sibalic, A., Beck-Schimmer, B., Oertli, B. and Wuthrich, R.P., 1999. Enhanced hyaluronan synthesis in the MRL-Fas(lpr) kidney: role of cytokines. *Nephron*, **83,** 66-73.

Fioretto, P., Kim, Y. and Mauer, M., 1998. Diabetic nephropathy as a model of reversibility of established renal lesions. *Curr Opin Nephrol Hypertens*, **7,** 489-94.

Fischle, W., Wang, Y. and Allis, C.D., 2003. Histone and chromatin cross-talk. *Curr Opin Cell Biol*, **15,** 172-83.

Fitzgerald, K.A., Bowie, A.G., Skeffington, B.S. and O'Neill, L.A., 2000. Ras, protein kinase C zeta, and I kappa B kinases 1 and 2 are downstream effectors of CD44 during the activation of NF-kappa B by hyaluronic acid fragments in T-24 carcinoma cells. *J Immunol*, **164,** 2053-63.

Florquin, S., Nunziata, R., Claessen, N., van den Berg, F.M., Pals, S.T. and Weening, J.J., 2002. CD44 expression in IgA nephropathy. *Am J Kidney Dis*, **39,** 407-14.

Francki, A., Bradshaw, A.D., Bassuk, J.A., Howe, C.C., Couser, W.G. and Sage, E.H., 1999. SPARC regulates the expression of collagen type I and transforming growth factor-beta1 in mesangial cells. *J Biol Chem*, **274,** 32145-52.

Fraser, D., Wakefield, L. and Phillips, A., 2002. Independent regulation of transforming growth factor-beta1 transcription and translation by glucose and platelet-derived growth factor. *Am J Pathol*, **161,** 1039-49.

Fraser, J.R., Laurent, T.C. and Laurent, U.B., 1997. Hyaluronan: its nature, distribution, functions and turnover. *J Intern Med*, **242,** 27-33.

Gerdin, B. and Hallgren, R., 1997. Dynamic role of hyaluronan (HYA) in connective tissue activation and inflammation. *J Intern Med*, **242,** 49-55.

Gesualdo, L., Di Paolo, S., Milani, S., Pinzani, M., Grappone, C., Ranieri, E., Pannarale, G. and Schena, F.P., 1994. Expression of platelet-derived growth factor receptors in normal and diseased human kidney. An immunohistochemistry and in situ hybridization study. *J Clin Invest*, **94,** 50-8.

Gibbs, D.A., Merrill, E.W., Smith, K.A. and Balazs, E.A., 1968. Rheology of hyaluronic acid. *Biopolymers*, **6,** 777-91.

Gilbert, R.E., Cox, A., Wu, L.L., Allen, T.J., Hulthen, U.L., Jerums, G. and Cooper, M.E., 1998. Expression of transforming growth factor-beta1 and type IV collagen in the renal tubulointerstitium in experimental diabetes: effects of ACE inhibition. *Diabetes*, **47,** 414-22.

Ginetzinsky, A.G., 1958. Role of hyaluronidase in the re-absorption of water in renal tubules: the mechanism of action of the antidiuretic hormone. *Nature*, **182,** 1218-9.

Goetinck, P.F., Stirpe, N.S., Tsonis, P.A. and Carlone, D., 1987. The tandemly repeated sequences of cartilage link protein contain the sites for interaction with hyaluronic acid. *J Cell Biol*, **105,** 2403-8.

Goldberg, G., Caldwell, P., Weissbach, H. and Brot, N., 1979. In vitro regulation of DNA-dependent synthesis of Escherichia coli ribosomal protein L12. *Proc Natl Acad Sci U S A*, **76,** 1716-20.

Gomez, D.E., Alonso, D.F., Yoshiji, H. and Thorgeirsson, U.P., 1997. Tissue inhibitors of metalloproteinases: structure, regulation and biological functions. *Eur J Cell Biol*, **74,** 111-22.

Goransson, V., Johnsson, C., Jacobson, A., Heldin, P., Hallgren, R. and Hansell, P., 2004. Renal hyaluronan accumulation and hyaluronan synthase expression after ischaemia-reperfusion injury in the rat. *Nephrol Dial Transplant*, **19,** 823-30.

Gou, Q., Liu, C.H., Ben-Av, P. and Hla, T., 1998. Dissociation of basal turnover and cytokine-induced transcript stabilization of the human cyclooxygenase-2 mRNA by mutagenesis of the 3'-untranslated region. *Biochem Biophys Res Commun*, **242,** 508-12.

Goumenos, D.S., Brown, C.B., Shortland, J. and el Nahas, A.M., 1994. Myofibroblasts, predictors of progression of mesangial IgA nephropathy? *Nephrol Dial Transplant*, **9,** 1418-25.

Grandaliano, G., Gesualdo, L., Ranieri, E., Monno, R., Montinaro, V., Marra, F. and Schena, F.P., 1996. Monocyte chemotactic peptide-1 expression in acute and chronic human nephritides: a pathogenetic role in interstitial monocytes recruitment. *J Am Soc Nephrol*, **7,** 906-13.

Grobe, K. and Esko, J.D., 2002. Regulated translation of heparan sulfate N-acetylglucosamine N-deacetylase/n-sulfotransferase isozymes by structured 5'-untranslated regions and internal ribosome entry sites. *J Biol Chem*, **277,** 30699-706.

Guo, G., Morrissey, J., McCracken, R., Tolley, T. and Klahr, S., 1999. Role of TNFR1 and TNFR2 receptors in tubulointerstitial fibrosis of obstructive nephropathy. *Am J Physiol*, **277,** F766-72.

Hall, C.L., Lange, L.A., Prober, D.A., Zhang, S. and Turley, E.A., 1996. pp60(c-src) is required for cell locomotion regulated by the hyaluronanreceptor RHAMM. *Oncogene*, **13,** 2213-24.

Hallgren, R., Gerdin, B. and Tufveson, G., 1990. Hyaluronic acid accumulation and redistribution in rejecting rat kidney graft. Relationship to the transplantation edema. *J Exp Med*, **171,** 2063-76.

Hansell, P., Goransson, V., Odlind, C., Gerdin, B. and Hallgren, R., 2000. Hyaluronan content in the kidney in different states of body hydration. *Kidney Int*, **58,** 2061-8.

Hansen, J.C., 2002. Conformational dynamics of the chromatin fiber in solution: determinants, mechanisms, and functions. *Annu Rev Biophys Biomol Struct*, **31,** 361-92.

Hardingham, T.E., 1979. The role of link-protein in the structure of cartilage proteoglycan aggregates. *Biochem J*, **177,** 237-47.

Hascall, V. and Laurent, T., 2000. Hyaluronan: structure and physical properties. http://www.glycoforum.gr.jp/science/hyaluronan/

Hascall, V.C., Majors, A.K., De La Motte, C.A., Evanko, S.P., Wang, A., Drazba, J.A., Strong, S.A. and Wight, T.N., 2004. Intracellular hyaluronan: a new frontier for inflammation? *Biochim Biophys Acta*, **1673,** 3-12.

Haubeck, H.D., Kock, R., Fischer, D.C., Van de Leur, E., Hoffmeister, K. and Greiling, H., 1995. Transforming growth factor beta 1, a major stimulator of hyaluronan synthesis in human synovial lining cells. *Arthritis Rheum*, **38,** 669-77.

Heldin, P., Asplund, T., Ytterberg, D., Thelin, S. and Laurent, T.C., 1992. Characterization of the molecular mechanism involved in the activation of hyaluronan synthetase by platelet-derived growth factor in human mesothelial cells. *Biochem J*, **283 (Pt 1),** 165-70.

Hofmann, M., Fieber, C., Assmann, V., Gottlicher, M., Sleeman, J., Plug, R., Howells, N., von Stein, O., Ponta, H. and Herrlich, P., 1998. Identification of IHABP, a 95 kDa intracellular hyaluronate binding protein. *J Cell Sci*, **111 (Pt 12),** 1673-84.

Hoogendoorn, B., Coleman, S.L., Guy, C.A., Smith, K., Bowen, T., Buckland, P.R. and O'Donovan, M.C., 2003. Functional analysis of human promoter polymorphisms. *Hum Mol Genet*, **12,** 2249-54.

Horton, M.R., McKee, C.M., Bao, C., Liao, F., Farber, J.M., Hodge-DuFour, J., Pure, E., Oliver, B.L., Wright, T.M. and Noble, P.W., 1998. Hyaluronan fragments synergize with interferon-gamma to induce the C-X-C chemokines mig and interferon-inducible protein-10 in mouse macrophages. *J Biol Chem*, **273,** 35088-94.

Huang, L., Grammatikakis, N., Yoneda, M., Banerjee, S.D. and Toole, B.P., 2000. Molecular characterization of a novel intracellular hyaluronan-binding protein. *J Biol Chem*, **275,** 29829-39.

Hughes, T.R., Tengku-Muhammad, T.S., Irvine, S.A. and Ramji, D.P., 2002. A novel role of Sp1 and Sp3 in the interferon-gamma -mediated suppression of macrophage lipoprotein lipase gene transcription. *J Biol Chem*, **277,** 11097-106.

Hugo, C., Shankland, S.J., Pichler, R.H., Couser, W.G. and Johnson, R.J., 1998. Thrombospondin 1 precedes and predicts the development of tubulointerstitial fibrosis in glomerular disease in the rat. *Kidney Int*, **53,** 302-11.

Ijuin, C., Ohno, S., Tanimoto, K., Honda, K. and Tanne, K., 2001. Regulation of hyaluronan synthase gene expression in human periodontal ligament cells by tumour necrosis factor-alpha, interleukin-1beta and interferon-gamma. *Arch Oral Biol*, **46,** 767-72.

Itano, N., Atsumi, F., Sawai, T., Yamada, Y., Miyaishi, O., Senga, T., Hamaguchi, M. and Kimata, K., 2002. Abnormal accumulation of hyaluronan matrix diminishes contact inhibition of cell growth and promotes cell migration. *Proc Natl Acad Sci U S A*, **99,** 3609-14.

Itano, N. and Kimata, K., 1996. Molecular cloning of human hyaluronan synthase. *Biochem Biophys Res Commun*, **222,** 816-20.

Itano, N. and Kimata, K., 1996. Expression cloning and molecular characterization of HAS protein, a eukaryotic hyaluronan synthase. *J Biol Chem*, **271,** 9875-8.

Itano, N., Sawai, T., Yoshida, M., Lenas, P., Yamada, Y., Imagawa, M., Shinomura, T., Hamaguchi, M., Yoshida, Y., Ohnuki, Y., Miyauchi, S., Spicer, A.P., McDonald, J.A. and Kimata, K., 1999. Three isoforms of mammalian hyaluronan synthases have distinct enzymatic properties. *J Biol Chem*, **274,** 25085-92.

Ito, A., Shimada, M. and Mori, Y., 1993. Regulation of hyaluronate production by interleukin 1 in cultured human chorionic cells. *Biochim Biophys Acta*, **1158,** 91-7.

Ito, T., Williams, J.D., Fraser, D. and Phillips, A.O., 2004. Hyaluronan attenuates transforming growth factor-beta1-mediated signaling in renal proximal tubular epithelial cells. *Am J Pathol*, **164,** 1979-88.

Ito, T., Williams, J.D., Fraser, D.J. and Phillips, A.O., 2004. Hyaluronan regulates transforming growth factor-beta1 receptor compartmentalization. *J Biol Chem*, **279,** 25326-32.

Ito, Y., Aten, J., Bende, R.J., Oemar, B.S., Rabelink, T.J., Weening, J.J. and Goldschmeding, R., 1998. Expression of connective tissue growth factor in human renal fibrosis. *Kidney Int*, **53,** 853-61.

Jacobson, A., Brinck, J., Briskin, M.J., Spicer, A.P. and Heldin, P., 2000. Expression of human hyaluronan synthases in response to external stimuli. *Biochem J*, **348 Pt 1,** 29-35.

Jenkins, R.H., Thomas, G.J., Williams, J.D. and Steadman, R., 2004. Myofibroblastic differentiation leads to hyaluronan accumulation through reduced hyaluronan turnover. *J Biol Chem*, **279,** 41453-60.

Jernigan, S.M. and Eddy, A.A., 2000. Experimental insights into the mechanisms of tubulo-interstitial scarring. In: El Nahas, M., Harris, K. and Anderson, S. (Eds), Mechanisms and clinical management of chronic renal failure. *Oxford University Press*, 104-145.

Johnsson, C., Tufveson, G., Wahlberg, J. and Hallgren, R., 1996. Experimentally-induced warm renal ischemia induces cortical accumulation of hyaluronan in the kidney. *Kidney Int*, **50,** 1224-9.

Jones, C.L., Buch, S., Post, M., McCulloch, L., Liu, E. and Eddy, A.A., 1992. Renal extracellular matrix accumulation in acute puromycin aminonucleoside nephrosis in rats. *Am J Pathol*, **141,** 1381-96.

Jones, S. and Phillips, A.O., 2001. Regulation of renal proximal tubular epithelial cell hyaluronan generation: implications for diabetic nephropathy. *Kidney Int*, **59,** 1739-49.

Jones, S.G., Ito, T. and Phillips, A.O., 2003. Regulation of proximal tubular epithelial cell CD44-mediated binding and internalisation of hyaluronan. *Int J Biochem Cell Biol*, **35,** 1361-77.

Jun, Z., Hill, P.A., Lan, H.Y., Foti, R., Mu, W., Atkins, R.C. and Nikolic-Paterson, D.J., 1997. CD44 and hyaluronan expression in the development of experimental crescentic glomerulonephritis. *Clin Exp Immunol*, **108,** 69-77.

Kadonaga, J.T., 2002. The DPE, a core promoter element for transcription by RNA polymerase II. *Exp Mol Med*, **34,** 259-64.

Kakizaki, I., Kojima, K., Takagaki, K., Endo, M., Kannagi, R., Ito, M., Maruo, Y., Sato, H., Yasuda, T., Mita, S., Kimata, K. and Itano, N., 2004. A novel mechanism for the inhibition of hyaluronan biosynthesis by 4-methylumbelliferone. *J Biol Chem*, **279,** 33281-9.

Kamikura, D.M., Khoury, H., Maroun, C., Naujokas, M.A. and Park, M., 2000. Enhanced transformation by a plasma membrane-associated met oncoprotein: activation of a phosphoinositide 3'-kinase-dependent autocrine loop involving hyaluronic acid and CD44. *Mol Cell Biol*, **20,** 3482-96.

Karin, M. and Ben-Neriah, Y., 2000. Phosphorylation meets ubiquitination: the control of NF-[kappa]B activity. *Annu Rev Immunol*, **18,** 621-63.

Karvinen, S., Pasonen-Seppanen, S., Hyttinen, J.M., Pienimaki, J.P., Torronen, K., Jokela, T.A., Tammi, M.I. and Tammi, R., 2003. Keratinocyte growth factor stimulates migration and hyaluronan synthesis in the epidermis by activation of keratinocyte hyaluronan synthases 2 and 3. *J Biol Chem*, **278,** 49495-504.

Kaya, G., Rodriguez, I., Jorcano, J.L., Vassalli, P. and Stamenkovic, I., 1997. Selective suppression of CD44 in keratinocytes of mice bearing an antisense CD44 transgene driven by a tissue-specific promoter disrupts hyaluronate metabolism in the skin and impairs keratinocyte proliferation. *Genes Dev*, **11,** 996-1007.

Kennedy, B.J., 1972. Mithramycin therapy in testicular cancer. *J Urol*, **107,** 429-32.

Kennedy, C.I., Diegelmann, R.F., Haynes, J.H. and Yager, D.R., 2000. Proinflammatory cytokines differentially regulate hyaluronan synthase isoforms in fetal and adult fibroblasts. *J Pediatr Surg*, **35,** 874-9.

Kent, W.J., 2002. BLAT--the BLAST-like alignment tool. *Genome Res*, **12,** 656-64.

Kim, S., Kang, B.Y., Cho, S.Y., Sung, D.S., Chang, H.K., Yeom, M.H., Kim, D.H., Sim, Y.C. and Lee, Y.S., 2004. Compound K induces expression of hyaluronan synthase 2 gene in transformed human keratinocytes and increases hyaluronan in hairless mouse skin. *Biochem Biophys Res Commun*, **316,** 348-55.

Kinyamu, H.K. and Archer, T.K., 2004. Modifying chromatin to permit steroid hormone receptor-dependent transcription. *Biochim Biophys Acta*, **1677,** 30-45.

Kirov, G., Williams, N., Sham, P., Craddock, N. and Owen, M.J., 2000. Pooled genotyping of microsatellite markers in parent-offspring trios. *Genome Res*, **10,** 105-15.

Klewes, L. and Prehm, P., 1994. Intracellular signal transduction for serum activation of the hyaluronan synthase in eukaryotic cell lines. *J Cell Physiol*, **160,** 539-44.

Kliem, V., Johnson, R.J., Alpers, C.E., Yoshimura, A., Couser, W.G., Koch, K.M. and Floege, J., 1996. Mechanisms involved in the pathogenesis of tubulointerstitial fibrosis in 5/6-nephrectomized rats. *Kidney Int*, **49,** 666-78.

Knepper, M.A., Saidel, G.M., Hascall, V.C. and Dwyer, T., 2003. Concentration of solutes in the renal inner medulla: interstitial hyaluronan as a mechano-osmotic transducer. *Am J Physiol Renal Physiol*, **284,** F433-46.

Knudson, C.B. and Knudson, W., 1993. Hyaluronan-binding proteins in development, tissue homeostasis, and disease. *Faseb J*, **7,** 1233-41.

Knudson, W., Biswas, C., Li, X.Q., Nemec, R.E. and Toole, B.P., 1989. The role and regulation of tumour-associated hyaluronan. *Ciba Found Symp*, **143,** 150-9; discussion 159-69, 281-5.

Knudson, W. and Knudson, C.B., 2000. The hyaluronan receptor, CD44. http://www.glycoforum.gr.jp/science/hyaluronan/HA10/HA10E.html

Kockar, F.T., Foka, P., Hughes, T.R., Kousteni, S. and Ramji, D.P., 2001. Analysis of the Xenopus laevis CCAAT-enhancer binding protein alpha gene promoter demonstrates species-specific differences in the mechanisms for both auto-activation and regulation by Sp1. *Nucleic Acids Res*, **29,** 362-72.

Kohda, D., Morton, C.J., Parkar, A.A., Hatanaka, H., Inagaki, F.M., Campbell, I.D. and Day, A.J., 1996. Solution structure of the link module: a hyaluronan-binding domain involved in extracellular matrix stability and cell migration. *Cell*, **86,** 767-75.

Kopp, J.B., Factor, V.M., Mozes, M., Nagy, P., Sanderson, N., Bottinger, E.P., Klotman, P.E. and Thorgeirsson, S.S., 1996. Transgenic mice with increased plasma levels of TGF-beta 1 develop progressive renal disease. *Lab Invest*, **74,** 991-1003.

Kosaki, R., Watanabe, K. and Yamaguchi, Y., 1999. Overproduction of hyaluronan by expression of the hyaluronan synthase Has2 enhances anchorage-independent growth and tumorigenicity. *Cancer Res*, **59,** 1141-5.

Kozak, M., 1987. At least six nucleotides preceding the AUG initiator codon enhance translation in mammalian cells. *J Mol Biol*, **196,** 947-50.

Krawczak, M., Reiss, J. and Cooper, D.N., 1992. The mutational spectrum of single base-pair substitutions in mRNA splice junctions of human genes: causes and consequences. *Hum Genet*, **90,** 41-54.

Lan, H.Y., Nikolic-Paterson, D.J., Mu, W. and Atkins, R.C., 1995. Local macrophage proliferation in multinucleated giant cell and granuloma formation in experimental Goodpasture's syndrome. *Am J Pathol*, **147,** 1214-20.

Lan, H.Y., Nikolic-Paterson, D.J., Zarama, M., Vannice, J.L. and Atkins, R.C., 1993. Suppression of experimental crescentic glomerulonephritis by the interleukin-1 receptor antagonist. *Kidney Int*, **43,** 479-85.

Laurent, T.C. and Fraser, J.R., 1992. Hyaluronan. *Faseb J*, **6,** 2397-404.

Laurent, T.C., Laurent, U.B. and Fraser, J.R., 1996. The structure and function of hyaluronan: An overview. *Immunol Cell Biol*, **74,** A1-7.

Lee, G.M., Johnstone, B., Jacobson, K. and Caterson, B., 1993. The dynamic structure of the pericellular matrix on living cells. *J Cell Biol*, **123,** 1899-907.

Lee, J.Y. and Spicer, A.P., 2000. Hyaluronan: a multifunctional, megaDalton, stealth molecule. *Curr Opin Cell Biol*, **12,** 581-6.

Lepperdinger, G., Mullegger, J. and Kreil, G., 2001. Hyal2--less active, but more versatile? *Matrix Biol*, **20,** 509-14.

Lesley, J., Hyman, R. and Kincade, P.W., 1993. CD44 and its interaction with extracellular matrix. *Adv Immunol*, **54,** 271-335.

Lewin, B., 2000. Genes VII. *Oxford University Press*, 990.

Li, M., Rosenfeld, L., Vilar, R.E. and Cowman, M.K., 1997. Degradation of hyaluronan by peroxynitrite. *Arch Biochem Biophys*, **341,** 245-50.

Lin, Y.Z., Yao, S.Y., Veach, R.A., Torgerson, T.R. and Hawiger, J., 1995. Inhibition of nuclear translocation of transcription factor NF-kappa B by a synthetic peptide containing a cell membrane-permeable motif and nuclear localization sequence. *J Biol Chem*, **270,** 14255-8.

Lokeshwar, V.B., Fregien, N. and Bourguignon, L.Y., 1994. Ankyrin-binding domain of CD44(GP85) is required for the expression of hyaluronic acid-mediated adhesion function. *J Cell Biol*, **126,** 1099-109.

Lokeshwar, V.B., Iida, N. and Bourguignon, L.Y., 1996. The cell adhesion molecule, GP116, is a new CD44 variant (ex14/v10) involved in hyaluronic acid binding and endothelial cell proliferation. *J Biol Chem*, **271,** 23853-64.

Lokeshwar, V.B., Schroeder, G.L., Carey, R.I., Soloway, M.S. and Iida, N., 2002. Regulation of hyaluronidase activity by alternative mRNA splicing. *J Biol Chem*, **277,** 33654-63.

Lokeshwar, V.B. and Selzer, M.G., 2000. Differences in hyaluronic acid-mediated functions and signaling in arterial, microvessel, and vein-derived human endothelial cells. *J Biol Chem*, **275,** 27641-9.

Luger, K. and Hansen, J.C., 2005. Nucleosome and chromatin fiber dynamics. *Curr Opin Struct Biol*, **15,** 188-96.

Lynn, B.D., Li, X., Cattini, P.A., Turley, E.A. and Nagy, J.I., 2001. Identification of sequence, protein isoforms, and distribution of the hyaluronan-binding protein RHAMM in adult and developing rat brain. *J Comp Neurol*, **439,** 315-30.

Ma, X.T., Qian, M.P. and Tang, H.X., 2004. Predicting polymerase II core promoters by cooperating transcription factor binding sites in eukaryotic genes. *Acta Biochim Biophys Sin (Shanghai)*, **36,** 250-8.

Mack, J.A., Abramson, S.R., Ben, Y., Coffin, J.C., Rothrock, J.K., Maytin, E.V., Hascall, V.C., Largman, C. and Stelnicki, E.J., 2003. Hoxb13 knockout adult skin exhibits high levels of hyaluronan and enhanced wound healing. *Faseb J*, **17,** 1352-4.

MacPhee, P.J., 1998. Estimating rat renal medullary interstitial oncotic pressures and the driving force for fluid uptake into ascending vasa recta. *J Physiol*, **506 (Pt 2),** 529-38.

Mahadevan, P., Larkins, R.G., Fraser, J.R. and Dunlop, M.E., 1996. Effect of prostaglandin E2 and hyaluronan on mesangial cell proliferation. A potential contribution to glomerular hypercellularity in diabetes. *Diabetes*, **45,** 44-50.

Mahadevan, P., Larkins, R.G., Fraser, J.R., Fosang, A.J. and Dunlop, M.E., 1995. Increased hyaluronan production in the glomeruli from diabetic rats: a link between glucose-induced prostaglandin production and reduced sulphated proteoglycan. *Diabetologia*, **38,** 298-305.

Majors, A.K., Austin, R.C., de la Motte, C.A., Pyeritz, R.E., Hascall, V.C., Kessler, S.P., Sen, G. and Strong, S.A., 2003. Endoplasmic reticulum stress induces hyaluronan deposition and leukocyte adhesion. *J Biol Chem*, **278,** 47223-31.

Mantovani, R., 1998. A survey of 178 NF-Y binding CCAAT boxes. *Nucleic Acids Res*, **26,** 1135-43.

Mantovani, R., 1999. The molecular biology of the CCAAT-binding factor NF-Y. *Gene*, **239,** 15-27.

Marcussen, N., 1992. Atubular glomeruli and the structural basis for chronic renal failure. *Lab Invest*, **66,** 265-84.

Margolis, R.K., Crockett, C.P., Kiang, W.L. and Margolis, R.U., 1976. Glycosaminoglycans and glycoproteins associated with rat brain nuclei. *Biochim Biophys Acta*, **451,** 465-9.

Masellis-Smith, A., Belch, A.R., Mant, M.J., Turley, E.A. and Pilarski, L.M., 1996. Hyaluronan-dependent motility of B cells and leukemic plasma cells in blood, but not of bone marrow plasma cells, in multiple myeloma: alternate use of receptor for hyaluronan-mediated motility (RHAMM) and CD44. *Blood*, **87,** 1891-9.

McKee, C.M., Lowenstein, C.J., Horton, M.R., Wu, J., Bao, C., Chin, B.Y., Choi, A.M. and Noble, P.W., 1997. Hyaluronan fragments induce nitric-oxide synthase in murine macrophages through a nuclear factor kappaB-dependent mechanism. *J Biol Chem*, **272,** 8013-8.

Meyer, K. and Palmer, J.W., 1934. The polysaccharide of the vitreous humor. *J Biol Chem*, **107,** 629-634.

Miner, J.H., 1999. Renal basement membrane components. *Kidney Int*, **56,** 2016-24.

Mohamadzadeh, M., DeGrendele, H., Arizpe, H., Estess, P. and Siegelman, M., 1998. Proinflammatory stimuli regulate endothelial hyaluronan expression and CD44/HA-dependent primary adhesion. *J Clin Invest*, **101,** 97-108.

Mohapatra, S., Yang, X., Wright, J.A., Turley, E.A. and Greenberg, A.H., 1996. Soluble hyaluronan receptor RHAMM induces mitotic arrest by suppressing Cdc2 and cyclin B1 expression. *J Exp Med*, **183,** 1663-8.

Monslow, J., Williams, J.D., Norton, N., Guy, C.A., Price, I.K., Coleman, S.L., Williams, N.M., Buckland, P.R., Spicer, A.P., Topley, N., Davies, M. and Bowen, T., 2003. The human hyaluronan synthase genes: genomic structures, proximal promoters and polymorphic microsatellite markers. *Int J Biochem Cell Biol*, **35,** 1272-83.

Monslow, J., Williams, J.D., Guy, C.A., Price, I.K., Craig, K.J., Williams, H.J., Williams, N.M., Martin, J., Coleman, S.L., Topley, N., Spicer, A.P., Buckland, P.R., Davies, M. and Bowen, T., 2004. Identification and analysis of the promoter region of the human hyaluronan synthase 2 gene. *J Biol Chem*, **279,** 20576-81.

Morrissey, J.J. and Klahr, S., 1998. Differential effects of ACE and AT1 receptor inhibition on chemoattractant and adhesion molecule synthesis. *Am J Physiol*, **274,** F580-6.

Muller, G.A., Zeisberg, M. and Strutz, F., 2000. The importance of tubulointerstitial damage in progressive renal disease. *Nephrol Dial Transplant*, **15 Suppl 6,** 76-7.

Munthe, E. and Aasheim, H.C., 2002. Characterization of the human ephrin-A4 promoter. *Biochem J*, **366,** 447-58.

Nagamatsu, T., Hayashi, K., Oka, T. and Suzuki, Y., 1999. Angiotensin II type I receptor antagonist suppresses proteinuria and glomerular lesions in experimental nephritis. *Eur J Pharmacol*, **374,** 93-101.

Nangaku, M., Pippin, J. and Couser, W.G., 1999. Complement membrane attack complex (C5b-9) mediates interstitial disease in experimental nephrotic syndrome. *J Am Soc Nephrol*, **10,** 2323-31.

Nardini, M., Ori, M., Vigetti, D., Gornati, R., Nardi, I. and Perris, R., 2004. Regulated gene expression of hyaluronan synthases during Xenopus laevis development. *Gene Expr Patterns*, **4,** 303-8.

Nathan, C.F., 1987. Secretory products of macrophages. *J Clin Invest*, **79,** 319-26.

Nentwich, H.A., Mustafa, Z., Rugg, M.S., Marsden, B.D., Cordell, M.R., Mahoney, D.J., Jenkins, S.C., Dowling, B., Fries, E., Milner, C.M., Loughlin, J. and Day, A.J., 2002. A novel allelic variant of the human TSG-6 gene encoding an amino acid difference in the CUB module. Chromosomal localization, frequency analysis, modeling, and expression. *J Biol Chem*, **277,** 15354-62.

Nikolov, D.B. and Burley, S.K., 1997. RNA polymerase II transcription initiation: a structural view. *Proc Natl Acad Sci U S A*, **94,** 15-22.

Nishida, Y., Knudson, C.B., Kuettner, K.E. and Knudson, W., 2000. Osteogenic protein-1 promotes the synthesis and retention of extracellular matrix within bovine articular cartilage and chondrocyte cultures. *Osteoarthritis Cartilage*, **8,** 127-36.

Nishida, Y., Knudson, C.B., Nietfeld, J.J., Margulis, A. and Knudson, W., 1999. Antisense inhibition of hyaluronan synthase-2 in human articular chondrocytes inhibits proteoglycan retention and matrix assembly. *J Biol Chem*, **274,** 21893-9.

Nishikawa, K., Andres, G., Bhan, A.K., McCluskey, R.T., Collins, A.B., Stow, J.L. and Stamenkovic, I., 1993. Hyaluronate is a component of crescents in rat autoimmune glomerulonephritis. *Lab Invest*, **68,** 146-53.

Noble, P.W., McKee, C.M., Cowman, M. and Shin, H.S., 1996. Hyaluronan fragments activate an NF-kappa B/I-kappa B alpha autoregulatory loop in murine macrophages. *J Exp Med*, **183,** 2373-8.

Nomura, A., Morita, Y., Maruyama, S., Hotta, N., Nadai, M., Wang, L., Hasegawa, T. and Matsuo, S., 1997. Role of complement in acute tubulointerstitial injury of rats with aminonucleoside nephrosis. *Am J Pathol*, **151,** 539-47.

Oertli, B., Beck-Schimmer, B., Fan, X. and Wuthrich, R.P., 1998. Mechanisms of hyaluronan-induced up-regulation of ICAM-1 and VCAM-1 expression by murine kidney tubular epithelial cells: hyaluronan triggers cell adhesion molecule expression through a mechanism involving activation of nuclear factor-kappa B and activating protein-1. *J Immunol*, **161,** 3431-7.

Ohkawa, T., Ueki, N., Taguchi, T., Shindo, Y., Adachi, M., Amuro, Y., Hada, T. and Higashino, K., 1999. Stimulation of hyaluronan synthesis by tumor necrosis factor-alpha is mediated by the p50/p65 NF-kappa B complex in MRC-5 myofibroblasts. *Biochim Biophys Acta*, **1448,** 416-24.

Ohno, S., Tanimoto, K., Fujimoto, K., Ijuin, C., Honda, K., Tanaka, N., Doi, T., Nakahara, M. and Tanne, K., 2001. Molecular cloning of rabbit hyaluronic acid synthases and their expression patterns in synovial membrane and articular cartilage. *Biochim Biophys Acta*, **1520,** 71-8.

Okada, H., Moriwaki, K., Kalluri, R., Imai, H., Ban, S., Takahama, M. and Suzuki, H., 2000. Inhibition of monocyte chemoattractant protein-1 expression in tubular epithelium attenuates tubulointerstitial alteration in rat Goodpasture syndrome. *Kidney Int*, **57,** 927-36.

Oliferenko, S., Kaverina, I., Small, J.V. and Huber, L.A., 2000. Hyaluronic acid (HA) binding to CD44 activates Rac1 and induces lamellipodia outgrowth. *J Cell Biol*, **148,** 1159-64.

Otsuka, F., Yamauchi, T., Kataoka, H., Mimura, Y., Ogura, T. and Makino, H., 1998. Effects of chronic inhibition of ACE and AT1 receptors on glomerular injury in dahl salt-sensitive rats. *Am J Physiol*, **274,** R1797-806.

Papakonstantinou, E., Roth, M., Block, L.H., Mirtsou-Fidani, V., Argiriadis, P. and Karakiulakis, G., 1998. The differential distribution of hyaluronic acid in the layers of human atheromatic aortas is associated with vascular smooth muscle cell proliferation and migration. *Atherosclerosis*, **138,** 79-89.

Parks, C.L. and Shenk, T., 1996. The serotonin 1a receptor gene contains a TATA-less promoter that responds to MAZ and Sp1. *J Biol Chem*, **271,** 4417-30.

Pasonen-Seppanen, S., Karvinen, S., Torronen, K., Hyttinen, J.M., Jokela, T., Lammi, M.J., Tammi, M.I. and Tammi, R., 2003. EGF upregulates, whereas TGF-beta downregulates, the hyaluronan synthases Has2 and Has3 in organotypic keratinocyte cultures: correlations with epidermal proliferation and differentiation. *J Invest Dermatol*, **120,** 1038-44.

Perez-Gomez, C., Mates, J.M., Gomez-Fabre, P.M., del Castillo-Olivares, A., Alonso, F.J. and Marquez, J., 2003. Genomic organization and transcriptional analysis of the human l-glutaminase gene. *Biochem J*, **370,** 771-84.

Perin, J.P., Bonnet, F., Thurieau, C. and Jolles, P., 1987. Link protein interactions with hyaluronate and proteoglycans. Characterization of two distinct domains in bovine cartilage link proteins. *J Biol Chem*, **262,** 13269-72.

Pichler, R.H., Hugo, C., Shankland, S.J., Reed, M.J., Bassuk, J.A., Andoh, T.F., Lombardi, D.M., Schwartz, S.M., Bennett, W.M., Alpers, C.E., Sage, E.H., Johnson, R.J. and Couser, W.G., 1996. SPARC is expressed in renal interstitial fibrosis and in renal vascular injury. *Kidney Int*, **50,** 1978-89.

Pienimaki, J.P., Rilla, K., Fulop, C., Sironen, R.K., Karvinen, S., Pasonen, S., Lammi, M.J., Tammi, R., Hascall, V.C. and Tammi, M.I., 2001. Epidermal growth factor activates hyaluronan synthase 2 in epidermal keratinocytes and increases pericellular and intracellular hyaluronan. *J Biol Chem*, **276,** 20428-35.

Pitcock, J.A., Lyons, H., Brown, P.S., Rightsel, W.A. and Muirhead, E.E., 1988. Glycosaminoglycans of the rat renomedullary interstitium: ultrastructural and biochemical observations. *Exp Mol Pathol*, **49,** 373-87.

Ponta, H., Sherman, L. and Herrlich, P.A., 2003. CD44: from adhesion molecules to signalling regulators. *Nat Rev Mol Cell Biol*, **4,** 33-45.

Prehm, P., 1985. Inhibition of hyaluronate synthesis. *Biochem J*, **225,** 699-705.

Quandt, K., Frech, K., Karas, H., Wingender, E. and Werner, T., 1995. MatInd and MatInspector: new fast and versatile tools for detection of consensus matches in nucleotide sequence data. *Nucleic Acids Res*, **23,** 4878-84.

Rao, C.M., Deb, T.B., Gupta, S. and Datta, K., 1997. Regulation of cellular phosphorylation of hyaluronan binding protein and its role in the formation of second messenger. *Biochim Biophys Acta*, **1336,** 387-93.

Razik, M.A., Lee, K., Price, R.R., Williams, M.R., Ongjoco, R.R., Dole, M.K., Rudner, X.L., Kwatra, M.M. and Schwinn, D.A., 1997. Transcriptional regulation of the human alpha1a-adrenergic receptor gene. Characterization Of the 5'-regulatory and promoter region. *J Biol Chem*, **272,** 28237-46.

Recklies, A.D., White, C., Melching, L. and Roughley, P.J., 2001. Differential regulation and expression of hyaluronan synthases in human articular chondrocytes, synovial cells and osteosarcoma cells. *Biochem J*, **354,** 17-24.

Remuzzi, G. and Bertani, T., 1998. Pathophysiology of progressive nephropathies. *N Engl J Med*, **339,** 1448-56.

Ricardo, S.D., Levinson, M.E., DeJoseph, M.R. and Diamond, J.R., 1996. Expression of adhesion molecules in rat renal cortex during experimental hydronephrosis. *Kidney Int*, **50,** 2002-10.

Rilla, K., Siiskonen, H., Spicer, A.P., Hyttinen, J.M., Tammi, M.I. and Tammi, R.H., 2005. Plasma membrane residence of hyaluronan synthase is coupled to its enzymatic activity. *J Biol Chem*.

Riser, B.L., Denichilo, M., Cortes, P., Baker, C., Grondin, J.M., Yee, J. and Narins, R.G., 2000. Regulation of connective tissue growth factor activity in cultured rat mesangial cells and its expression in experimental diabetic glomerulosclerosis. *J Am Soc Nephrol*, **11,** 25-38.

Roberts, I.S., Burrows, C., Shanks, J.H., Venning, M. and McWilliam, L.J., 1997. Interstitial myofibroblasts: predictors of progression in membranous nephropathy. *J Clin Pathol*, **50,** 123-7.

Ropponen, K., Tammi, M., Parkkinen, J., Eskelinen, M., Tammi, R., Lipponen, P., Agren, U., Alhava, E. and Kosma, V.M., 1998. Tumor cell-associated hyaluronan as an unfavorable prognostic factor in colorectal cancer. *Cancer Res*, **58,** 342-7.

Rouschop, K.M., Sewnath, M.E., Claessen, N., Roelofs, J.J., Hoedemaeker, I., van der Neut, R., Aten, J., Pals, S.T., Weening, J.J. and Florquin, S., 2004. CD44 deficiency increases tubular damage but reduces renal fibrosis in obstructive nephropathy. *J Am Soc Nephrol*, **15,** 674-86.

Roy-Chaudhury, P., Wu, B., King, G., Campbell, M., Macleod, A.M., Haites, N.E., Simpson, J.G. and Power, D.A., 1996. Adhesion molecule interactions in human glomerulonephritis: importance of the tubulointerstitium. *Kidney Int*, **49,** 127-34.

Rozen, S. and Skaletsky, H., 2000. Primer3 on the WWW for general users and for biologist programmers. *Methods Mol Biol*, **132,** 365-86.

Ryan, M.J., Johnson, G., Kirk, J., Fuerstenberg, S.M., Zager, R.A. and Torok-Storb, B., 1994. HK-2: an immortalized proximal tubule epithelial cell line from normal adult human kidney. *Kidney Int*, **45,** 48-57.

Saavalainen, K., Pasonen-Seppanen, S., Dunlop, T.W., Tammi, R., Tammi, M.I. and Carlberg, C., 2005. The human hyaluronan synthase 2 gene is a primary retinoic acid and epidermal growth factor responding gene. *J Biol Chem.*

Sampson, P.M., Rochester, C.L., Freundlich, B. and Elias, J.A., 1992. Cytokine regulation of human lung fibroblast hyaluronan (hyaluronic acid) production. Evidence for cytokine-regulated hyaluronan (hyaluronic acid) degradation and human lung fibroblast-derived hyaluronidase. *J Clin Invest*, **90,** 1492-503.

Savani, R.C., Cao, G., Pooler, P.M., Zaman, A., Zhou, Z. and DeLisser, H.M., 2001. Differential involvement of the hyaluronan (HA) receptors CD44 and receptor for HA-mediated motility in endothelial cell function and angiogenesis. *J Biol Chem*, **276,** 36770-8.

Sayo, T., Sugiyama, Y., Takahashi, Y., Ozawa, N., Sakai, S., Ishikawa, O., Tamura, M. and Inoue, S., 2002. Hyaluronan synthase 3 regulates hyaluronan synthesis in cultured human keratinocytes. *J Invest Dermatol*, **118,** 43-8.

Schaefer, L., Hausser, H., Altenburger, M., Ugorcakova, J., August, C., Fisher, L.W., Schaefer, R.M. and Kresse, H., 1998. Decorin, biglycan and their endocytosis receptor in rat renal cortex. *Kidney Int*, **54,** 1529-41.

Schenck, P., Schneider, S., Miehlke, R. and Prehm, P., 1995. Synthesis and degradation of hyaluronate by synovia from patients with rheumatoid arthritis. *J Rheumatol*, **22,** 400-5.

Selbi, W., de la Motte, C., Hascall, V. and Phillips, A., 2004. BMP-7 modulates hyaluronan-mediated proximal tubular cell-monocyte interaction. *J Am Soc Nephrol*, **15,** 1199-211.

Serio, K.J., Hodulik, C.R. and Bigby, T.D., 2000. Sp1 and Sp3 function as key regulators of leukotriene C(4) synthase gene expression in the monocyte-like cell line, THP-1. *Am J Respir Cell Mol Biol*, **23,** 234-40.

Seron, D., Alexopoulos, E., Raftery, M.J., Hartley, B. and Cameron, J.S., 1990. Number of interstitial capillary cross-sections assessed by monoclonal antibodies: relation to interstitial damage. *Nephrol Dial Transplant*, **5,** 889-93.

Setala, L.P., Tammi, M.I., Tammi, R.H., Eskelinen, M.J., Lipponen, P.K., Agren, U.M., Parkkinen, J., Alhava, E.M. and Kosma, V.M., 1999. Hyaluronan expression in gastric cancer cells is associated with local and nodal spread and reduced survival rate. *Br J Cancer*, **79,** 1133-8.

Shimabukuro, Y., Ichikawa, T., Takayama, S., Yamada, S., Takedachi, M., Terakura, M., Hashikawa, T. and Murakami, S., 2004. Fibroblast growth factor-2 regulates the synthesis of hyaluronan by human periodontal ligament cells. *J Cell Physiol.*

Shyjan, A.M., Heldin, P., Butcher, E.C., Yoshino, T. and Briskin, M.J., 1996. Functional cloning of the cDNA for a human hyaluronan synthase. *J Biol Chem*, **271,** 23395-9.

Sibalic, V., Fan, X., Loffing, J. and Wuthrich, R.P., 1997. Upregulated renal tubular CD44, hyaluronan, and osteopontin in kdkd mice with interstitial nephritis. *Nephrol Dial Transplant*, **12,** 1344-53.

Sibalic, V., Sun, L., Sibalic, A., Oertli, B., Ritthaler, T. and Wuthrich, R.P., 1998. Characteristic matrix and tubular basement membrane abnormalities in the CBA/Ca-kdkd mouse model of hereditary tubulointerstitial disease. *Nephron*, **80,** 305-13.

Slavik, M. and Carter, S.K., 1975. Chromomycin A3, mithramycin, and olivomycin: antitumor antibiotics of related structure. *Adv Pharmacol Chemother*, **12,** 1-30.

Sleeman, J., Rudy, W., Hofmann, M., Moll, J., Herrlich, P. and Ponta, H., 1996. Regulated clustering of variant CD44 proteins increases their hyaluronate binding capacity. *J Cell Biol*, **135,** 1139-50.

Smale, S.T., 1997. Transcription initiation from TATA-less promoters within eukaryotic protein-coding genes. *Biochim Biophys Acta*, **1351,** 73-88.

Spicer, A.P., Augustine, M.L. and McDonald, J.A., 1996. Molecular cloning and characterization of a putative mouse hyaluronan synthase. *J Biol Chem*, **271,** 23400-6.

Spicer, A.P. and McDonald, J.A., 1998. Characterization and molecular evolution of a vertebrate hyaluronan synthase gene family. *J Biol Chem*, **273,** 1923-32.

Spicer, A.P. and McDonald, J.A., 2000. Eukaryotic hyaluronan synthases. http://www.glycoforum.gr.jp/science/hyaluronan/HA07/HA07E.html

Spicer, A.P. and Nguyen, T.K., 1999. Mammalian hyaluronan synthases: investigation of functional relationships in vivo. *Biochem Soc Trans*, **27,** 109-15.

Spicer, A.P., Olson, J.S. and McDonald, J.A., 1997. Molecular cloning and characterization of a cDNA encoding the third putative mammalian hyaluronan synthase. *J Biol Chem*, **272,** 8957-61.

Spicer, A.P., Seldin, M.F., Olsen, A.S., Brown, N., Wells, D.E., Doggett, N.A., Itano, N., Kimata, K., Inazawa, J. and McDonald, J.A., 1997. Chromosomal localization of the human and mouse hyaluronan synthase genes. *Genomics*, **41,** 493-7.

Stahl, P.J. and Felsen, D., 2001. Transforming growth factor-beta, basement membrane, and epithelial-mesenchymal transdifferentiation: implications for fibrosis in kidney disease. *Am J Pathol*, **159,** 1187-92.

Stamenkovic, I., Amiot, M., Pesando, J.M. and Seed, B., 1989. A lymphocyte molecule implicated in lymph node homing is a member of the cartilage link protein family. *Cell*, **56,** 1057-62.

Stern, R., 2000. Mammalian hyaluronidases. http://www.glycoforum.gr.jp/science-/hyaluronan/HA15/HA15E.html

Stock, A.E., Bouchard, N., Brown, K., Spicer, A.P., Underhill, C.B., Dore, M. and Sirois, J., 2002. Induction of hyaluronan synthase 2 by human chorionic gonadotropin in mural granulosa cells of equine preovulatory follicles. *Endocrinology*, **143,** 4375-84.

Stokes, M.B., Holler, S., Cui, Y., Hudkins, K.L., Eitner, F., Fogo, A. and Alpers, C.E., 2000. Expression of decorin, biglycan, and collagen type I in human renal fibrosing disease. *Kidney Int*, **57,** 487-98.

Strachan, T. and Read, A.P., 1999. Human Molecular Genetics 2. In: Kingston, F. (Ed). *BIOS Scientific Publishers Ltd.*, 576.

Strutz, F., 2001. Potential methods to prevent interstitial fibrosis in renal disease. *Expert Opin Investig Drugs*, **10,** 1989-2001.

Strutz, F. and Muller, G.A., 1995. On the progression of chronic renal disease. *Nephron*, **69,** 371-9.

Stuhlmeier, K.M. and Pollaschek, C., 2004. Differential effect of transforming growth factor beta (TGF-beta) on the genes encoding hyaluronan synthases and utilization of the p38 MAPK pathway in TGF-beta-induced hyaluronan synthase 1 activation. *J Biol Chem*, **279,** 8753-60.

Stuhlmeier, K.M. and Pollaschek, C., 2004. Glucocorticoids inhibit induced and non-induced mRNA accumulation of genes encoding hyaluronan synthases (HAS): hydrocortisone inhibits HAS1 activation by blocking the p38 mitogen-activated protein kinase signalling pathway. *Rheumatology (Oxford)*, **43,** 164-9.

Stylianou, E., Jenner, L.A., Davies, M., Coles, G.A. and Williams, J.D., 1990. Isolation, culture and characterization of human peritoneal mesothelial cells. *Kidney Int*, **37,** 1563-70.

Stylianou, E., Nie, M., Ueda, A. and Zhao, L., 1999. c-Rel and p65 trans-activate the monocyte chemoattractant protein-1 gene in interleukin-1 stimulated mesangial cells. *Kidney Int*, **56,** 873-82.

Sugimoto, K., Iizawa, T., Harada, H., Yamada, K., Katsumata, M. and Takahashi, M., 2004. Cartilage degradation independent of MMP/aggrecanases. *Osteoarthritis Cartilage*, **12,** 1006-14.

Sussmann, M., Sarbia, M., Meyer-Kirchrath, J., Nusing, R.M., Schror, K. and Fischer, J.W., 2004. Induction of hyaluronic acid synthase 2 (HAS2) in human vascular smooth muscle cells by vasodilatory prostaglandins. *Circ Res*, **94,** 592-600.

Szabo, A., Lutz, J., Schleimer, K., Antus, B., Hamar, P., Philipp, T. and Heemann, U., 2000. Effect of angiotensin-converting enzyme inhibition on growth factor mRNA in chronic renal allograft rejection in the rat. *Kidney Int*, **57,** 982-91.

Takeda, M., Babazono, T., Nitta, K. and Iwamoto, Y., 2001. High glucose stimulates hyaluronan production by renal interstitial fibroblasts through the protein kinase C and transforming growth factor-beta cascade. *Metabolism*, **50,** 789-94.

Tammi, R., Pasonen-Seppanen, S., Kolehmainen, E. and Tammi, M., 2005. Hyaluronan synthase induction and hyaluronan accumulation in mouse epidermis following skin injury. *J Invest Dermatol*, **124,** 898-905.

Tammi, R., Rilla, K., Pienimaki, J.P., MacCallum, D.K., Hogg, M., Luukkonen, M., Hascall, V.C. and Tammi, M., 2001. Hyaluronan enters keratinocytes by a novel endocytic route for catabolism. *J Biol Chem*, **276,** 35111-22.

Tang, W.W., Qi, M., Warren, J.S. and Van, G.Y., 1997. Chemokine expression in experimental tubulointerstitial nephritis. *J Immunol*, **159,** 870-6.

Tang, W.W., Van, G.Y. and Qi, M., 1997. Myofibroblast and alpha 1 (III) collagen expression in experimental tubulointerstitial nephritis. *Kidney Int*, **51,** 926-31.

Tatusova, T.A. and Madden, T.L., 1999. BLAST 2 Sequences, a new tool for comparing protein and nucleotide sequences. *FEMS Microbiol Lett*, **174,** 247-50.

Teder, P., Vandivier, R.W., Jiang, D., Liang, J., Cohn, L., Pure, E., Henson, P.M. and Noble, P.W., 2002. Resolution of lung inflammation by CD44. *Science*, **296,** 155-8.

Toole, B.P., 2000. Hyaluronan is not just a goo! *J Clin Invest*, **106,** 335-6.

Toole, B.P., 2001. Hyaluronan in morphogenesis. *Semin Cell Dev Biol*, **12,** 79-87.

Toole, B.P., 2004. Hyaluronan: from extracellular glue to pericellular cue. *Nat Rev Cancer*, **4,** 528-39.

Toole, B.P., Wight, T.N. and Tammi, M.I., 2002. Hyaluronan-cell interactions in cancer and vascular disease. *J Biol Chem*, **277,** 4593-6.

Topley, N., Mackenzie, R.K. and Williams, J.D., 1996. Macrophages and mesothelial cells in bacterial peritonitis. *Immunobiology*, **195,** 563-73.

Topley, N. and Williams, J.D., 1994. Role of the peritoneal membrane in the control of inflammation in the peritoneal cavity. *Kidney Int Suppl*, **48,** S71-8.

Triggs-Raine, B., Salo, T.J., Zhang, H., Wicklow, B.A. and Natowicz, M.R., 1999. Mutations in HYAL1, a member of a tandemly distributed multigene family encoding disparate hyaluronidase activities, cause a newly described lysosomal disorder, mucopolysaccharidosis IX. *Proc Natl Acad Sci U S A*, **96,** 6296-300.

Turley, E.A., 1989. The role of a cell-associated hyaluronan-binding protein in fibroblast behaviour. *Ciba Found Symp*, **143,** 121-33; discussion 133-7, 281-5.

Turley, E.A., Noble, P.W. and Bourguignon, L.Y., 2002. Signaling properties of hyaluronan receptors. *J Biol Chem*, **277,** 4589-92.

Udabage, L., Brownlee, G.R., Waltham, M., Blick, T., Walker, E.C., Heldin, P., Nilsson, S.K., Thompson, E.W. and Brown, T.J., 2005. Antisense-mediated suppression of hyaluronan synthase 2 inhibits the tumorigenesis and progression of breast cancer. *Cancer Res*, **65,** 6139-50.

Ueki, N., Taguchi, T., Takahashi, M., Adachi, M., Ohkawa, T., Amuro, Y., Hada, T. and Higashino, K., 2000. Inhibition of hyaluronan synthesis by vesnarinone in cultured human myofibroblasts. *Biochim Biophys Acta*, **1495,** 160-7.

Urnov, F.D. and Wolffe, A.P., 2001. Chromatin remodeling and transcriptional activation: the cast (in order of appearance). *Oncogene*, **20,** 2991-3006.

Usui, T., Amano, S., Oshika, T., Suzuki, K., Miyata, K., Araie, M., Heldin, P. and Yamashita, H., 2000. Expression regulation of hyaluronan synthase in corneal endothelial cells. *Invest Ophthalmol Vis Sci*, **41,** 3261-7.

van der Velden, A.W. and Thomas, A.A., 1999. The role of the 5' untranslated region of an mRNA in translation regulation during development. *Int J Biochem Cell Biol*, **31,** 87-106.

Vines, C.A., Li, M.W., Deng, X., Yudin, A.I., Cherr, G.N. and Overstreet, J.W., 2001. Identification of a hyaluronic acid (HA) binding domain in the PH-20 protein that may function in cell signaling. *Mol Reprod Dev*, **60,** 542-52.

Wang, A. and Hascall, V.C., 2004. Hyaluronan structures synthesized by rat mesangial cells in response to hyperglycemia induce monocyte adhesion. *J Biol Chem*, **279,** 10279-85.

Wang, C., Thor, A.D., Moore, D.H., 2nd, Zhao, Y., Kerschmann, R., Stern, R., Watson, P.H. and Turley, E.A., 1998. The overexpression of RHAMM, a hyaluronan-binding protein that regulates ras signaling, correlates with overexpression of mitogen-activated protein kinase and is a significant parameter in breast cancer progression. *Clin Cancer Res*, **4,** 567-76.

Wang, S.N., Lapage, J. and Hirschberg, R., 1999. Glomerular ultrafiltration and apical tubular action of IGF-I, TGF-beta, and HGF in nephrotic syndrome. *Kidney Int*, **56,** 1247-51.

Wang, Y., Chen, J., Chen, L., Tay, Y.C., Rangan, G.K. and Harris, D.C., 1997. Induction of monocyte chemoattractant protein-1 in proximal tubule cells by urinary protein. *J Am Soc Nephrol*, **8,** 1537-45.

Watanabe, H., Cheung, S.C., Itano, N., Kimata, K. and Yamada, Y., 1997. Identification of hyaluronan-binding domains of aggrecan. *J Biol Chem*, **272,** 28057-65.

Watanabe, H. and Yamada, Y., 1999. Mice lacking link protein develop dwarfism and craniofacial abnormalities. *Nat Genet*, **21,** 225-9.

Watanabe, K. and Yamaguchi, Y., 1996. Molecular identification of a putative human hyaluronan synthase. *J Biol Chem*, **271,** 22945-8.

Weigel, P.H., 2004. Bacterial hyaluronan synthases. http://www.glycoforum.gr.jp-/science/hyaluronan/HA06/HA06E.html

Weigel, P.H., Hascall, V.C. and Tammi, M., 1997. Hyaluronan synthases. *J Biol Chem*, **272,** 13997-4000.

Weiss, R.A., Madaio, M.P., Tomaszewski, J.E. and Kelly, C.J., 1994. T cells reactive to an inducible heat shock protein induce disease in toxin-induced interstitial nephritis. *J Exp Med*, **180,** 2239-50.

Weissmann, B., Meyer, K., Sampson, P. and Linker, A., 1954. Isolation of oligosaccharides enzymatically produced from hyaluronic acid. *J Biol Chem*, **208,** 417-29.

Wells, A., Larsson, E., Hanas, E., Laurent, T., Hallgren, R. and Tufveson, G., 1993. Increased hyaluronan in acutely rejecting human kidney grafts. *Transplantation*, **55,** 1346-9.

Wells, A.F., Larsson, E., Tengblad, A., Fellstrom, B., Tufveson, G., Klareskog, L. and Laurent, T.C., 1990. The localization of hyaluronan in normal and rejected human kidneys. *Transplantation*, **50,** 240-3.

West, D.C., Hampson, I.N., Arnold, F. and Kumar, S., 1985. Angiogenesis induced by degradation products of hyaluronic acid. *Science*, **228,** 1324-6.

Williams, H.J., Bray, N., Murphy, K.C., Cardno, A.G., Jones, L.A. and Owen, M.J., 1999. No evidence for allelic association between schizophrenia and a functional variant of the human dopamine beta-hydroxylase gene (DBH). *Am J Med Genet*, **88,** 557-9.

Williams, N.M., Bowen, T., Spurlock, G., Norton, N., Williams, H.J., Hoogendoorn, B., Owen, M.J. and O'Donovan, M.C., 2002. Determination of the genomic structure and mutation screening in schizophrenic individuals for five subunits of the N-methyl-D-aspartate glutamate receptor. *Mol Psychiatry*, **7,** 508-14.

Winzen, R., Kracht, M., Ritter, B., Wilhelm, A., Chen, C.Y., Shyu, A.B., Muller, M., Gaestel, M., Resch, K. and Holtmann, H., 1999. The p38 MAP kinase pathway signals for cytokine-induced mRNA stabilization via MAP kinase-activated protein kinase 2 and an AU-rich region-targeted mechanism. *Embo J*, **18,** 4969-80.

Wuthrich, R.P., 1999. The proinflammatory role of hyaluronan-CD44 interactions in renal injury. *Nephrol Dial Transplant*, **14,** 2554-6.

Yamada, Y., Itano, N., Hata, K., Ueda, M. and Kimata, K., 2004. Differential regulation by IL-1beta and EGF of expression of three different hyaluronan synthases in oral mucosal epithelial cells and fibroblasts and dermal fibroblasts: quantitative analysis using real-time RT-PCR. *J Invest Dermatol*, **122,** 631-9.

Yamada, Y., Itano, N., Zako, M., Yoshida, M., Lenas, P., Niimi, A., Ueda, M. and Kimata, K., 1998. The gene structure and promoter sequence of mouse hyaluronan synthase 1. *Biochem J*, **330 (Pt 3),** 1223-7.

Yang, B., Yang, B.L., Savani, R.C. and Turley, E.A., 1994. Identification of a common hyaluronan binding motif in the hyaluronan binding proteins RHAMM, CD44 and link protein. *Embo J*, **13,** 286-96.

Yonemura, S., Hirao, M., Doi, Y., Takahashi, N., Kondo, T. and Tsukita, S., 1998. Ezrin/radixin/moesin (ERM) proteins bind to a positively charged amino acid cluster in the juxta-membrane cytoplasmic domain of CD44, CD43, and ICAM-2. *J Cell Biol*, **140,** 885-95.

Yoo, J., Jeong, M.J., Kwon, B.M., Hur, M.W., Park, Y.M. and Han, M.Y., 2002. Activation of dynamin I gene expression by Sp1 and Sp3 is required for neuronal differentiation of N1E-115 cells. *J Biol Chem*, **277,** 11904-9.

Yung, S., Coles, G.A. and Davies, M., 1996. IL-1 beta, a major stimulator of hyaluronan synthesis in vitro of human peritoneal mesothelial cells: relevance to peritonitis in CAPD. *Kidney Int*, **50,** 1337-43.

Yung, S., Thomas, G.J. and Davies, M., 2000. Induction of hyaluronan metabolism after mechanical injury of human peritoneal mesothelial cells in vitro. *Kidney Int*, **58,** 1953-62.

Yung, S., Thomas, G.J., Stylianou, E., Williams, J.D., Coles, G.A. and Davies, M., 1995. Source of peritoneal proteoglycans. Human peritoneal mesothelial cells synthesize and secrete mainly small dermatan sulfate proteoglycans. *Am J Pathol*, **146,** 520-9.

Zhang, H. and Martin-DeLeon, P.A., 2003. Mouse Spam1 (PH-20) is a multifunctional protein: evidence for its expression in the female reproductive tract. *Biol Reprod*, **69,** 446-54.

Zhang, S., Chang, M.C., Zylka, D., Turley, S., Harrison, R. and Turley, E.A., 1998. The hyaluronan receptor RHAMM regulates extracellular-regulated kinase. *J Biol Chem*, **273,** 11342-8.

Zhu, D. and Bourguignon, L.Y., 2000. Interaction between CD44 and the repeat domain of ankyrin promotes hyaluronic acid-mediated ovarian tumor cell migration. *J Cell Physiol*, **183,** 182-95.

Zoja, C., Morigi, M., Figliuzzi, M., Bruzzi, I., Oldroyd, S., Benigni, A., Ronco, P. and Remuzzi, G., 1995. Proximal tubular cell synthesis and secretion of endothelin-1 on challenge with albumin and other proteins. *Am J Kidney Dis*, **26,** 934-41.